JOURNAL

OF

MINING AND GEOLOGICAL SCIENCES

Editor-in-chief

Prof. Dr. Pavel Pavlov

University of Mining and Geology "St. Ivan Rilski"
1, Prof. Boyan Kamenov Str., 1700 Sofia, Bulgaria
e-mail: srs@mgu.bg; http://www.mgu.bg/nis

EDITORIAL BOARD

Technical secretary: **Kalina Marinova**

Printig: **Publishing House "St. Ivan Rilski"**

CONTENTS

DETERMINING THE IMPACT OF THE FRACTION SIZE OF THE FEEDING PRODUCT AND THE WIDTH OF THE DISCHARGE PORT OF A COMPLEX PENDULUM JAW CRUSHER ON ITS PERFORMANCE

Ivan Minin[1], Dimitar Mitev[2], Simeon Savov[3]

[1]University of Mining and Geology „St. Ivan Rilski", 1700 Sofia, minin_ivan@abv.bg
[2]University of Mining and Geology „St. Ivan Rilski", 1700 Sofia, dimitar_i_radi@abv.bg
[3]University of Mining and Geology „St. Ivan Rilski", 1700 Sofia, ss.ss@abv.bg

ABSTRACT. In the literature describing the theory of operation of jaw crushers, the topic of the influence of the constructive parameters on the technological ones is is touched upon, but separately. For example, when determining the performance of jaw crushers with a complex swinging of the jaw (or complex pendulum jaw crushers), the size of the discharge port is indicated as the main parameter of influence. However, it is not clear how the fraction size of the product to be crushed affects the performance of the mill. This is shown partially in the fraction size characteristics of the crushers, but it is not possible to be analytically determined. In the present study, an attempt is made to determine the simultaneous impact of these two parameters on the performance of a laboratory-scaled jaw crusher with complex swinging of the jaw used for a coarse crushing. For this purpose, an experiment was performed with a laboratory-scaled complex pendulum jaw with the size of the feeding gap of 0.7 x 1.05m. After processing the results of the experiment, several mathematical models were obtained describing the influence of the width of the sizing gap for the discharge and the fraction size of the feeding material on the productivity of the crusher. The model with the highest values of confidence has been chosen and the relevant conclusions were made.

Keywords: jaw crushers, analytical determination, productivity, rate of crushing

ОПРЕДЕЛЯНЕ ВЛИЯНИЕТО НА ЕДРИНАТА НА ПОСТЪПВАЩИЯ ПРОДУКТ И ШИРОЧИНАТА НА ИЗПУСКАТЕЛНИЯ ОТВОР НА ЧЕЛЮСТНА ТРОШАЧКА СЪС СЛОЖНО ЛЮЛЕЕНЕ ВЪРХУ ПРОИЗВОДИТЕЛНОСТТА Й

Иван Минин[1], Димитър Митев[2], Симеон Савов[3]
[1]Минно-геоложки университет „Св. Иван Рилски",1700 София, minin_ivan@abv.bg,
[2]Минно-геоложки университет „Св. Иван Рилски",1700 София, dimitar_i_radi@abv.bg
[3]Минно-геоложки университет „Св. Иван Рилски",1700 София, ss.ss@abv.bg

РЕЗЮМЕ. В литературата, описваща теорията на работа на челюстните трошачки, е засегнат въпросът за влиянието на конструктивните параметри върху технологичните, но поотделно. Например, при определяне на производителността на челюстните трошачки със сложно люлеене на подвижната челюст като основен параметър, оказващ влияние, е посочена широчината на изпускателния отвор на трошачката. Не е ясно обаче какво е влиянието на зърнометричния състав на постъпващия за трошене продукт върху производителността на машината. Това е показано частично в зърнометричните характеристики на трошачките, но не е възможно да се определи аналитично. В настоящата разработка е направен опит да се определи едновременното влияние на тези два параметъра върху производителността на челюстна трошачка със сложно люлеене на подвижната челюст, използвана най-често за едро трошене. За целта е направен експеримент с лабораторна челюстна трошачка със сложно люлеене на подвижната челюст с размери на приемния отвор 0,7 x 1,05m. След обработка на резултатите от експеримента са получени няколко математически модела, описващи влиянието на широчината на изпускателния отвор и зърнометричния състав на постъпващия за трошене материал върху производителността на машината. Избран е моделът с най-високи стойности на достоверност и са направени съответните изводи от получения резултат.

Ключови думи: челюстна трошачка, аналитично определяне, продуктивност, степен на трошене

Introduction

In the analytical determination of the performance of jaw crushers, the width of the sizing gap for discharge (or: the discharge port) and the movement of the jaw are indicated as main parameters of influence (Цветков, 1976; Минин, 2012). This is determined according to the following formula:

$$Q_v = 60.k_1.k_p.n\frac{(2b+s).s.L}{2.tg\alpha}, m^3/s \qquad (1)$$

where:

Q_v is the volumetric efficiency of the crusher;

b, m is the maximum width of the discharge port;

k_1 is a coefficient that depends on the type of the crusher. For crushers with a complex swinging of the jaw, it is in the range of > 1 because the jaw moves downwards, thus increasing the productivity of the machine.

k_p is a coefficient of ore bulking;

s, m is the movement of the jaw;

$n, \min^{-1}$ are the RPMs of the eccentric shaft of the crusher;

α^0 is the angle between the jaws;

L, m is the length of the inlet gap.

The mass performance is calculated by the formula:

$$Q = \rho.Q_v, t/h \qquad (2)$$

where $\rho, t/m^3$ is the density of the ore to be crushed.

From the formulae shown, it is not clear how the fraction size of the product to be crushed affects the productivity of the machine. This can be roughly defined by the fraction size characteristics of crushers, but it is not possible to be determined analytically. With the present study, an attempt is made to determine the simultaneous impact of two parameters (the width of the sizing gap for discharge and the fraction size of the feeding product) on the performance of a laboratory-scaled complex pendulum jaw crusher used for coarse crushing through an experiment with a laboratory-scaled jaw crusher (Fig. 1) with a complex swinging of the movable jaw with the size of the feeding gap of 0.7 x 1.05m.
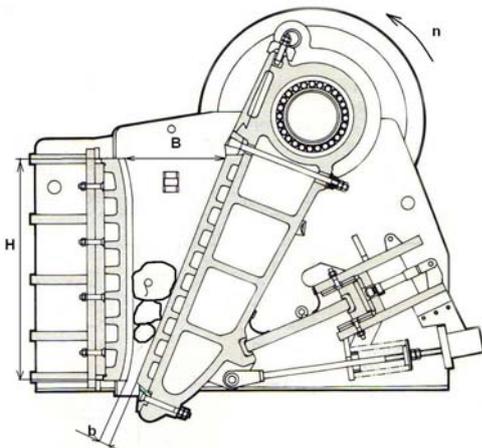
Fig.1. A schematic view of the laboratory-scaled crusher

Results from the experiment on a laboratory - scaled crusher with a complex swinging of the movable jaw

In the study, the following possible parameters were identified as driving factors:

1. An average diameter of the fractions that are fed into the crusher. This size is the average of the appropriate class of selected and pre-cut material. The experiments were made with the materials of dimensions shown in Table 1. They are consistent with the width of the inlet gap of the laboratory-scaled crusher.

Table 1.

Class	D	Class	D
+45-55	50	+35-45	40
+25-35	30	+15-25	20

2. The width discharge port of the crusher. This parameter has also been selected according to the dimensions and capabilities of the laboratory machine and with values of 6, 8, 12, 16, and 20 mm.

Measurements of the productivity were performed. The productivity was obtained after measuring the crushing time of a certain quantity of material, pre-weighed with a digital balance.

The performance of the machine can be calculated using the formula:

$$q = \frac{M_{сум.}}{t}, g/s \qquad (3)$$

where:

q is the productivity of the machine;

$M_{сум.}, g$ is the total amount of the crushed material. This parameter is measured by an electronic balance.

t, s is the time for ore crushing.

The obtained results and calculations are given in Table 2:

Table 2.

D, mm	b, mm	q, g/s
50	20	364.9969
50	16	235.9133
50	12	171.9044
50	8	166.18
50	6	101.1798
40	20	334.7136
40	16	263.2581
40	12	191.3529
40	8	147.937
40	6	115.9501
30	20	421.9943
30	16	312.0862
30	12	245.5491
30	8	158.1779
30	6	111.9926
30	20	334.3384
20	16	386.9281
20	12	346.6667
20	8	134.9
20	6	127.2314
20	6	107.1524

As a result of the experiment, the parameters were transformed into a Fisher matrix shown in Table 3:

Table 3.

№	X_1	X_2	Y_2
	D, mm	b, mm	q, g/s
1	50	20	364.9969
2	50	16	235.9133
3	50	12	171.9044
4	50	8	166.18
5	50	6	101.1798
6	40	20	334.7136
7	40	16	263.2581
8	40	12	191.3529
9	40	8	147.937
10	40	6	115.9501
11	30	20	421.9943
12	30	16	312.0862

13	30	12	245.5491
14	30	8	158.1779
15	30	6	111.9926
16	30	20	334.3384
17	20	16	386.9281
18	20	12	346.6667
19	20	8	134.9
20	20	6	127.2314
21	20	6	107.1524

For the purpose of the practical study of the performance process, models and regression coefficients were sought which can be assumed with confidence levels of 95%. It is expected that acceptable engineering error margins of 5% are normal for technical devices such as jaw crushers. The method of operation (Божанов,1979) is illustrated at Figure 2.
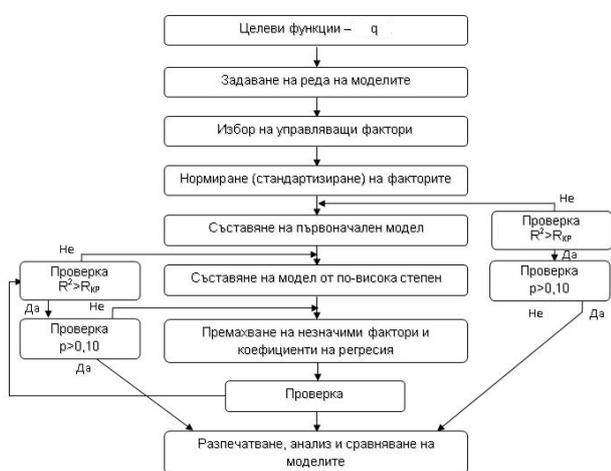
Fig. 2. A flow-chart of the operation mode

The results of the conducted experiment were statically processed with the STATGRAPHICS program, because it is appropriate for this study.

As a result of the experiment, 10 mathematical models with the parameters were obtained and they are shown in Table 4:

Table 4.

Model №	P-value criterion	Significance of F	$R^2(adj)$ %	R^2 %
1	>0.05	0	88.9	88
2	>0.05	0	97.1	97
3	>0.05	<0.05	33.4	36
4	0	0	84	84
5	0	0	55	57
6	0	0	42.9	43
7	>0.05	0	89.2	90
8	0	0	98.3	98
9	>0.05	0	84.6	85
10	>0.05	0	96.6	97

The assessment of the significance of the coefficients of regression is performed according to the Student`s t-test criterion at a level of significance and 8 degrees of freedom

(Минин, 2012). In the program, this procedure is known to evaluate the expectancy of significance of the regression coefficients. If this probability is

$$P\text{-}value < \alpha \tag{4},$$

the coefficient of regression is significant (α-confidence probability).

Similarly, the adequacy of the equation is evaluated by means of the significance of the Fisher criterion (Significance of F). If the significance of the criterion is < α, the equation is adequate.

Model № 8 is the best-performing of all obtained models (Table 4) and it can be evaluated as a high-performance model. The multiple correlation coefficient is 98.36% and the corrected multi-correlation factor is over 98%. This model has the best performance among all others. The confidence probability index (P-criterion) for the model is below the critical value of 0.05, i.e. it can be assumed that the model is adequate with a confidence probability of over 98%. The parameters of Model № 8 are shown in Table 5.

Table 5.

Parameters	Value	Standard error		P-value criterion
b	26.4465	2.05081		0.0000
D*b	-0.215449	0.0548965		0.0009
	Sum of squares of the model	*Degrees of freedom*	*F-value criterion*	Significance of *F*
Model	1.288986	2	570.57	0.0000
Residual	21461	19		
Total	1.310446	21		
Multiple correlation coefficient				98.3623%
Adjusted coefficient of multiple correlation				98.2761%
Standard error				33.6085
Average absolute error				24.2421
Statistics of Durbin - Watson				2.04736

Then, the equation of the model with natural variables is logically chosen to be:

$$q = 26,446.b - 0,215.D.b \ , g/s \tag{5}$$

The model is presented graphically in Figure 3.
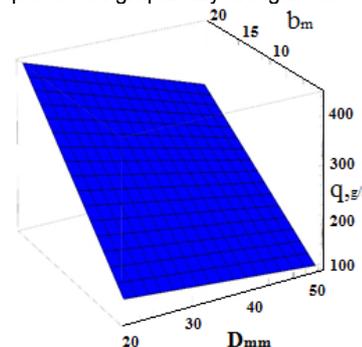
Fig.3. The productivity of the crusher depending on the width of the sizing discharge gap and the fraction size of the feeding product

Conclusions

1. The performance of the jaw crusher is significantly affected by two parameters: the size of the feeding fractions and the width of the discharging port.

2. An increase of the width of the outlet gap leads to an increase in the productivity of the machine, possibly due to the fact that it reduces the discharging time of the crushing chamber.

3. An increase of the size of the ore fractions feeding the machine results in a reduction in the productivity, possibly due to the fact that the time of discharging the crush chamber is increased.

References

Божанов С., И. Н. Вучков. Статистически решения в производството и начини на изследване. С., Техника, 1979. (Bozhanov, S., I. N. Vuchkov. Statisticheski reshenia v proizvodstvoto i nachini na izsledvane. Sofia, Tehnika, 1979.)

Минин, И. Техника и технологии за обогатяване на полезни изкопаеми – I част, Учебник, С., Авангард Прима, 2012. (Minin, I. Tehnika i technologii za obogatyavane na polezni izkopaemi -I chast. Sofia, Avangard Prima, 2012.)

Цветков, Хр. Обогатителни машини. С., Техника, 1976. (Tsvetkov, Hr. Obogatitelni mashini. Sofia, Tehnika, 1976.)

CHARACTERISTICS OF THE FRACTION SIZE DISTRIBUTION AND THE RATE OF CRUSHING FOR A LABORATORY-SCALED COMPLEX PENDULUM JAW CRUSHER

Ivan Minin[1], Valerya Kovacheva-Ninova[2], Dimitar Dimitrov[3]

[1]*University of Mining and Geology "St. Ivan Rilski", 1700 Sofia, minin_ivan@abv.bg*
[2]*University of Mining and Geology "St. Ivan Rilski", 1700 Sofia, valeria.kovacheva@mgu.bg,*
[3]*University of Mining and Geology "St. Ivan Rilski", 1700 Sofia, dimitardim61@gmail.com*

ABSTRACT. Some of the paramount technological parameters of jaw crushers are the fraction size characteristics of the crushed product and the rate of crushing (*i*). The manual of every machine outlines those but very often it does not specify the width of the discharge gap (b) of the crusher and how this affects the fraction size characteristics of the crushing process and the achieved rate of crushing. All these factors aggravate the choice of crusher purchase and result in errors. For this reason, an experiment has been carried out with a laboratory-scaled complex pendulum jaw crusher with the size of the feeding gap of 100 x 155 mm. The sieve analyses performed have helped construct fraction size characteristics for the crushing products and define the degree of crushing of the mineral at varying widths of the jaw crusher's outlet gap and at varying lump or grain sizes of the input material to be crushed. The results obtained have been analysed and conclusions have been drawn regarding the technological parameters of the jaw crusher under the specified working conditions.

Keywords: jaw crushers, discharge gap, fraction size distribution characteristics, rate of crushing

ЗЪРНОМЕТРИЧНИ ХАРАКТЕРИСТИКИ И СТЕПЕН НА ТРОШЕНЕ НА ЛАБОРАТОРНА ЧЕЛЮСТНА ТРОШАЧКА СЪС СЛОЖНО ЛЮЛЕЕНЕ НА ПОДВИЖНАТА ЧЕЛЮСТ
Иван Минин[1], Валерия Ковачева-Нинова[2], Димитър Димитров[3]
[1]*Минно-геоложки университет „Св. Иван Рилски", 1700 София, minin_ivan@abv.bg*
[2]*Минно-геоложки университет „Св. Иван Рилски", 1700 София, valeria.kovacheva@mgu.bg*
[3]*Минно-геоложки университет „Св. Иван Рилски", 1700 София, dimitardim61@gmail.com*

РЕЗЮМЕ. Едни от основните технологични параметри на челюстните трошачки са зърнометричната характеристика на натрошения продукт и степента на трошене (*i*). Те се дават в проспекта на всяка машина, но много често не е уточнено за каква широчина на разтоварващия отвор (b) на трошачката се отнасят и какво е влиянието на *b* върху зърнометричната характеристика на продукта от трошенето и постиганата степен на трошене. Всичко това затруднява избора на трошачка при закупуване на нова машина и води до грешки. За целта е направен експеримент с лабораторна челюстна трошачка със сложно люлеене на подвижната челюст и размери на приемния отвор 100 x 155 mm. От извършени ситови анализи са построени зърнометрични криви на продуктите от трошенето и е определена степента на трошене на минерална суровина при различни широчини на *b* на челюстната трошачка и едрини на постъпващия за трошене материал. След анализа на получените резултати са обобщени съответните изводи относно технологичните параметри на челюстната трошачка, при зададени размер на разтоварващ отвор и едрина на изходния материал.

Ключови думи: челюстна трошачка, разтоварващ отвор, зърнометрични характеристики, степен на трошене

Introduction

The jaw crushers are widely used for crushing of a variety of raw materials. The advantages of complex pendulum jaw crushers are their small dimensions and weight and their simple construction. These crushers provide a higher rate of crushing and 15-20% less energy demand than the jaw crushers with a simple swinging of the movable jaw. The choice of the dimension-type of the crusher is related to the following conditions: the feeding gap has to be at least 10-15% wider than the maximum particle size of the feeding product and the size of the sizing gap for discharge has to be suitable for achieving the required fraction size of the crushed product, the rate of crushing, and the productivity.

A number of technological parameters characterising the operation of the jaw crusher are determined under laboratory conditions, the most important being the rate of crushing and the fraction size characteristic of the crushed product. The establishment of the fraction size of the crushed material and the crushing rate are essential conditions for good management of the crushing process and its optimisation.

The purpose of the present study is to determine the fraction size and crushing rate of a laboratory-scaled complex pendulum jaw crusher at different widths of the discharge port and fraction grain sizes of the feeding material.

Materials and methods

The grain size distribution, or the grain size characteristics, shows the quantitative distribution of the grains/fractions in a certain material according to their size. The grain size distribution is determined by the methods of the grain size

analysis. The grain size analysis of the grain materials is unified and is performed by the method of the sieve analysis. For this purpose, average samples are collected from representative samples of the crushed products and they are sieved through a set of sieves of different mesh sizes (16.0, 12.5, 8.0, 4.0, 2.5, and 1.0 mm). Thus, average samples of the crushed products are sieved by size, obtaining the following classes: +16 mm, -16 + 12.5 mm, -12.5 + 8 mm, -8 + 4 mm, -4 + 2.5 mm, -2.5 +1 mm, and -1 + 0 mm.

The results of the sieve analyses are presented in a graphical form. To determine the total sum production of the resulting classes, their private productions (y_i) are calculated using the formula:

$$\gamma_i = \frac{M_i}{Q}.100, \%$$ (1)

where:
M_i is the mass of the respective class, kg;
Q is the total mass of the sample, kg.

The total sum grain size curves of the material passed through the meshes (by "–" in Fig. 2, 3, 4, 5, and 6)) represents the regularity of grain size distribution in the crushed products obtained after the crushing of the feeding material of different sizes and at different widths of the discharge port of the crusher.

The achieved rate of crushing (*i*) under the set test conditions (size of *b* and size of the input material) is determined by the formula:

$$i = \frac{D_{av}}{d_{av}}$$ (2)

where:
D_{av}, d_{av} are the average diameters of the material, respectively before and after the crushing, mm.
The average diameters of the crushed material are defined with the following formula:

$$d_{av} = \frac{\sum_{i=1}^{n} \gamma_i.d_i}{\sum_{i=1}^{n} \gamma_i}$$ (3)

where:
d_{av} is the average diameter of the grains of the whole material, mm;
d_i is the arithmetic mean diameter of the grains in the different classes, mm;
γ_i is the production of a class with a diameter d_i %.

The experiment sets the following parameter that defines the test conditions: average diameter of the material to be crushed (D_{av}, mm).

The material is pre-selected and sieved until the relevant crushed class is obtained. The dimensions of the prepared classes are shown in Table 1.

Table 1.
Dimensions of the feeding material for crushing.

Class, mm	D_{av}, mm
-55+45	50
-45+35	40
-35+25	30
-25+15	20

The sizing gap for discharge is selected and compliant to the dimensions and capabilities of the laboratory-scaled facility. The experiments were performed at widths of the sizing gap for discharge of 6, 8, 12, 16, and 20 mm.

For the experiment, a laboratory-scaled complex pendulum jaw crusher and a feeding gap of 100 x 155 mm was used. Fig. 1 presents the longitudinal section of a jaw crusher with a complex swinging.
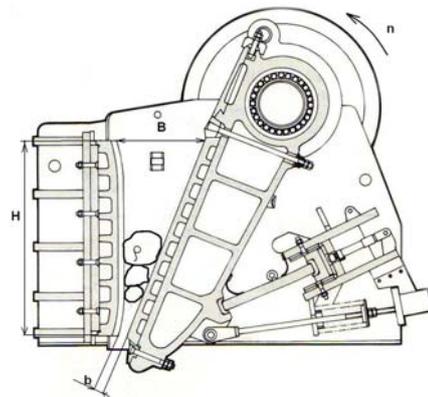
Fig. 1. Complex pendulum jaw crusher
➢ Width of the discharge port of the crusher (*b, mm*).

Results and discussions

The total sum of grain size curves (drawn by "-") of the crushed products at different widths of the discharge port and fraction sizes of the feeding material are shown in Figures 2, 3, 4, 5, and 6.

The characteristics of the grain sizes in Figures 2, 3, and 4 (at *b* = 20, 16 and 12 mm) show that the larger classes at all sizes of the feeding material (D_{av} = 50, 40, 30 and 20 mm) predominate in the crushed products. This is less prominent in the products obtained by crushing the material with a fraction size D_{av} = 50 mm. The dominance of larger classes increases with the reduction of the size of the material to be crushed. By decreasing the size of the discharge port from 20 mm to 12 mm, the content of the class +16 mm is reduced in the crushed products, respectively for:
✓ D_{av} 50 mm: from 41,5% to 5,2%;
✓ D_{av} 40 mm: from 47,2% to 0%;
✓ D_{av} 30 mm: from 46,5% to 0%;
✓ D_{av} 20 mm (at *b*=16 and 12 mm): 0%.

The grain size curves in Figure 5 show that for a discharging gap of the crusher *b* = 8 mm, a steady distribution of classes in the crushed products for all fraction sizes of the feeding material is achieved. This is most evident in the crushed product obtained from the material with D_{av} = 50 mm. All the

crushed products are with fraction sizes less than 12.5 mm. The resulting contents of the +8 mm class in the crushed products are respectively:

- ✓ for D_{av} 50 mm: 30.0%;
- ✓ for D_{av} 40 mm: 26.6%;
- ✓ for D_{av} 30 mm: 23.2%;
- ✓ for D_{av} 20 mm: 20.6%.

The grain size characteristics in Figure 6 (at b = 6 mm) show the predominance of the fine classes in the crushed products for all fraction sizes of the input material. With this size of the discharging port, the content of the +8 mm class in the products from the crushing of the relevant in sizes material is:

- ✓ for D_{av} 50 mm: 9.6%;
- ✓ for D_{av} 40 mm: 9.4%;
- ✓ for D_{av} 30 mm: 6.7%;
- ✓ for D_{av} 20 mm: 5.0%.

At the same sizing gap for discharge (b = 6 mm) of the jaw crusher, the content of the class -1,0 + 0 mm in the crushed products is similar for all fraction sizes of the feeding material. The content of the class -1,0 + 0 mm in the crushed products is respectively:

- ✓ for D_{av} 50 mm: 19.0%;
- ✓ for D_{av} 40 mm: 20.4%;
- ✓ for D_{av} 30 mm: 20.4%;
- ✓ for D_{av} 20 mm: 19.5%.
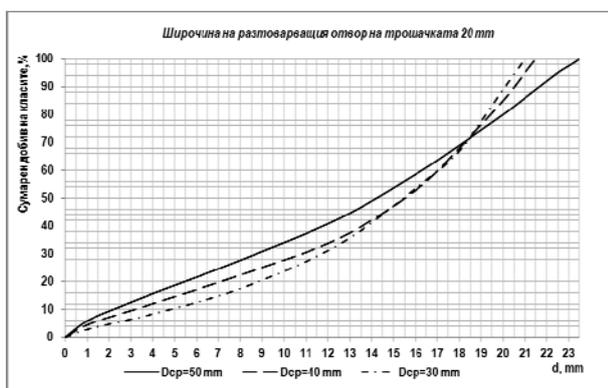
Fig. 2. Grain size distribution characteristics of the crushed products at b=20 mm
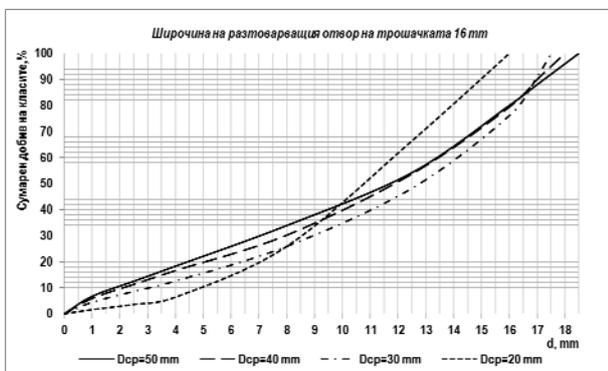
Fig. 3. Grain size distribution characteristics of the crushed products at b=16 mm
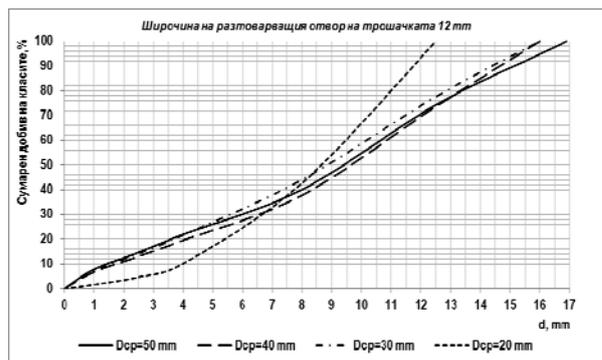
Fig. 4. Grain size distribution characteristics of the crushed products at b=12 mm
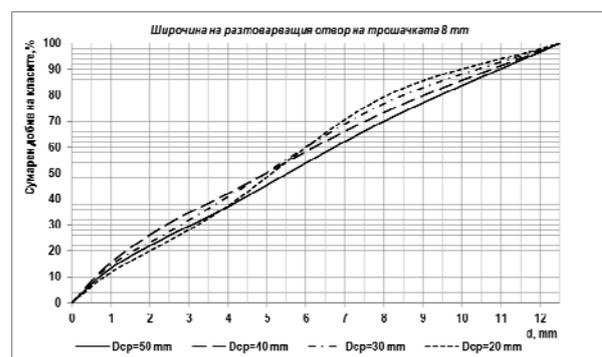
Fig. 5. Grain size distribution characteristics of the crushed products at b=8 mm
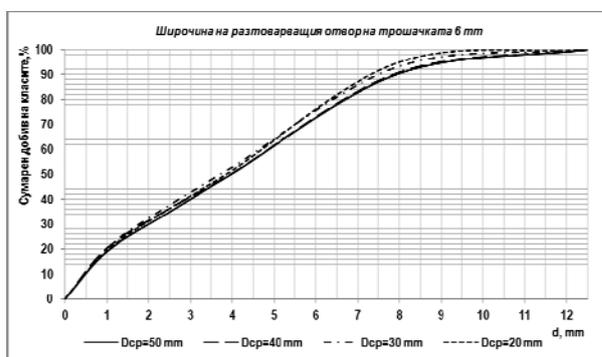
Fig. 6. Grain size distribution characteristics of the crushed products at b=6 mm

Table 2 shows thethe results of the calculations performed through formulae (2) and (3) regarding the crushing rates (*i*) and average diameters (d_{av}) of the crushed products at the different fraction sizes of the feeding material and the widths of the discharge port of the jaw crusher. Also, the table shows the fraction sizes d_{50} in the crushed products obtained under different test conditions. The fraction size d_{50} (mm) is a grain size corresponding to a 50% total sum production by minus, reported at the grain size curves represented in figures 2 - 6. The data in the table shows that the d_{av} and d_{50} of the crushed products obtained at the relevant widths of the discharging port have similar values that do not depend on the D_{av} of the feeding material. The rate of crushing decreases with a reduction in the size of the material to be crushed for each one of the chosen widths of the discharge port of the crusher.

Table 2.

Obtained values of i, d_{av} and d_{50} for the crushed products under the certain conditions for the experiments (D_{av} and b, mm).

D_{av}, mm	b=20 mm			b=16 mm			b=12 mm			b=8 mm			b=6 mm		
	D_{av} mm	d_{50} mm	l mm	D_{av} mm	d_{50} mm	l mm	d_{av} mm	d_{50} mm	l mm	D_{av} mm	d_{50} mm	l mm	D_{av} mm	d_{50} mm	l mm
50	13.0	14.3	3.8	10.5	11.8	4.8	8.8	9.3	5.7	5.7	5.5	8.8	4.3	4.0	11.6
40	13.5	15.5	3.0	10.7	12.0	3.7	8.9	9.6	4.5	5.3	5.0	7.5	4.2	4,0	9.5
30	13.8	15.5	2.2	11.2	12.8	2.7	8.4	8.8	3.6	5.3	5.3	5.7	4.0	3.7	7.5
20	-	-	-	10.2	11.0	2.0	8.6	8.6	2.3	5.3	5.2	3.8	4.0	3.9	5.0

For all fraction sizes of the feeding material, the crushing rate is increased by the reduction of the width of the discharging port. The highest rate of crushing is achieved by crushing the raw material with D_{av} = 50 mm, at all widths of the discharge port.

Conclusions

1. By the adjustment of the width of the sizing gap for discharge of the jaw crusher (b), the crushing process is controlled in order to obtain products of different fraction size composition. The total sum grain size characteristics of the crushed products indicate that they are characterised by:

   - a dominance of the larger classes at b > 12 mm;

   - a dominance of the finer classes at *b* = 6 mm;

   - a steady distribution of grain fractions at *b* = 8 mm.

2. For the studied widths of the discharging port of the crusher, a similar value of d_{av} and d_{50} is obtained for the crushed material and it does not depend on the D_{av} of the feeding material. The values of d_{av} and d_{50} vary within the range, respectively
   - at *b*=20 mm – d_{av} from 13.0 to 13.8 mm; d_{50} from 14.3 to 15.5 mm;
   - at *b*=16 mm – d_{av} from 10.2 to 11.2 mm; d_{50} from 11.0 to 12.8 mm;
   - at *b*=12 mm – d_{av} from 8.4 to 8.9 mm; d_{50} from 8.6 to 9.6 mm;
   - at *b*=8 mm – d_{av} from 5.3 to 5.7 mm; d_{50} from 5.0 to 5.5 mm;
   - at *b*=6 mm - d_{av} from 4.0 to 4.3 mm; d_{50} from 3.7 to 4.0 mm.

3. For all the investigated fraction sizes of the feeding material, the rate of crushing increases with the reduction of the width of the discharge port.

It is known that the rate of crushing, as well as the frequency of rotation of the eccentric shaft (swing frequency of the movable jaw), exert influence on the performance of the crusher and the consumed power. In order to determine these dependencies, it is necessary to continue the experiments for the actual crusher.

References

Андреев, С. Е. Дробление, измельчение и грохочение полезных ископаемых. М., Недра, 1980. (Andreev, S. E. Droblenie, izmelchenie i grohochenie poleznaih iskopaemaih. Moskva, Nedra, 1979.)

Гайдарджиев, Ст., Щ. Джендова, Г. Клисуранов, Р. Русев. Практикум по обогатяване на полезните изкопаеми. С., Техника, 1982. (Gaidardzhiev, St., Sht. Dzhendova, G. Klisuranov, R. Russev. Praktikum po obogatyavane na poleznite izkopaemi. Sofia, Tehnika, 1982.)

Денев, С. Зърнометрична подготовка на суровините. С., Техника, 1982. (Denev, St. Zarnometrichna podgotovka na surovinite. Sofia, Tehnika, 1982.)

Ковачева-Нинова, В. Практикум по минерални технологии. С., изд. МГУ „Св. Ив. Рилски", 2004. (Kovacheva-Ninova, V. Praktikum po mineralni technologii. Sofia, izd. MGU "Sv. Iv. Rilski", 2004.)

Минин, И. Техника и технологии за обогатяване на полезни изкопаеми – I част. С., Авангард Прима, 2012. (Minin, I. Tehnika i technologii za obogatyavane na polezni izkopaemi -I chast. Sofia, Avangard Prima, 2012.)

DETERMINING THE RELATIVE ENERGY CONSUMPTON OF A JAW CRUSHER DEPENDING ON THE WIDTH OF THE DISCHARGE PORT AND ON THE PARTICLE SIZE DISTRIBUTION OF THE CRUSHING PRODUCT

Teodora Hristova[1], Ivan Minin[2], Dimitar Mitev[3],

[1] *University of Mining and Geology "St. Ivan Rilski", 1700 Sofia, teodora@mgu.bg*
[2] *University of Mining and Geology "St. Ivan Rilski", 1700 Sofia, minin@abv.bg*
[3] *University of Mining and Geology "St. Ivan Rilski", 1700 Sofia, dimitar_i_radi@abv.bg*

ABSTRACT. The article discusses the topic of the specific energy consumption of a complex pendulum jaw crusher. It is driven by an induction motor with a squirrel-cage rotor. The purpose of the study is to determine the effect of two basic parameters on the relative energy consumption of the crusher: the width of the discharge port and the particle size distribution of the product to be crushed. In order to determine the energy performance, some basic parameters have been measured, such as the average diameter of the fragments fed into the crusher, the width of the crusher discharge port, the weight of the crushed material, the average power of the engine phase, the crushing time of the sample, etc. In accordance with the selected target function, energy consumption patterns have been synthesized depending on the width of the discharge port and the particle size distribution of the crushing product. The models obtained have been evaluated using statistical criteria to determine their adequacy in relation to the selected target function. Data processing has been performed through the STATGRAPHICS computer program. It has been found that the relative energy consumption is affected by the two control parameters - the size of the incoming pieces and the width of the crusher discharge port. Relevant conclusions have been made.

Keywords: jaw crusher, asynchronous engine, energy consumption, particle size distribution, discharge port

ОПРЕДЕЛЯНЕ НА ОТНОСИТЕЛЕН ЕНЕРГОРАЗХОД НА ЧЕЛЮСТНА ТРОШАЧКА В ЗАВИСИМОСТ ОТ ШИРОЧИНАТА НА ИЗПУСКАТЕЛНИЯ И ОТВОР И ЗЪРНОМЕТРИЧНИЯ СЪСТАВ НА ПРОДУКТА ЗА ТРОШЕНЕ
Теодора Христова[1], Иван Минин[2], Димитър Митев[3],
[1] *Минно-геоложки университет "Св. Иван Рилски", 1700 София, teodora@mgu.bg*
[2] *Минно-геоложки университет "Св. Иван Рилски", 1700 София, minin@abv.bg*
[3] *Минно-геоложки университет "Св. Иван Рилски", 1700 София, dimitar_i_radi@abv.bg*

РЕЗЮМЕ. В статията е изследван специфичният разход на електроенергия на челюстна трошачка със сложно люлеене на подвижната челюст. Тя е задвижвана от асинхронен двигател с накъсо съединен ротор. Цел на изследването е да се определи влиянието на два основни параметъра – широчина на изпускателния отвор и зърнометричен състав на продукта за разтрошаване върху относителния енергоразход на трошачката. За определяне на енергоразхода са измерени основни параметри като среден диаметър на постъпващите в трошачката късове, широчина на изпускателния отвор на трошачката, тегло на разтрошаваното количество материал, средна мощност на едната фаза на двигателя, време за разтрошаване на пробата и др. Според избраната целева функция са синтезирани модели на енергоразхода в зависимост от широчината на изпускателния отвор и зърнометричния състав на продукта за трошене. Получените модели са оценени посредством статистически критерии за определяне на адекватността им към избраната целева функция. Обработката на данните е извършен чрез компютърна програмата STATGRAPHICS. Установено е, че относителният енергоразход се влияе от двата управляващи параметъра - едрината на постъпващите късове и широчината на изпускателния отвор на трошачката и са направени съответните изводи.

Ключови думи: трошачка, асинхронен двигател, енергоразход, зърнометричен състав, изпускателен отвор

Introduction

Increased demand for production, reduced machine downtime, increased productivity, and the lowering of costs are of all of major importance to the mining industry. To maintain these priorities, the crushing process can be managed in accordance with various goals: minimum costs, high productivity, product quality, high efficiency, energy efficiency, and many more. The task is complicated due to the multitude of factors of the object. In such a case, it is appropriate to select a target that can be estimated from the point of view of real measured values which affect the production process.

Determining the target function and the control factors

The choice of machine mode of operation is made according to various criteria. In this case, a complex pendulum jaw crusher is considered. It is necessary to choose an operating mode for a laboratory jaw crusher in accordance with a specified criterion. To automate the process, the crusher must be considered as a control object. In terms of technological mode, the jaw crusher is classified as an uneven load mechanism. The performance of such mechanisms depends on a number of random factors such as: the particle size distribution, the physical properties of the ore, the mutual

arrangement of the individual ore fragments in the feed opening of the crusher, the wear of the lining of the moving and fixed jaws (Irinkov, 1971).

Typically, the objective of automatic control is the stabilisation of: the productivity, the active power of the electric drive or the ore level in the feed opening of the crusher (Radulov et al., 2009). Classical theory recommends that the crusher be automated for maximum productivity (Irinkov, 1971).

The output parameters of the crushing process are:
- the productivity of the jaw crusher in terms of crushed product - q;
- the active power of the crusher's electric drive - P;
- the particle size distribution of the crushed product C_{x2}.

The managed parameters are the ore level in the feed opening and the active power. They are changed through the control parameters: the change of the quantity of feed ore Q, g, the width of the discharge opening - b, mm, and the jaw movement frequency n, s^{-1} (Radulov et al., 2009).

Consequently, the control criteria can be defined according to the power, according to the ore level in the feed opening, as well as according to the particle size distribution. Since a laboratory crusher with a small feed opening is considered, the second criterion hasn't been accepted. The appropriate criteria are the pproductivity and the low energy consumption.

As a criterion, productivity is obtained after measuring the crushing time of a certain quantity of weighed material. Based on performance, the energy consumption $E, kWh/t$ can be calculated as the ratio of the measured crush engine power to the crusher productivity per finished product per unit of time. In this case, for the object under examination, the energy consumption is considered to be the appropriate target function. The energy consumption E is calculated using the formula:

$$E = \frac{P}{Q.t}, \text{kWh/t} \tag{1}$$

where:
- E is the power consumed by the crusher's engine;
- Q is the productivity of the crushed product.

For the laboratory crusher tested, there are no energy consumption characteristics specified in relation to the change in the particle size distribution and to the variation in the width of the discharge port. This is the object of the present study.

Experiment Description

The choice of factors in accordance with which the specific energy consumption will be determined is subject to the following requirements:
• each factor must have a certain limit of change i.e. be controllable;

• each factor must be manageable, i.e. to determine the levels in the definition area;
• the parameters of each factor must be measured with accuracy;
• the parameters must be independent i.e. not to be functionally linked;
• the parameters must be compatible so that the joint relationships could be defined.

The following possible parameters have been identified as the managing factors in the study:

1. D, mm - Average diameter of the fragments entering the crusher. This size is average for the respective fraction class of the selected and pre-sieved material. The experiments were performed with materials of the sizes shown in Table 1. They are consistent with the width of the feed opening of the laboratory crusher.

Table 1
The average diameter of the Fraction class

Fraction class	D	Fraction class	D
+45-55	50	+35-45	40
Fraction class	D	Fraction class	D
+25-35	30	+15-25	20

2. b, mm - Width of the discharge port of the crusher. This parameter has also been selected in accordance with the dimensions and capabilities of the laboratory machine. The width of the discharge port has the following values: 6, 8, 12, 16, and 20 mm.

The relative energy consumption as a target function is obtained as the ratio of the average crusher engine power measured by means of the measuring and recording device to the performance per unit of time - $E, Ws/g$. The three-phase digital multi-function AC powermeter of SATEC PM130EH is used as a measuring instrument.

A parameter such as the angular rotation speed of the eccentric shaft cannot be changed, so it does not participate as a control factor.

Due to the uniqueness requirement, the interconnected factors are eliminated, e.g. the crusher's degree of crushing which is related to the average diameter of the fragments entering the crusher and the width of the discharge port (Ackermann et al., 1982).

When determining the energy consumption, the disturbing effects that affect the performance and the size of the crushed product are as follows: the particle size distribution of the ore; the ore hardness; the uneven material feed. To neutralise the influence of the above disturbing factors, material of the same hardness was examined and parameter measurements were made under the conditions of continuous feed of material.

The following parameters were measured during the experiment:

- D, mm the average diameter of the pieces entering the crusher;
- b, mm - the discharge port width of the crusher;
- M_{CYM}, g - the weight of the crushed material;
- P_1, W - the average power of one phase of the engine;
- -t, s - the time taken to crush the sample.

Results

To determine the energy consumption, a mathematical model needs to be created that will take into account the real statistical properties of the dependencies in the object. Since there is a change in a number of factors, such as the power, the engine load, and the different shape of the crushed product, it is appropriate to make a non-deterministic rather than a statistical model (Bozhanov, 1971). The first step of the modeling is converting the results obtained through the experimental measurements with a laboratory crusher into a Fischer matrix. The matrix is visualised in Table 2.

Table 2
Fischer matrix

	X_1	X_2	Y_2
№	D, mm	b, mm	E,Ws/g
1	50	20	0.006
2	50	16	0.009
3	50	12	0.011
4	50	8	0.01
5	50	6	0.020
6	40	20	0.006
7	40	16	0.008
8	40	12	0.010
9	40	8	0.014
10	40	6	0.015
11	30	20	0.006
12	30	16	0.007
13	30	12	0.008
14	30	8	0.014
15	30	6	0.016
16	30	20	0.006
17	20	16	0.006
18	20	12	0.006
19	20	8	0.014
20	20	6	0.014
21	20	6	0.016

The processing of the data from Table 2 is performed through a statistical analysis (Bozhanov, 1979; Nalimov, 1965) by the STATGRAPHICS program which is suitable for scientific research. Energy consumption patterns have been synthesised by means of the program, and various criteria have been calculated for determining the reliability and adequacy of the model. Among those are the Student's t-criterion, the P-criterion, the F-criterion, the multiple correlation criterion, the corrected multi-correlation coefficient, and the mean absolute error.

Using these statistical means, an interval known as the confidence interval is defined in which the highly probable true value of the parameter evaluated is determined. The P-criterion gives us the confidence probability and it must be less than 0.05.

In addition to the confidence interval, the significance of each factor is checked. The significance of the coefficients is determined according to the Student's t-criterion for certain degrees of freedom, which, in this case, must be more than 8.

The F-criterion shows the influence of the controllable (managed) factors on the output parameter. Its value is aimed to be high, i.e. the energy consumption is manageable.

The Multiple Correlation Criterion and the Multiple Correlation Factor provide information on the extent of the relationship between the output parameter and the functions included in the model, as well as on the adequacy of the resulting model.

Various models have been obtained from the statistical surveys, most of which have a low multiple correlation factor R^2 (for example, 85.38% for the M3 model, or 41.5% for the M7 model) and an adjusted multiple correlation factor $R^2_{(adj)}$ (for example, 83.75% for M3 or 38.45% for M7).

The value of the confidence probability indicator (P-criterion = 0 or P = 0.0016) for the cited models is below the critical, i.e. these models are assumed as inadequate. The basic values of the parameters of all models are given in Table 3. Based on the values in the table, it can be determined that the M6 model has the best parameter and it is the only adequate one for the selected control function of energy consumption.

Table 3
Values of model parameters

model	R^2, %	$R^2_{(adj)}$, %	P-criterion	F-criterion
M 1	85.64	84.04	0.0302	46.96
M 2	82.86	81.96	0.0807	45.96
M 3	41.5	38.45	0.0016	13.48
M 4	47,66	47,66	0.0004	18,22
M 5	68.91	67.28	0.0027	42.13
M 6	92.92	92.92	0.0000	262.46
M 7	85.38	83.75	0.0000	52.56
M 8	93.01	92.85	0.6081	126.59
M 9	88.66	87.40	0.0029	70.42
M 10	93.72	93.39	0.1344	141.93

Table 4
M6 model parameters

Parameters	Value	Standard error	T-statistics of Student		P criterion
$\frac{D}{b}$	0.00283042	$1.747*10^{-4}$	16.2005		0.0000
	Amount of squares of the model	Degrees of freedom	Average on squares of the model	F criterion	Significance of F
Model	$2.554*10^{-3}$	1	0.00255424	262.46	0.0000
residue	$1.946*10^{-4}$	20	$9.7321 0^{-6}$		
Total	0.00274888	21			
Multiple correlation coefficient					92.9193%
Corrected Multiple Correlation Factor					92.9193%
Standard error					0.00311962
Average Absolute Error					0.00230522
Stats Darban- Otsan					0.654328

Among the examined models, M 7 and M 8 have excellent parameters of the correlation coefficients, but in model M 8 the value of the confidence probability index (P-criterion = 0.6081) for the model is above the critical, i.e. it can be assumed that the model is inadequate for the selected target function.

Analysing the parameters of this model, it can be seen that the multi-correlation coefficient R^2 is 92.92% and the adjusted multi-correlation coefficient $R^2_{(adj)}$ is over 92.92%. The value of the confidence probability index (P-criterion = 0.0000) for the model is below the critical one, i.e. it can be assumed that the model is adequate.

Of all obtained models, the best-performing is the M 6 model (Table 4) and it can be considered as a model of great adequacy. This model has the best performance indicators among all others.

Then we choose the equation of the model with natural variables to be as follows:

$$E = 2,83 10^{-3}\frac{D}{b}, KWh/t \tag{2}$$

Table 5 shows the basic parameters along with the obtained values for each examined model.

Table 5
Basic parameters of model study

MODEL №	D	b	D.b	constant	$\dfrac{D}{b}$
1.	$8.2937*10^{-5}$	$-7.69796*10^{-4}$	-	0.0170376	-
2.	$-3.8988*10^{-4}$	$-3.39282*10^{-4}$	-	-	-
3.	-	-	$1.1457*10^{-5}$	0.0155199	-
4.	-	-	$1,6125*10^{-5}$	-	-
5.	-	-	-	0.00399301	$-1.1457*10^{-5}$
6.	-	-	-	-	$2.83042*10^{-3}$
7.	$-7.69796*10^{-4}$	-	-	0.00847669	$1.84803*10^{-4}$
8.	$2.437*10^{-4}$	-	-	-	$2.622*10^{-3}$
9.	-	$-5.193*10^{-4}$	-	$3.413*10^{-3}$	$8.959*10^{-4}$
10.	-	$1.063*10^{-4}$	-	-	$2.587*10^{-3}$

Conclusions

The results obtained from the measurements and the statistical analysis of the relative energy consumption of the crusher show the following:
- the relative energy consumption is influenced to a large extent by two parameters, namely the size of the incoming pieces and the width of the discharge port of the crusher;
- when increasing the size of the input fragments, the relative energy consumption of the machine is increased, which is most probably due to the fact that the larger of size of the material increases the degree of crushing, which in turn increases the power required for the material to be crushed;

- increasing the width of the discharge port of the crusher reduces the relative energy consumption which is due to the fact that a larger-sized material at the discharge port of the machine means a low rate of crushing and a higher productivity that is the denominator of the energy consumption.

The aim of a future study of the team is to determine the effect of the swing frequency of the pendulum jaw on the energy consumption. For this purpose, an induction motor needs to be driven by an inverter. When adjusting the swing frequency of the jaw by means of a frequency inverter, it distorts the sine curve of the supply current. This state is described as the "presence of harmonics". Thus, in productivity management by means of the motion frequency of the jaw, it is likely to have harmonic constituents in excess of the standard allowances.

References

Акерман, Ю., Г. Букаты, В. Олевский и др. Справочник по обогащению руд, М., Недра, 1982. (Ackerman, Yu, G. Bukaty, V. Olevskyi et al., Spravochnik po obogashteniyu rud, Moskva, Nedra, 1982.)

Божанов, Емил С., Иван Н. Вучков. Статистически решения в производството и научните изследвания, С., Техника, 1979. (Bozhanov, Emil S., Ivan N. Vuchkov. Statisticheski reshenia v proizvodstvoto i nauchnite izsledvania, Sofia, Technika, 1979.)

Иринков, Ст. Автоматизация на процесите в мините и обогатителните фабрики, ДИ Техника, 1971. (Irinkov, S. Avtomatizatsia na protsesite v minite i obogatitelnite fabriki, DI Technika, 1971.)

Налимов, В. В., И. А. Чернова, Статистические методы планирования экспериментов, М., Наука, 1965. (Nalimov, V. V., I. A. Chernova. Statisticheskie metodai planirovaniya eksperimentov, Moskva, Nauka, 1965.)

Радулов, Г., Д. Парашкевова. Автоматизация на производството в минните предприятия, МГУМ, С., 2009. (Radulov, G., D. Parashkevova. Avtomatizatsia na proizvodstvoto na minnite predpriatia, MGUM, Sofia, 2009.)

COMPARISON OF THE METHODOLOGIES FOR DETERMINING THE CROSS SECTION OF THE MATERIAL ON A MOVING CONVEYOR BELT

Hristo Sheiretov

University of Mining and Geology "St.Ivan Rilski" Sofia, sheiretov@abv.bg

ABSTRACT. Three methodologies for determining the cross section of the transported material are discussed: the first one - based on the DIN German standard for the calculation of belt conveyors used by the Dunlop company; the second one - based on the ISO and CEMA American standards for calculation used by the Sandvik company; and the third one - based on the GOST Russian standard. The second methodology assumes that the form of the material is a segment of a circle, whereas the first and the third methodologies consider the form as an isosceles triangle. Calculations are accomplished with the three methodologies for a concrete solved example - a belt conveyor with three roll idlers with assigned length of the rollers, angle of inclination of the side rollers, and type of the transported material. In the calculations, the recommended values of the material surcharge angle are taken for the corresponding methodology.

The following conclusions are drawn: 1. When the recommended values of the material surcharge angle are used for the area of the material cross section, approximately equal values are received by the three methodologies; 2. In order to obtain an equal cross section area of the transported material, the value of the surcharge angle in the first and the third methodologies must be taken smaller than that in the second methodology.

Keywords: cross section of the material, surcharge angle, methodology

СРАВНЯВАНЕ НА МЕТОДИКИТЕ ЗА ОПРЕДЕЛЯНЕ НА СЕЧЕНИЕТО НА МАТЕРИАЛА ВЪРХУ ДВИЖЕЩА СЕ ТРАНСПОРТНА ЛЕНТА

Христо Шейретов
Минно-геоложки университет „Св.Иван Рилски", 1700 София, sheiretov@abv.bg

РЕЗЮМЕ. Разгледани са три методики за определяне на сечението на транспортирания материал: първата - по немския стандарт за изчисляване на лентови транспортьори DIN, използвана от фирма Dunlop; втората - по американските стандарти за изчисляване ISO и CEMA, използвана от фирма Sandvik; и третата - по руския стандарт за изчисляване ГОСТ. При втората методика се приема, че формата на материала е сегмент от окръжност, а при първата и третата методика – формата е равнобедрен триъгълник. Направени са изчисления по трите методики за конкретно решаван пример - транспортьор с триролкови опори със зададени дължина на ролките, ъгъл на наклон на страничните ролки и вид на транспортирания материал. При изчисленията са взети препоръчителните за съответните методики стойности на ъгъла на откоса на материала при движение.

Направени са следните изводи: 1. При използване на препоръчителните стойности на ъгъла на откоса на материала при движение за площта на сечението се получават приблизително еднакви стойности по трите методики; 2. За да се получи еднаква площ на сечението на транспортирания материал, трябва ъгълът на откоса на материала при движение по първата и третата методика да се приема по-малък от този по втората методика.

Ключови думи: сечение на материала, ъгъл на откос при движение, методика

Introduction

On a moving conveyor belt, the cross section of the transported material can be divided into two parts: lower part with the form of an isosceles trapezium with an area S_2, and upper part with the form of a segment from a circle with an area S_1 (Fig.2). The angle θ, between the tangent to the circle in the point of intersection of the circle with the belt, and the horizontal line, is called *surcharge angle*. This angle is used for determining the area of the cross section of the material in the methodology of the American standards ISO and CEMA, which is used by the Swedish company Sandvik (HA 200 Idlers design manual, Sandvik, 2008).

The surcharge angle (dynamic angle) θ is usually with 5° to 15° smaller than the angle of repose (static angle) θ_0, but in some materials it can be by 20° smaller. It is recommended that the surcharge angle θ be chosen from Table 1.

Table 1.
Surcharge angle of the material

Angle of repose of the material θ_0 [º]				
0 - 19	20 - 29	30 - 34	35 - 39	40 - 50
Flow ability of the material				
Very high	High	Medium	Low	
Surcharge angle of the material θ [º]				
5	10	20	25	30

In the methodology of the German DIN 22101 standard (Phoenix conveyor belt design fundamentals, 2004), used by the Netherlands company Dunlop (Conveyor belt design and calculation, Dunlop, 2009), an *equivalent angle of surcharge β* (Fig.1) is introduced for determining the area of the cross section of the transported material. It is assumed that the area of the upper part of the cross section A_1 is equal to the area of an isosceles triangle with base angle $β$. The equivalent angle

of surcharge β is smaller than the angle of surcharge θ, used in the first methodology.

The values of the angle β for the various materials are given in tables. At medium flow ability of the material (these are the majority of the materials), the angle β is recommended to be assumed as 15°, at low flow ability - to be $\beta=20°$, and at high flow ability - to be $\beta=5°$ or 10°.

In the methodology of the Russian GOST standard (Vasiliev, 1991), it is assumed that the area of the upper part of the material's cross section A_1 (Fig.3) is equal to the area of an isosceles triangle with base angle φ (this is the angle of surcharge of the material). The area of the lower part of the cross section A_2 which is an isosceles trapezium is equal to the area of an isosceles triangle with base angle α'. For determining the area of the whole cross section, empirical coefficients are introduced.

The aim of the present study is the calculation of the area of the cross section using the three methodologies and the comparison of the results. A concrete example is solved - a belt conveyor with three roll idlers with a given length of the rollers, an angle of inclination of the side rollers, and the type of the transported material. In the calculations, the recommended values of the angle of surcharge for the corresponding methodology are taken.

Another aim of the study is to determine the ratio of the angles of surcharge of the material which must be accepted in the calculations in the different methodologies.

Determining the area of the cross section of the transported material in the different methodologies

Determining the area of the cross section in the methodology of the DIN 22101 standard

The area of the cross section of the material A is a sum of the areas of the cross sections A_1 and A_2 (Conveyor belt design and calculation, Dunlop, 2009) (Fig.1):
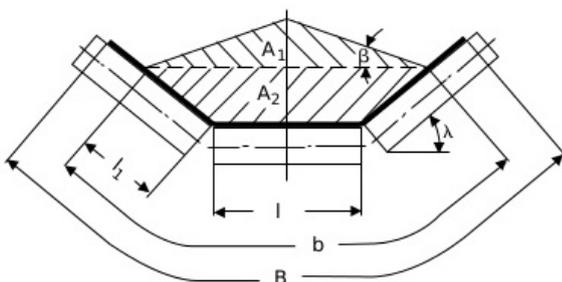

Fig.1. Scheme for determining the area of the cross section of the transported material according to DIN 22101

$$A = A_1 + A_2 \tag{1}$$

The area of the section A_1 which is an isosceles triangle is equal to:

$$A_1 = \frac{x.h_1}{2} = \frac{x}{2}.\frac{x}{2}.tg\beta = 0,25.tg\beta.x^2, \tag{2}$$

where β is an equivalent angle of surcharge of the material.

The length of the base of the triangle x is equal to:

$$x = l + 2.\left(\frac{b-l}{2}.\cos\lambda\right) = l + (b-l).\cos\lambda, \text{ m}, \tag{3}$$

where:
l is the length if the rollers;
b is the working width of the belt;
λ is the angle of inclination of the side rollers.

When substituting equation (3) in equation (2), it is received:

$$A_1 = 0,25.tg\beta.\left[l + (b-l).\cos\lambda\right]^2 \tag{4}$$

The area of the section A_2 which is an isosceles trapezium is equal to:

$$A_2 = \frac{x+l}{2}.h_2 = \frac{x+l}{2}.l_1.\sin\lambda \tag{5}$$

After substitution of equation (3) in equation (5), it is received:

$$A_2 = \frac{l + 2.\left(\frac{b-l}{2}.\cos\lambda\right) + l}{2}.l_1.\sin\lambda =$$

$$= \frac{l + 2.(l_1.\cos\lambda) + l}{2}.l_1.\sin\lambda = l_1.\sin\lambda(l + l_1.\cos\lambda), \tag{6}$$

where l_1 is the working length of the side rollers and is determined by equation (7):

$$l_1 = \frac{b-l}{2} \tag{7}$$

For the working length of the belt, it is assumed:

$$b = 0,9.B - 0,05 \text{ , m ,} \tag{8}$$

where B [m] is the width of the belt.

The length of the rollers for three roll idlers is assumed from Table 2.

Table 2.
Recommended length of the rollers l [mm]

Width of the belt B [mm]	500	650	800	1000
Three roll idlers l [mm]	200	250	315	380

1200	1400	1600	1800	2000	2200	2400
465	530	600	670	750	800	900

When $\beta=15°$ (the recommended value when a composite of sand and gravel is transported), $\lambda=30°$, and $B=1.2$m, it is received: $l=0.465$m (from Table 2); $b=1.03$m (from equation (8)); $A_1=0.061$m^2 (from equation (4)); $l_1=0.2825$m (from equation (7)); $A_2=0.1$m^2 (from equation (6)); and $A=0.161$m^2 (from equation (1)).

In Table 3 (Conveyor belt design and calculation, Dunlop, 2009), the volume capacities of the conveyors Q_v [m^3/h] are given at belt velocity $v=1$m/s, according to the methodology of the DIN 22101 standard used by the company Dunlop.

Table 3.
Volume capacities of the conveyor Q_v [m³/h] for three roll idlers at belt velocity v=1m/s according to DIN 22101

B [mm]	β [°]	20	30	35	40	45
				Q_v [m³/h] at λ [°]		
400	0	21	30	34	-	-
	10	35	43	47	-	-
	15	42	50	53	-	-
	20	50	57	60	-	-
500	0	36	51	58	-	-
	10	59	73	79	-	-
	15	72	84	90	-	-
	20	85	97	102	-	-
650	0	67	95	108	118	127
	10	109	134	145	153	159
	15	131	155	165	176	176
	20	155	176	184	190	193
800	0	105	149	168	185	198
	10	171	210	227	240	249
	15	206	243	257	268	276
	20	243	276	289	299	303
1000	0	173	246	278	304	326
	10	280	344	370	391	407
	15	336	396	419	436	448
	20	394	449	469	484	492
1200	0	253	360	406	445	477
	10	411	505	543	573	596
	15	493	**580**	614	640	658
	20	578	659	688	709	722
1400	0	355	504	567	622	666
	10	572	703	755	797	828
	15	685	806	852	888	912
	20	803	915	954	964	1001
1600	0	472	669	753	825	883
	10	758	931	1000	1055	1096
	15	906	1067	1128	1175	1207
	20	1062	1209	1263	1301	1323
1800	0	605	858	965	1057	1131
	10	969	1194	1279	1350	1402
	15	1159	1364	1443	1502	1543
	20	1357	1546	1614	1662	1690
2000	0	750	1064	1197	1311	1404
	10	1204	1478	1588	1675	1741
	15	1439	1694	1791	1865	1916
	20	1685	1919	2003	2064	2099
2200	0	948	1343	1509	1650	1765
	10	1509	1855	1990	2099	2178
	15	1801	2121	2241	2332	2393
	20	2107	2399	2503	2576	2618

B - width of the belt,
β [°] - angle of surcharge of the material,
Q_v [m³/h] - volume capacity,
λ [°] - angle of inclination of the side rollers.

The area of the cross section of the transported material is received by the formula:

$$A = \frac{Q_v}{3600}, \text{m}^2 \tag{9}$$

For the concrete example, when β=15°, λ=30° and B=1.2m, from Table 3 it is checked that Q_v=580m³/h and for the area of the cross section from formula (9), it is received A=0.161m². Consequently, for the areas of the cross section determined by formula (1) and Table 3, equal values are received.

Determining the area of the cross section in the methodology of the ISO (CEMA) standard

The area of the cross section of the material S is a sum of the areas of the cross sections S_1 и S_2 (Hrabovsky, 2011) (Fig.2):
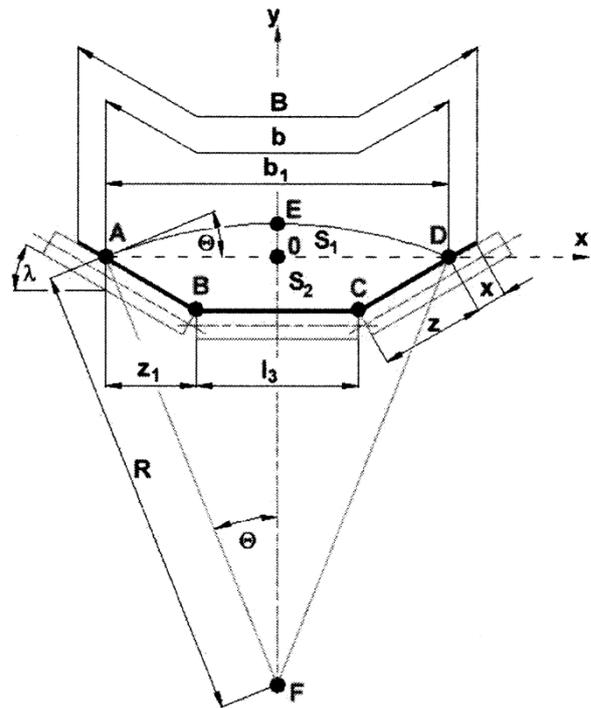
Fig. 2. Scheme for determining the area of the cross section of the transported material according to ISO (CEMA)

$$S = S_1 + S_2 \tag{10}$$

The area of the section S_1 which is the segment *AED* is the substitution of the area of the sector *FAEDF* and the areas of the triangles *FA0* and *FD0*.

$$S_1 = S_{AED} = S_{FAEDF} - S_{FAO} - S_{FDO} \tag{11}$$

The area of the sector *FAEDF* is:

$$S_{FAEDF} = \pi.R^2.\frac{2.\theta}{2.\pi} = R^2.\theta, \tag{12}$$

where:
R is the radius of the arc *AED*;
θ [rad] is half of the central angle of the arc *AED*.

After the substitution of the angle θ in [°], formula (12) is transformed to:

$$S_{FAEDF} = \frac{\pi.\theta}{180}.R^2 \qquad (13)$$

The areas of the triangles *FA0 и FD0* are equal to:

$$S_{FAO} = S_{FDO} = \frac{1}{2}.R.\sin\theta.R.\cos\theta = \frac{1}{2}.R^2.\sin\theta.\cos\theta \qquad (14)$$

After substituting equations (13) and (14) in equation (11), it is received:

$$S_1 = \frac{\pi.\theta}{180}.R^2 - 2.\frac{1}{2}.R^2.\sin\theta.\cos\theta =$$
$$= \frac{1}{2}.R^2.\left(\frac{2.\pi.\theta}{180} - \sin 2\theta \right) \qquad (15)$$

The radius of the arc *AED* is equal to:

$$R = \frac{z.\cos\lambda + \frac{l_3}{2}}{\sin\theta} = \frac{2.z.\cos\lambda + l_3}{2.\sin\theta}, \qquad (16)$$

where:
z is the working width of the side rollers;
l_3 is the length of the rollers.

After the substitution of equation (16) in equation (15), the area of the cross section S_1 is finally obtained:

$$S_1 = \frac{1}{2}.\left(\frac{2.z.\cos\lambda + l_3}{2.\sin\theta} \right).\left(\frac{2.\pi.\theta}{180} - \sin 2\theta \right), \qquad (17)$$

where:

$$z = \frac{b - l_3}{2} \qquad (18)$$

The working width of the belt b is determined by formula (8).

The area of the section S_2 is determined by a formula analogous to formula (6):

$$S_2 = z.\sin\lambda.\left(l_3 + z.\cos\lambda \right) \qquad (19)$$

When $\theta = 25°$ (the recommended value when a composite of sand and gravel is transported, or it is accepted from Table 1 at $\theta_0 = 38°$), $\lambda = 30°$, and $B = 1.2$m, it is received: $l_3 = 0.465$m (from Table.2); $b = 1.03$m (from formula (8)); $z = 0.2825$m (from formula (18)); $S_1 = 0.069$m² (from formula (17)); $S_2 = 0.1$m² (from formula (19)); $S = 0.169$m² (from formula (10)).

In Table 4 (HA 200 Idlers design manual, Sandvik, 2008), the areas of the cross section of the transported material are given according to the methodology of the ISO (CEMA) standard, used by the company Sandvik. For the concrete example, when $\theta = 15°$, $\lambda = 30°$, and $B = 1.2$m, it is checked that $S = 0.169$m². Consequently, equal values are received for the areas of the cross section determined by formula (10) and Table 4.

In order to receive equal areas of the cross section in the two examined methodologies (DIN and ISO), it must be assumed that $\beta = 16.5°$ and then $A = S = 0.169$m². Consequently, the ratio $\beta/\theta = 16.5°/25° = 0.67$.

Determining the area of the cross section in the methodology of the GOST standard

The area of the cross section of the material *F* is a sum of the areas of the sections A_1 and A_2 (Vasiliev, 1991) (Fig.3):

$$A = A_1 + A_2 \qquad (20)$$

Table 4.
Area of the cross section of the transported material for three roll idlers S [m²] according to ISO (CEMA)

λ [°]	B [mm]	θ [°]				
		10	15	20	**25**	30
20	500	0.015	0.017	0.020	0.022	0.026
	650	0.027	0.031	0.035	0.039	0.047
	800	0.042	0.049	0.055	0.062	0.078
	1000	0.068	0.078	0.088	0.099	0.133
	1200	0.100	0.115	0.130	0.145	0.206
30	650	0.035	0.038	0.042	0.046	0.052
	800	0.054	0.060	0.066	0.072	0.081
	1000	0.087	0.096	0.105	0.115	0.144
	1200	0.128	0.141	0.155	0.169	0.208
	1400	0.176	0.94	0.213	0.232	0.289
	1600	0.232	0.256	0.281	0.306	0.383
	1800	0.296	0.327	0.358	0.390	0.489
	2000	0.368	0.406	0.445	0.485	0.544
35	800	0.059	0.064	0.070	0.075	0.083
	1000	0.095	0.103	0.112	0.121	0.135
	1200	0.139	0.151	0.164	0.177	0.197
	1400	0.191	0.209	0.226	0.245	0.272
	1600	0.252	0.275	0.298	0.322	0.358
	1800	0.322	0.351	0.380	0.411	0.456
	2000	0.400	0.436	0.472	0.510	0.566
45	800	0.066	0.071	0.075	0.080	0.088
	1000	0.106	0.113	0.121	0.129	0.142
	1200	0.155	0.166	0.177	0.189	0.207
	1400	0.214	0.229	0.244	0.260	0.285
	1600	0.282	0.302	0.322	0.343	0.376
	1800	0.360	0.385	0.410	0.437	0.479
	2000	0.447	0.478	0.510	0.542	0.594
	2250	0.543	0.581	0.620	0.659	0.670
	2500	0.705	0.754	0.804	0.856	0.883
	3000	1.023	1.094	1.166	1.240	1.262

B - width of the belt,
θ [°] - angle of surcharge of the material,
λ [°] - angle of inclination of the side rollers.

The area of the section A_1 which is isosceles triangle is equal to:

$$A_1 = \frac{b^2}{4}.tg\varphi = b^2.\frac{tg\varphi}{4}, \qquad (21)$$

where:

b is determined by formula (8),
*φ* is the angle of surcharge of the material.
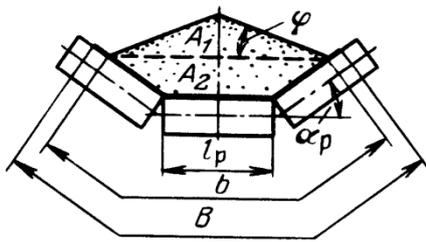
Fig. 3. Scheme for determining the area of the cross section of the material according to GOST

The area of the section A_2 which is isosceles trapezium is assumed to be equal to the area of an isosceles triangle with base *b* and base angle *α'*. Then it is received:

$$A_2 = \frac{b^2}{4} . tg\alpha' = b^2 . \frac{tg\alpha'}{4}, \tag{22}$$

When equations (21) and (22) are substituted in equation (20), it is received:

$$A = b^2 . \left(\frac{tg\varphi}{4} + \frac{tg\alpha'}{4} \right) = b^2 . C, \tag{23}$$

The following values for the coefficient *C* are recommended for α_p=30° (Vasiliev, 1991): *C*=0.153 at *φ* =15° and *C*=0.174 at *φ* =20°. When *φ* =15°, α_p=30°, and *B*=1.2m it is received: *b*=1.03m (from formula (8)), *C*=0.153, and *A*=0.162m² (from formula (23)).

Conclusions

From the calculations using the three methodologies, the following conclusions are drawn:

1. For the area of the cross section of the transported material, close values are received for the concrete example solved: *A*=0.161m² using the DIN 22101 methodology, *S*=0.167m² using the ISO (CEMA) methodology, and *A*=0.162m² using the GOST methodology.

2. If the methodologies of DIN and GOST are used, a smaller value for the angle of surcharge of the material must be accepted, in comparison with the methodology of ISO (CEMA). For the concrete example solved, for the ratio of the angles of surcharge it is received 0.67, i.e. *β*≈0,67.*θ*. This is why, when a certain methodology is used, the surcharge angle for the given material must be taken according the recommendations and tables of this methodology.

References

Васильев, К. А. Транспортные устройства и склады. М., Недра, 1991. - 321 с. (Vasiliev, K. A. Transportnie ustroistva i skladai. Moskva, Nedra, 1991. - 321 p.)

Conveyor belt technique. Design and calculation. Dunlop, 2009, available at: https://www.slideshare.net/RicardoGarayReinoso/belt-conveyor-designdunlop (accessed 08 June 2018).

HA 200 Idlers design manual. Engineering user reference and guidelines book. Sandvik, 2008., available at: https://www.yumpu.com/en/document/view/47116184/ha200-idlers-design-manual-sandvik-mining-and-construction (accessed 08 June 2018).

Hrabovsky, L. Cross-sectional area of the belt conveyor with three-idler set., 2011, available at: http://pernerscontacts.upce.cz/22_2011/Hrabovsky.pdf (accessed 08 June 2018).

Phoenix conveyor belt design fundamentals. DIN 22101. Hamburg, 2004.

CHECKING THE STABILITY OF A TRUCK MOUNTED CRANE AND DETERMINING THE REACTION FORCES IN THE SUPPORTS

Hristo Sheiretov

University of Mining and Geology "St.Ivan Rilski" Sofia, sheiretov@abv.bg

ABSTRACT. A methodology for the calculation of the mechanism for side movement and stretching of the supports of truck mounted cranes is developed. Checks are made for the stability of a truck mounted crane with load (at maximum range) and without load (at minimum range). The paper determines the turnover and establishes moments of the gravity and wind forces upon the boom, the platform, the load, the counterweight, and the truck, as well as the inertial and centrifugal forces upon the load. Two cases are considered - at maximum and at minimum length of the boom. The reaction forces in the left and the right hydraulic supports of the crane in the four end positions of the load are determined, which are obtained at minimum and maximum angle of inclination of the boom and at maximum and minimum length of the boom.
A concrete example for the KC-45717 crane mounted on the chassis of a KamAZ truck is solved.

Keywords: hydraulic support, load stability, own stability, reaction force

ПРОВЕРКА НА УСТОЙЧИВОСТТА НА АВТОМОБИЛЕН КРАН И ОПРЕДЕЛЯНЕ НА РЕАКЦИИТЕ В ОПОРИТЕ
Христо Шейретов
Минно-геоложки университет „Св.Иван Рилски", 1700 София, sheiretov@abv.bg

РЕЗЮМЕ. Разработена е методика за изчисляване на механизма за изнасяне и разпъване на страничните опори на автокранове. В настоящата статия са направени проверки на товарната (при максимален обсег) и собствената (при минимален обсег) устойчивост на автомобилен кран. Определени са обръщащите и установяващите моменти от силите на тежестта и вятъра върху стрелата, платформата, товара, противотежестта и ходовата част на крана и от инерционната и центробежната сила върху товара. Разгледани са два случая - при максимална и при минимална дължина на стрелата. Определени са опорните реакции в левите и десните изнесени хидравлични опори при четирите крайни положения на товара, които се получават при минимален и максимален ъгъл на наклон на стрелата и при максимална и минимална дължина на стрелата.
Решен конкретен пример за кран КС-45717, монтиран на автомобилно шаси КамАЗ.

Ключови думи: хидравлична опора, товарна устойчивост, собствена устойчивост, опорна реакция

Introduction

The mobile cranes are automotive boom slewing cranes which move on railless tracks. They are used for assembly and load handling operations in the construction, industrial, and mining enterprises. The mobile cranes are mounted on standard trucks or on special truck or crawler chassis. They have great maneuverability and travelling speed and quickly change over from working- to transport position. In order to assure enough stability during operation, additional side supports are let down.

The aim of the present work is to determine the coefficients of load stability and the reaction forces in the supports at various lengths and angles of inclination of the boom. A concrete example for a truck mounted crane is solved.

As a result of the accomplished study, a methodology for the calculation of the mechanism for side shifting and stretching of the supports of mobile cranes is developed (choice of hydraulic supports and hydraulic cylinders for their side movement, time for the stretching and shifting of the supports, work liquid consumption).

In order to choose hydraulic supports, it is necessary to determine the reaction forces in the supports when the crane is in work position. On the other hand, in order to determine the reaction forces, it is necessary to determine in advance the mass of the counterweight and the distance between the left and right supports.

Therefore, when the mass of the counterweight and the distance between the supports are given, checks for the crane load and own stability are performed; after that the reaction forces in the supports are determined.

Input data

The input data for the check of the crane stability and for determining the support reaction forces are (http://www.uks76.ru/upload/docs/Rukovodstvo_po_ekspluatat sii_KS-45717K-2.pdf):
- length of the boom L=9÷21 m;
- angle of inclination of the boom $β$=5÷75°;
- maximum lifting capacity of the crane at L=9 m and $β$=75° Q_1=25 t;
- lifting capacity of the crane at L=9 m and $β$=5° Q_2=6.35 t;
- lifting capacity of the crane at L=21 m and $β$=75° Q_3=6.35 t;

- lifting capacity of the crane at L=21 m and β=5° Q_4=0.9 t;
- mass of the boom m_c=1990 kg;
- mass of the slewing platform m_o=5100 kg;
- mass of the hook block $m_{p\delta}$=306 kg;
- mass of the counterweight m_n=357 kg;
- mass of the unslewing part of the crane m_H=14.27 t;
- slope angle of the ground when the supports are not shifted aside θ=0÷3° (Fig.1 and 2);
- slope angle of the ground when the supports are shifted aside θ=0÷1.5°;
- distance between the axis of the side shifted hydraulic support and the slewing axis of the crane a=2.8 m (Fig.1);
- distance between the axis of symmetry of the front wheel and the slewing axis of the platform a'=1.013 m (Fig.2);
- speed of load hoisting v=6.1 m/min;
- slewing speed of the platform n=0÷2.4 min^{-1}.

Check of the crane load stability

The crane load stability (Fig.1) is checked at maximum working radius of the crane (minimum angle of inclination of the boom β=5°) in a working position with stretched side supports and maximum permissible slope angle of the ground θ=1.5°. The turnover and stabilise moments of all forces are determined toward point B in which the right hydraulic supports contact with the ground.

Two cases are considered: at maximum boom length L=21m and lifting capacity Q=Q_4=0.9t; and at boom length L=9m and lifting capacity Q=Q_2=6.35t.

Turnover moment from the normal components of the gravity forces of the load, the hook block, and the boom (perpendicular to the ground plane)

$$M_{o\delta p1} = \left(G_m + G_{p\delta}\right).\left(l_m - a\right).\cos\theta + G_c.\left(l_c - a\right).\cos\theta \quad (1)$$

$$M_{o\delta p1} = \left(8,8 + 3\right).\left(20 - 2,8\right).\cos1,5° +$$

$$+19,5.\left(9,31 - 2,8\right).\cos1,5° = 329 \text{ kN.m}$$

where:
G_m, $G_{p\delta}$, and G_c [kN] are the gravity forces of the load, the hook block, and the boom (Fig.1) (they are determined by formulae 2÷4);
l_m and l_c [m] are the distances between the applied points of the gravity forces of the load and the boom and slewing axis of the crane (Fig.1) (they are determined by formulae 5 and 6);

$$G_m = Q_4.g = 0,9.9,81 = 8,8 \text{ kN} \quad (2)$$

$$G_{p\delta} = 0,001.m_{p\delta}g = 0,001.306.9,81 = 3 \text{ kN} \quad (3)$$

$$G_c = 0,001.m_c g = 0,001.1990.9,81 = 19,5 \text{ kN} \quad (4)$$

$$l_m = L\cos\beta - e + 0,3 = 21.\cos5° - 1,15 + 0,3 = 20 \text{ m} \quad (5)$$

$$l_c = 0,5.L\cos\beta - e = 0,5.21.\cos5° - 1,15 = 9,31 \text{ m} \quad (6)$$

where e [m] is the distance between the crane slewing axis and the boom suspension axis (Fig.1) (it is checked from the drawing of the slewing platform, e=1.15m).

Turnover moment from the tangential components of the gravity forces of the boom, the slewing platform, the unslewing part of the crane, and the counterweight (parallel to the ground plane)

$$M_{o\delta p2} = \left(G_c.h_c + G_o.h_o + G_H.h_H + G_n.h_n\right).\sin\theta \quad (7)$$

$$M_{o\delta p2} = \left(19,5.3,9 + 50.2,7 + 140.1,5 + 3,5.2,1\right).\sin1,5° = 11 \text{ kN.m},$$

where:
G_o, G_H, and G_n [kN] are the gravity forces of the slewing platform, the unslewing part of the crane, and the counterweight;
h_c, h_o, h_H, and h_n [m] are the distances between the applied points of the gravity forces of the boom, the slewing platform, the unslewing part of the crane, and the counterweight and the ground plane (Fig.1) (h_c is determined by formula (11), h_o, h_H and h_n are checked from the scheme given in Fig.1, proportionally to the boom length L=21m: h_o=2.7m; h_H=1.5m; and h_n=2.1m);

$$G_o = 0,001.m_o.g = 0,001.5100.9,81 = 50 \text{ kN} \quad (8)$$

$$G_H = m_H.g = 14,27.9,81 = 140 \text{ kN} \quad (9)$$

$$G_n = 0,001m_n.g = 0,001.357.9,81 = 3,5 \text{ kN} \quad (10)$$

$$h_c = 0,5.L.\sin\beta + h_{oc} = 0,5.21.\sin5° + 3,05 = 3,9\text{m}, \quad (11)$$

where: h_{oc} [m] - distance between the axle of suspension of the boom and the ground plane (it is checked by the scheme given on Fig.1, h_{oc}=3,05 m).

Turnover moment from the wind forces on the load, the boom and the slewing platform

$$M_{o\delta p3} = P_m.h_m + P_c.h_c + P_o.h_o \quad (12)$$

$$M_{o\delta p3} = 0,3.3,3 + 0,1.3,9 + 0,2.2,7 = 1 \text{ kN.m}$$

where:
P_m, P_c, and P_o [kN] are the wind forces on the load, the boom, and the slewing platform (Fig.1) (they are determined by formulae 13÷15);
h_m [m] is the distance between the applied point of the gravity force and the ground plane (Fig.1) (it is determined by formula 16);

$$P_m = A_m.q.k_3.c = 2,5.0,09.1,1.2 = 0,3\text{kN} \quad (13)$$

$$P_c = A_c.q.k_3.c = 0,78.0,09.1,1.4 = 0,1\text{kN} \quad (14)$$

$$P_o = A_o.q.k_3.c = 2,1.0,09.1,1.4 = 0,2 \text{ kN} \quad (15)$$

$$h_m = L\sin\beta + h_{oc} - 1,5 = 21.\sin5° + 3,05 - 1,5 = 3,3 \text{ m} \quad (16)$$

where:

A_m [m^2] is the wind-beaten area of the load (it is taken from Table1 according to the lifting capacity of the crane). At Q=0.9t A_m=2,5 m^2;

q [kPa] is the wind pressure at normal loading in work position (q=0.09 kPa);

k_3 is the filling coefficient of the crane construction (for loads and whole wall constructions k_3=1; for rod constructions k_3=0.2÷0.6). For the calculated crane k_3=1;

c is an aerodynamic coefficient (c=1.4 for the boom and the platform; c=1.2 for the load);
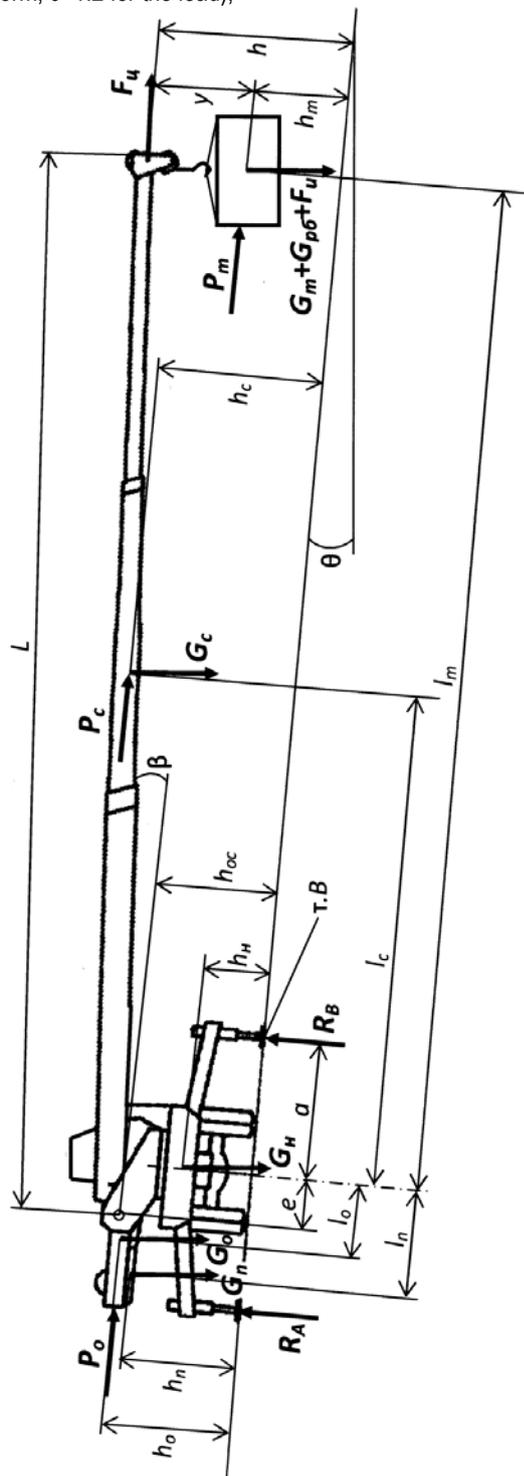
Fig.1. Scheme for determining the load stability and the reaction forces in the side supports of the crane

l_n, l_o, l_c, and l_m are the distances between the applied points of the gravity forces of the counterweight, the platform, the boom, and the load and the slewing axis;

e is the distance between the axis of boom suspension and the slewing axis;

a is the distance between the slewing axis and the side shifted support;

h_n, h_o, $h_н$, h_c, and h_m are the distances between the applies points of the gravity forces of the counterweight, the platform, the unslewing part of the crane, and the boom and the load and the ground plane;

h_{oc} is the distance between the axis of boom suspension and the ground plane;

h is the distance between the top of the boom and the ground plane;

y is the distance between the gravity center of the load and the top of the boom;

L, β are the length and the angle of inclination of the boom;

θ is the ground slope angle;

G_n, G_o, $G_н$, G_c, G_m, and $G_{pб}$ are the gravity forces of the counterweight, the platform, the unslewing part of the crane, the boom, the load, and the hook block;

P_o, P_c, and P_m are the wind forces on the platform, the boom, and the load;

F_u, F_u - centrifugal force and force of inertia on the load;

R_A, R_B - reaction forces in the side shifted supports.

A_c [m^2] is the wind-beaten area of the boom (it is determined by formula 17);

Table 1.
Wind-beaten area of the load A_m according to the lifting capacity of the crane Q

Q [t]	0.8	1	1.25	1.6	2	2.5	3.2	4
A_m [m^2]	2.5	2.8	3.2	3.6	4	5	5.6	6.3

Q [t]	5	6.3	8	10	12.5	16	20	25
A_m [m^2]	7.1	8	9	10	12	14	16	18

$$A_c = L.b_c.\sin\beta = 21.0,43.\sin 5° = 0,78 \text{ m}^2, \quad (17)$$

where b_c [m] is the width of the boom (b_c=430mm=0.43m - it is checked from the drawing of the boom).

Turnover moment from the force of inertia and the centrifugal force on the load

$$M_{oбp4} = F_u(l_m - a) + F_u.h = 0,09.(20-2,8)+11.1.4,8 = 54 \text{ kN.m}, \quad (18)$$

where:

F_u [kN] is the force of inertia from the load hoisting (Fig.1), (it is determined by formula 19);

F_u [kN] is the centrifugal force from the crane slewing (Fig.1), (it is determined by formula 20);

h [m] is the distance between the applied point of the centrifugal force and the ground plane (Fig.1) (it is determined by formula 21);

$$F_u = Q_4 \frac{V}{60.t_n} = 0,9.\frac{6,1}{60.1} = 0,09 \text{ kN} \quad (19)$$

$$F_{ц} = \frac{Q_4 . g . \omega^2 . l_m}{g - \omega^2 . y} = \frac{0,9.9,81.0,25^2.20}{9,81 - 0,25^2.2,5} = 11,1 \text{ kN} \qquad (20)$$

$$h = L.\sin\beta + h_{oc} = 21.\sin 5° + 3,05 = 4,8 \text{ m}, \qquad (21)$$

where:

t_n [s] is the starting time of the hoisting mechanism (it is assumed as the minimum permissible time, i.e. t_n=1s);

ω [rad/s] is the angular speed of the platform (it is determined by formula 22);

y [m] is the distance between the gravity center of the load and the top of the boom (Fig.1) (it is assumed y=2.5m according to the scheme in Fig.1).

$$\omega = \frac{\pi.n}{30} = \frac{3,14.2,4}{30} = 0,25 \text{ rad/s} \qquad (22)$$

Total turnover moment

$$M_{об p} = M_{об p1} + M_{об p2} + M_{об p3} + M_{об p4} = 329 + 11 + 1 + 54 = 395 \text{kN.m} \qquad (23)$$

Stabilise moment from the gravity forces of the counterweight, the slewing platform, and the unslewing part of the crane

$$M_{ycm} = G_n(l_n + a).\cos\theta + G_o.(l_o + a).\cos\theta + G_H.a.\cos\theta$$
$$M_{ycm} = 3,5(2,2 + 2,8).\cos 1,5° + 50.(1,3 + 2,8).\cos 1,5° +$$
$$+140.2,8.\cos 1,5° = 614 \text{ kN.m}, \qquad (24)$$

where:

l_n [m] is the distance between the gravity center of the counterweight and the slewing axis of the crane (Fig.1) (it is assumed from the drawing of the platform, l_n=2.2m);

l_o [m] is the distance between the gravity center of the platform and the slewing axis (Fig.1) (it is assumed from the drawing of the crane, l_o=1.3m).

Check of the coefficient of load stability

$$k_{my} = \frac{M_{ycm}}{M_{об p}} = \frac{614}{395} = 1,55 \geq 1,15 \qquad (25)$$

For the second case of loading at L=9m, β=5°, Q=Q_2=6.35t and A_m=8m², it is received: $M_{об p1}$=356kN.m; $M_{об p2}$=10kN.m; $M_{об p3}$=2kN.m; $M_{об p4}$=124kN.m; $M_{об p}$=492kN.m; M_{ycm}=606kN.m; k_{my}=1.23. Consequently, the condition (25) is also satisfied.

Check of the crane own stability

The crane own stability (Fig.2) is checked at minimum working radius of the crane (minimum boom length L=9m and maximum angle of inclination of the boom β=75°), load free position with unstretched side support, maximum permissible slope angle of the ground θ=3°, and wind pressure q=0.7kN/m² (the wind pressure is assumed for maximum loading in load free position). The turnover and stabilise moments of all forces are determined toward point A in which the left front wheel of the truck contacts with the ground.

Turnover moment from the normal components of the gravity forces of the slewing platform and the counterweight (perpendicular to the ground plane)

$$M'_{об p1} = G_o.(l_o - a').\cos\theta + G_n.(l_n - a').\cos\theta \qquad (26)$$

$$M'_{об p1} = 50.(1,3 - 1,013).\cos 3° + 3,5(2,2 - 1,013).\cos 3° = 18 \text{KN.m}$$

Turnover moment from the tangential components of the gravity forces of the boom, the slewing platform, the unslewing part of the crane and the counterweight (parallel to the ground plane)

$$M'_{об p2} = (G_c.h_c + G_o.h_o + G_H.h_H + G_n.h_n).\sin\theta \qquad (27)$$

$$M'_{об p2} = (19,5.7,3 + 50.2,7 + 140.1,5 + 3,2.1).\sin 3° = 25 \text{KN.m},$$

where:

$$h_c = 0,5.L.\sin\beta + h_{oc} = 0,5.9.\sin 75° + 3,05 = 7,3 \text{ m}, \qquad (28)$$

Turnover moment from the wind forces on the boom 28and the slewing platform

$$M'_{об p3} = P_c.h_c + P_o.h_o = 3,7.7,3 + 2.2,7 = 32 \text{ kN.m} \qquad (29)$$

where:

$$P_c = A_c.q.k_3.c = 3,73.0,7.1.1,4 = 3,7 \text{ kN} \qquad (30)$$

$$P_o = A_o.q.k_3.c = 2,1.0,7.1.1,4 = 2 \text{ kN} \qquad (31)$$

$$A_c = L.b_c.\sin\beta = 9.0,43.\sin 75° = 3,73 \text{ m}^2 \qquad (32)$$

Total turnover moment

$$M'_{об p} = M'_{об p1} + M'_{об p2} + M'_{об p3} = 18 + 25 + 32 = 75 \text{ kN.m} \qquad (33)$$

Stabilise moment from the gravity forces of the boom and the unslewing part of the crane

$$M'_{ycm} = G_c.(l_c + a').\cos\theta + G_H.a'.\cos\theta \qquad (34)$$

$$M'_{ycm} = 19,5.(0,01 + 1,013).\cos 3° + 140.1.0,13.\cos 3° = 161 \text{ kN.m}$$

where:

$$l_c = 0,5.L.\cos\beta - e = 0,5.9.\cos 75° - 1,15 = 0,015 \text{ m} \qquad (35)$$

Check of the coefficient of own stability

$$k_{cy} = \frac{M'_{ycm}}{M'_{об p}} = \frac{161}{67} = 2,14 \geq 1,15 \qquad (36)$$

Reaction forces in the side shifted hydraulic supports

Reaction forces in the left hydraulic supports
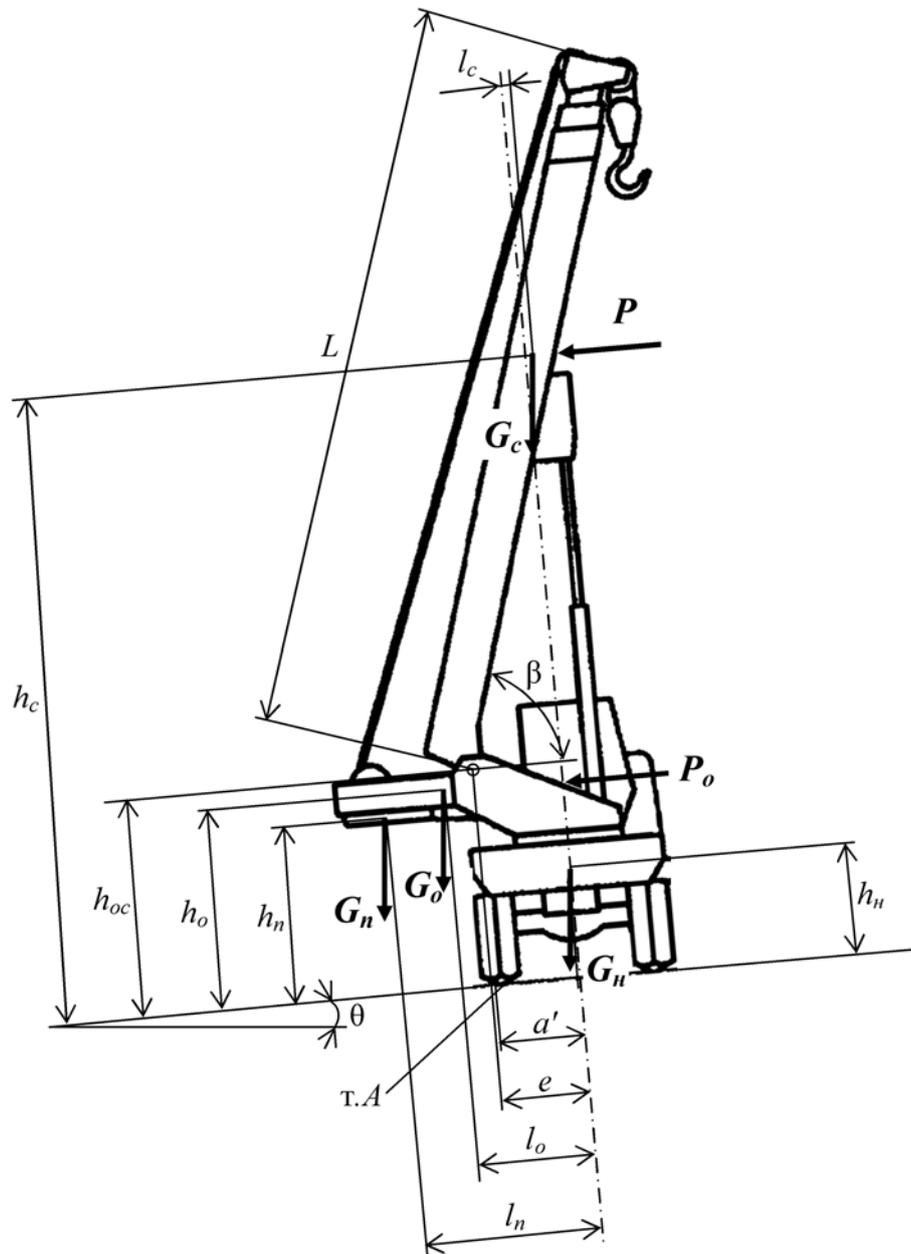
Fig. 2. Scheme for determining the own stability of the crane

h_n, h_o, $h_н$, and h_c are the distances between the applies points of the gravity forces of the counterweight, the platform, the unslewing part of the crane, and the boom and the ground plane;
h_{oc} is the distance between the axis of boom suspension and the ground plane;
l_n, l_o, and l_c are the distances between the applied points of the gravity forces of the counterweight, the platform, and the boom and the slewing axis;
e is the distance between the axis of boom suspension and the slewing axis;
a' is the distance between the axis of symmetry of the front wheel and the axis of rotation of the platform;
L and β are the length and the angle of inclination of the boom;
G_n, G_o, $G_н$, and G_c are the gravity forces of the counterweight, the platform, the unslewing part of the crane, and the boom;
P_o and P_c are the wind forces on the platform and the boom;
θ is the ground slope angle.

$$R_A = \frac{M_{уст} - M_{обр}}{4.a} = \frac{614 - 395}{4.2,8} = 19\,\text{kN} \tag{37}$$

Reaction forces in the right hydraulic supports

$$R_B = \frac{G_{кран} - 2.R_A}{2} = \frac{224 - 2.18}{2} = 93\,\text{kN}, \tag{38}$$

where $G_{кран}$ [kN] is the gravity force of the crane with the load (it is determined by formula 39);

$$G_{кран} = G_н + G_o + G_c + G_n + G_{рб} + G_m \tag{39}$$

$$G_{кран} = 140 + 50 + 19,5 + 3,5 + 3 + 8,8 = 224\ \text{kN}$$

The results from the calculation of the reaction forces R_A and R_B (Fig.1) for the forth end positions of the load are given in Table 2.

Table 2a.
Reaction forces in the side supports for the forth end positions of the load

Load position	L [m]	β [°]	Q [t]	$M_{уст}$ [kN.m]
1	9	75	25	614
2	9	5	6.35	614
3	21	75	6.35	614
4	21	5	0.9	614

Table2b.

Load position	$M_{обр}$ [kN.m]	$G_{кран}$ [kN]	R_A [kN]	R_B [kN]
1	-114	461	65	165
2	492	278	10	129
3	552	278	4	135
4	395	222	19	93

From Tables 2a and 2b, it is clear that the maximum reaction force is received in the right support *B* at load condition 1 which is R_B=165kN. The value of this reaction must be used for determining the piston diameter of the hydraulic supports.

Conclusions

1. In the calculations made for determining the coefficient of load stability of the crane for the two considered cases (maximum working radius of the crane with maximum boom length and maximum working radius with minimum boom length), it is received that, in the second case, the coefficient of load stability is smaller. But in both cases, the coefficient of load stability is greater than the minimum permissible coefficient.

2. In the calculations made for the forth end positions of the load, the maximum reaction forces are received in the right hydraulic supports (situated on the side of load lifting) at minimum boom length, maximum angle of inclination of the boom, and maximum lifting capacity.

3. For the calculated truck mounted crane, the permissible lifting capacities and the counterweight mass are chosen correctly, since as the checks of the load and own stability are satisfied.

References

Дивизиев, В. Й. Основи на товароподемните машини. С. Техника, 1986. - 386 с. (Divisiev, V. I. Osnovi na tovaropodemnite mashini. Sofia, Tehnika, 1986. - 386 p.)

Кран стреловой автомобильный КС45717К-2. Руководство по эксплуатации. (Kran strelovoi avtomobilnai КС45717К-2, Rukovodstvo po ekspluatatsii), available at: http://www.uks76.ru/upload/docs/Rukovodstvo_po_eksplua tatsii_KS-45717K-2.pdf (accessed 6 June 2018).

DETERMINING THE DIAGRAMS OF INTERNAL FORCES IN A KNIFE ON AN EXCAVATOR BUCKET

Raina Vucheva[1], Violeta Trifonova–Genova[2]

[1] University of Mining and Geology "St. Ivan Rilski", 1700 Sofia, r.wutschewa@abv.bg,

[2]University of Mining and Geology "St. Ivan Rilski", 1700 Sofia, violeta.trifonova@yahoo.com

ABSTRACT. The article examines the internal forces in a specific knife on the bucket of an excavator. The knife is modelled as a broken planar and spatial frame. The load on the teeth of the knife is asymmetric. It is located on the local axes of the sections of the frame. The case studied here is of loading that is composed of concentrated forces and moments. The former are transverse to the frame, the latter lie in its plane. The two ends of the frame are cramped. Furthermore, it is supported by four-point rods. To determine the internal forces in the undefined frame, a method of forces is used.
For a particular knife, the basic frame is selected. It consists of fifteen sections. The basic frame is then loaded both with concentrated single forces and moments applied in the places of redundancy, as well as with a load from the teeth of the knife. The torsions and the bending moments at the border points of each section are obtained. The coefficients of unknown reactions in the equations of the selected method are calculated through the energy methods of the resistance of the materials. The results obtained are only part of the developed methodology by which the internal forces in a bucket knife are determined.

Keywords: bucket knife, internal forces, spatial frame.

ОПРЕДЕЛЯНЕ НА ДИАГРАМИТЕ НА ВЪТРЕШНИ СИЛИ В НОЖ НА КОФА НА БАГЕР
Райна Вучева[1] , Виолета Трифонова – Генова[2]
[1] Минно-геоложки университет "Св. Иван Рилски", 1700 София, r.wutschewa@abv.bg,
[2] Минно-геоложки университет "Св. Иван Рилски ", 1700 София, violeta.trifonova@yahoo.com

РЕЗЮМЕ. В статията се изследват вътрешните сили в конкретен нож на кофа на багер. Ножът е моделиран като начупена равнинно-пространствена рамка. Натоварването върху зъбите на ножа е несиметрично. То е разположено върху локалните оси на участъците на рамката. Тук се разглежда случай на натоварване, състоящо се от съсредоточени сили и моменти. Първите са напречни на рамката, вторите лежат в нейната равнина. Двата края на рамката са запънати. Освен това в четири точки тя е подпряна с напречни пръти. За определяне на вътрешните сили в неопределената рамка се използва силов метод.
За конкретен нож е избрана основна система, която се състои от петнадесет участъка. Системата се натоварва последователно както със съсредоточени единични сили и моменти, приложени в местата на излишните връзки, така и с натоварване от зъбите на ножа. В граничните точки на всеки участък са получени стойностите на огъващите и усукващите моменти. С енергетичните методи на съпротивление на материалите са изчислени коефициентите пред неизвестните опорни реакции в уравненията на избрания метод. Тези резултати са само част от етапите на разработена методика, чрез която са определени вътрешните сили в ножа.

Ключови думи: нож на кофа, вътрешни сили, пространствена рамка.

Introduction

The model of a knife of the bucket of the SRS 4000 excavator is described in (Dinev et al., 2016). The dimensions of the concrete computational scheme and the load on the teeth for this model are obtained in the same article. A possible case of loading of a knife is considered in (Vucheva et al., 2017). It includes concentrated forces transverse to the plane of the frame and moments lying in its plane. The algorithm for determining the internal force at the border points of each section of the frame is described in detail. It includes the figures and analytical expressions of the internal forces. The purpose of this work is to obtain and analyse the numerical values of the internal moments at indicated points in the frame.

Methods

1. Application of the problem

The broken spatial frame is tilted at two ends (A, B_*). It is supported by four vertical rods at points K, I, A_3, and C (Fig.1). On the one hand, the load includes the forces (P_i^*) parallel to the axis and, on the other hand, the bending and torsion moments (M_{yi}, M_{xi}), which lie in the $y_* z_*$ plane. These concentrated forces and moments are applied at points A_i ($i = 1 \div 4$).
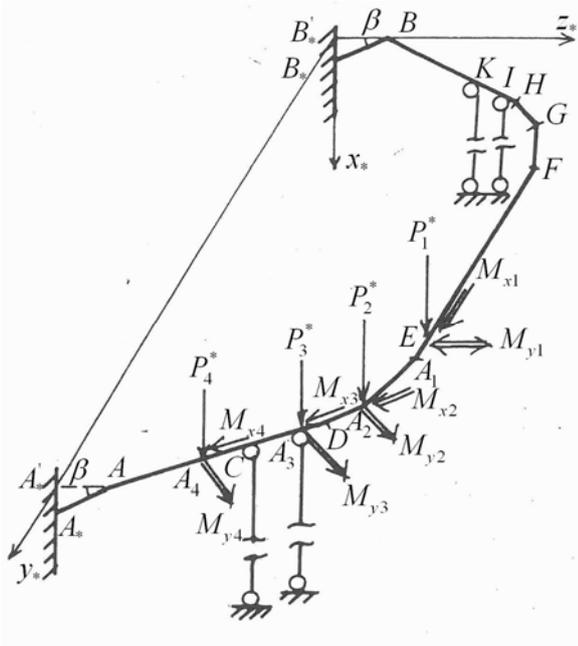
Fig. 1. Computational scheme

The frame is undetermined. For determining the reactions in the connections, a force method is used. According to it, the reactions at points B_*, K, I, A_3, and C are extracted and then the basic frame is obtained. It is tilted to point A_*. The reactions in the supports are determined by two sets of equations: for equilibrium and for deformations (Kisyov, 1978). The former equations are written for an undetermined frame. The latter set of equations has two kinds of coefficients. The first are obtained through moments as a result of the actions of the concentrated forces and the moments of magnitude one in basic frame. The other kind of coefficients is determined by using the values of moments by an external load in the same frame.

2. Diagrams of the moments
2.1. Diagrams of unit forces

The methods of the resistance of the materials are used here (Valkov, 2011; Trifonova-Genova et al., 2017). Each of the diagrams results from the consistent application of forces, equal to $1 kN$, applied at points B_*, K, I, A_3, and C of the basic frame. The moments M_y^j and M_x^j are projections of the moment M_k^j (Fig.2). The latter is equal to the distance d_k^j between point k of a given section and the applied point of force j (Valkov, 2004; Valkov et al., 2013). The angle δ_k is calculated by the slope β_k of the distance d_k^j and the slope α_i of section i by axis y_* (Vucheva et al., 2017).

The local moments in section AA_* are obtained by expressions (Fig.3):

$$M_x = M_{x'} \cos\beta; \; M_z = M_{x'} \sin\beta. \qquad (1)$$

The moment $M_{x'}$ lies in the $y_* z_*$ plane, but axis x' is parallel to z_*.
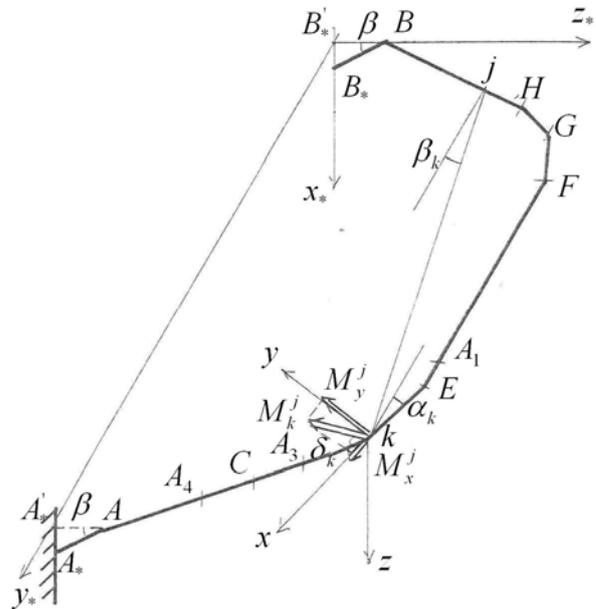

Fig. 2. Basic frame
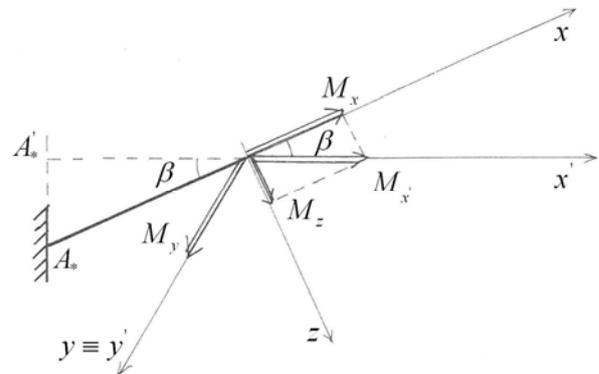
Fig. 3. Local moments in section AA_*

2.2. Diagrams of unit moments

The moments with a volume of $1 kNm$ are successfully applied to the direction of reactions $M_{B_* z_*}$ and $M_{B_* y_*}$. The local moments $M_{x,2}$, $M_{x,3}$, $M_{y,2}$, and $M_{y,3}$ are expressed by the trigonometric function of the slope α_i of each section in the chosen coordinate system.

2.3. Diagrams by external load

The basic frame is loaded by forces parallel to axis x_*, and by bending and torsion moments (Fig.4). To obtain the values of the moments, and consequently the operation of forces, the approach described in 2.1 is applied. The concentrated moments are projected to the local axis of the section. Finally, the values of the two types of moments are summed up.
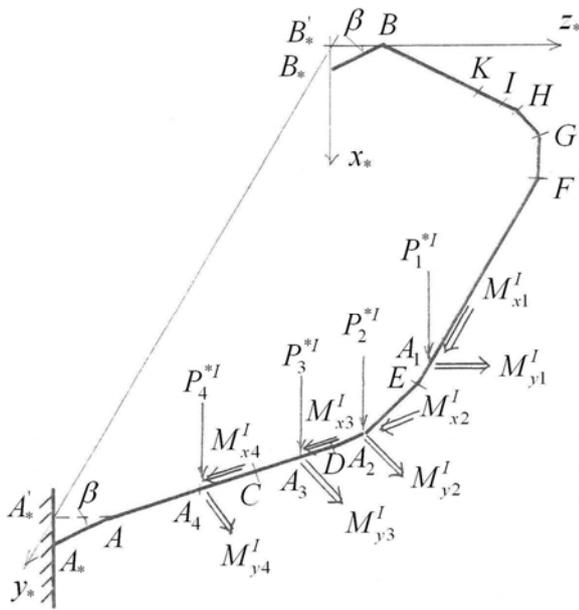
Fig. 4. External load on the basic frame

3. Numerical example

The frames in Figures 1, 2, and 4 have the dimensions taken by (Dinev et al., 2016). The load in Figure 4 can be seen in the same article.

The basic frame is loaded with three kinds of load: forces equal to $1kN$, moments equal to $1kNm$, and external load. The results of the first load are given in Tables 1, 2, and 3. These forces are loaded at points B_*, K, I, A_3, and C.

The results of the second kind of load are given in Table 4. These values correspond to the group of points which are explicated in Table 5. For Table 4, it is typical that some values are negative. These are the values of $M_{x,3}$ from point K to point F and the values of $M_{y,2}$ from point E to point A.

The third kind of load is taken from Tables 3 and 4 of the work of (Dinev et al., 2016). Thus, the values in Table 6 are obtained.

4. Key findings

The described algorithm for determining the values of the internal moments is applied to a concrete broken planar and spatial frame. It is the generalisation of a known solution for a rectangular plane-space frame (Kisyov, 1978). It can easily be adapted for other form of a frame. The values in the tables will be used to calculate the coefficients in the equations of deformation (Vucheva et al., 2017).

All values in the tables will be used for calculating coefficients δ_{ij} and Δ_{iP}. Their formulae can be seen in the work by (Vucheva et al., 2017). They are part of a system of equations whose solution is the subject of a future work.

Table 1.

Bending moments by units of force at points B_*, K, and I

point	$M_{y,1}$	$M_{y,4}$	$M_{y,5}$
B_*	0		
B	18.6		
B	17.11		
K	53.61		
K	53.63	0	
I	68.13	14.4	
I	68.34	14.4	0
H	80.31	26.5	12.0
H	74.80	25.33	11.42
G	93.84	44.43	30.58
G	64.06	33.63	24.03
F	80.40	49.98	45.57
F	41.48	35.58	37.46
A_1	121.42	107.09	101.48
A_1	121.39	107.09	101.48
E	129.13	114.84	109.20
E	90.90	94.23	93.20
A_2	107.25	110.58	109.50
A_2	20.69	52.05	58.81
D	39.80	71.17	86.90
D	1.92	29.26	50.20
A_3	2.05	41.32	51.63
A_3	2.16	44.71	54.80
C	16.6	59.14	69.22
C	14.55	57.50	67.70
A_4	29.12	72.08	82.26
A_4	34.67	75.71	85.39
A	55.57	97.61	107.58
A	18.600	33.59	46.90
A_*	0	52.20	65.50

Table 2.

Moments by units of force applied at points A_3 and C

point	$M_{x,6}$	$M_{x,7}$	$M_{y,6}$	$M_{y,7}$
A_3	0	-	0	-
C	0	-	14.1	-
C	0.17	0	14.4	0
A_4	0.17	0	29.0	14.6
A_4	0.06	0.37	29.0	14.6
A	0.58	0.58	51.0	36.5
A	18.34	13.16	46.95	33.58
A_*	18.33	13.16	65.54	52.18

Table 3.

Torsions moments by units of force at points B_*, K, and I.

point	$M_{x,1}$	$M_{x,4}$	$M_{x,5}$
B_*	0		
B	0		
B	7.28		
K	7.28		
K	5.99	0	
I	7.08	0	
I	5.43	0.35	0
H	5.43	0.35	0
H	29.75	7.78	3.67
G	29.93	7.77	3.68
G	74.82	30.05	19.27
F	74.74	30.02	17.47
F	101.66	44.57	31.27
A_1	96.81	44.59	31.29
A_1	97.45	44.59	31.30
E	96.82	44.61	31.30
E	133.36	79.37	64.95
A_2	133.32	79.34	64.95
A_2	169.85	125.76	113.01
D	169.89	125.76	106.30
D	174.48	141.51	127.79
A_3	173.88	140.46	131.42
A_3	173.88	140.46	130.13
C	173.91	140.46	130.13
C	174.09	141.14	130.93
A_4	174.08	141.16	130.89
A_4	173.27	139.27	128.40
A	173.30	139.19	128.77
A	166.66	153.4	148.30
A_*	166.61	153.46	148.29

Table 4.

Moments by units of concentrated moments at point B_*

Group of points	$M_{x,2}$	$M_{x,3}$	$M_{y,2}$	$M_{y,3}$
I	1	0	0	1
II	0.95	0.32	0.32	0.95
III	0.63	0.77	0.77	0.63
IV	0.37	0.93	0.93	0.37
V	0.39	0.91	0.91	0.39
VI	0.38	0.93	0.93	0.38
VII	0.40	0.92	0.93	0.40
VIII	0	O.92	1	0
IX	0.39	-0.92	0.92	0.39

Table 5.

Explication of Table 4

Group of points	points
I	A_1, E
II	G, F, E, A_2
III	G, H, A_2, D
IV	H, I, D, A_3
V	I, K, A_3, C
VI	C, A_4
VII	A_4, A
VIII	B, B_*, A, A_*
IX	B, K

Table 6.

Moments by external load

point	$M_x^{P,M}$	$M_y^{P,M}$	$M_z^{P,M}$
A_1	-4.13	-0.61	
E	107.60	-0.61	
E	324.88	115.35	
A_2	339.39	39.79	
A_2	459.10	374.71	
D	1 374.93	224.98	
D	1 533.06	726.06	
A_3	1 949.20	635.56	
A_3	2 119.73	706.74	
C	3 324.14	595.40	
C	3 498.67	712.04	
A_4	4 703.08	634.28	
A_4	5 009.25	651.64	
A	7 600.77	563.59	
A	6 940.19	3 359.75	1 430.27
A_*	9 230.73	3 560.33	1 511.16

Conclusion

The values of the internal moments at points on a plane-space frame are presented in this article. They are the result of two types of load. The first type of load is by forces and moments with value one. The second type is external load. These loads are applied on the basic frame.

The results will allow to calculate the coefficients of basic system of equations with the method of the forces, as well as to determine the unknown reactions.

References

Вълков, М. Съпротивление на материалите – част 1 еластостатика. Изд. къща „Св. Ив. Рилски", 2011. - 300 с. (Valkov, M., Saprotivlenie na materialite – chast 1 - elastostatika. Izd. kashta "Sv. Iv. Rilski", 2011. - 300 p.)

Вълков,М. Теоретична механика – част 1 - статика. Изд. къща „Св. Ив. Рилски", 2004. - 204 с. (Valkov, M. Teoretichna mehanika – chast 1- statika. Izd. kashta "Sv. Iv. Rilski", 2004. - 204 p.)

Вълков, М., Ст. Пулев. Ръководството за решаване на задачи по теоретична механика. Част I. Статика. С., Изд. къща „Св. Ив. Рилски", 2013. - 133 с. (Valkov, M., St. Pulev. Rakovodstvo za reshavane na zadachi po teoretichna mehanika. Chast I. Statika. Sofia, Izd. kashta "Sv. Iv. Rilski", 2013. - 133 p.)

Динев, Н., Р. Вучева, В. Трифонова-Генова. Относно численото моделиране на натоварване върху нож на кофа. Год. на МГУ „Св. Ив. Рилски", т. 59, св. III, 2016. - 38-40. (Dinev, N., R. Vucheva, V. Trifonova-Genova. Otnosno chislenoto modelirane na natovarvane varhu nozh na kofa, God. na MGU "Sv. Iv. Rilski", t. 59, sv. III, 2016. - 38–40.)

Кисьов, И. Съпротивление на материалите. С., Д. И. "Техника", 1978. - 594 с. (Kisyov, I. Saprotivlenie na materialite. Sofia, D. I. "Tehnika", 1978. - 594 p.)

Трифонова-Генова, В., М. Вълков, А. Стоянов, С. Сезонов. Съпротивление на материалите, Сборник от задачи и методични указания. Изд. къща „Св. Ив. Рилски", 2017. (Trifonova-Genova, V., M. Valkov, A. Stoyanov, S. Sezonov. Saprotivlenie na materialite, Sbornik ot zadachi i metodichni ukazania. Izd. kashta "Sv. Iv. Rilski", 2017.)

Vucheva, R., V. Trifonova-Genova, An approach for determining the internal forces in a knife bucket. Journal of Mining and Geological Sciences, t. 60, sv. III, 2017. - 34–38.

EXPERIMENTAL DETERMINATION OF A CURRENT OF GROUND CONNECTION IN THE MIDDLE VOLTAGE NETWORK IN AN OPENCAST MINE

Kiril Dzhustrov

University of Mining and Geology "St. Ivan Rilski", 1700 Sofia, justrov@mgu.bg

ABSTRACT. To determine the settings of relay protection from single-phase ground connection, an experiment was conducted in which the ground fault current was recorded on a conductor grounded on a rock mass and on soil. To determine the full current of a ground connection, the current of a metal ground connection was also recorded. The experiment was carried out in real conditions in an opencast mine and the results were compared with the theoretical ones. An assessment has been made of the possibility of setting relay protection from single-phase ground connection in opencast mines with high specific soil resistance.

Keywords: relay protection, single-phase ground connection

ЕКСПЕРИМЕНТАЛНО ОПРЕДЕЛЯНЕ НА ТОКА НА ЗЕМНО СЪЕДИНЕНИЕ В МРЕЖИТЕ ЗА СРЕДНО НАПРЕЖЕНИЕ НА ОТКРИТ РУДНИК
Кирил Джустров
Минно-геоложки университет „Св. Иван Рилски", 1700 София, justrov@mgu.bg

РЕЗЮМЕ. За определяне на настройките на релейни защити от еднофазни земни съединения е проведен експеримент, при който е регистриран токът на земно съединение при паднал на земята проводник върху скална маса и върху почва. За определяне на пълния ток на земно съединение е регистриран и токът на метално земно съединение. Експериментът е извършен в реални условия на открит рудник, като резултатите са сравнени с теоретично получените. Направена е оценка на възможността за настройване на релейни защити от еднофазни земни съединения при открити рудници с високо специфично съпротивление на почвата.

Ключови думи: релейни защити, еднофазни земни съединения

Introduction

Single-phase ground current in medium voltage grids in opencast mines are the most common failures. The reasons for this are the specifics of the operation of the electrical installations in the open mine - the supply of flexible cables for excavators and other electrical equipment, frequent transfer of the distribution line networks along with the movement of the mining operations, the influence of the environment on the condition of the cable insulation, conducting controlled blasts, etc. The consequences of the ground connections are manifested in prolonged periods of mechanisation downtime and in the development of contact and percolation stresses that are dangerous to the personnel.

Therefore, it is necessary to install relay protections against the single-phase ground current in medium voltage networks to quickly and selectively disconnect the damaged exit.

Problems with earth ground connections in the medium voltage electrical networks with an isolated neutral

In the event of ground connection, voltage and currents with zero sequence occur. The zero-sequence voltage is the same for the entire electrically connected network. Figure 1 shows the distribution of zero-sequence currents upon Earth-phase coupling of phase A from exit 1. In n, k, and m, current filters are provided with zero sequence. The filter at point n will show current $3I_{03}$ (Exit 3), the filter at point k will show current $3I_{02}$ (exit 2), and the one at point m will show current: $I_{0m}=I_{02}+I_{03}$.

Hence, follows the rule that the zero sequence current measured at the beginning of the damaged exit is equal to the sum of the zero sequence currents determined by the capacities relative to the ground of the entire network without the zero sequence current through the capacitance conduction of the damaged electrical exit.

$$I_{0m} = \sum_{1}^{n} 3I_{0n} - 3I_{0повр\,изв} \tag{1}$$

When the network has multiple branches, this rule can be used to detect the power line with the ground connection. In the branch with the ground connection, the largest zero-sequence current flows and this acts as the principle of action of the non-current current-earth protections. The zero sequence currents in the non-damaged phases (terminals) are small, determined only by the capacity of these branches relative to the ground.
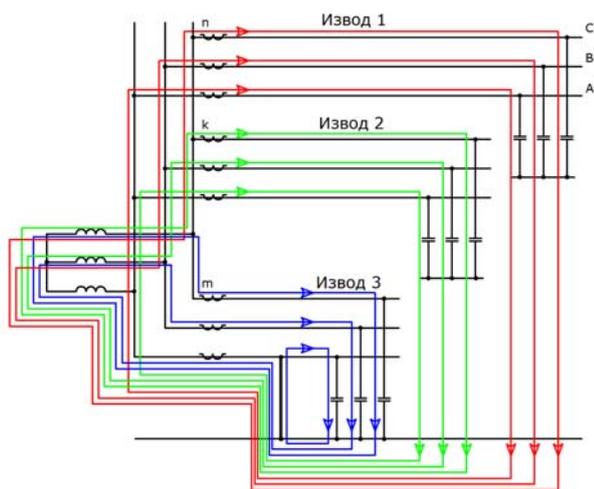
Fig. 1. Distribution of currents in a metallic ground connection

Experimental research

The occurrence of ground connections in networks with isolated star center is often followed by large values of the transient resistance at the fault site. The current of the ground connection may decrease below the cost of ground protection - it becomes ineffective. Another reason for lowering the current of the ground connection made mainly from distribution lines is that their capacity, compared to the ground, is 30 times lower than the cable line with the same length. The 6kV networks of *Asarel-Medet JSC* and the *Elatzite* Mine Complex can serve as an example.

The total length of the stationary cable network to the winding 1 of the transformer of *Asarel-Medet JSC* determines the capacitance current Ic=30.67A. The ratio of the common lines of the cable to the airline is 1.85. The air of the grid creates here a capacity current below 1A (Перпелицев и др., 2013). In the *Elatzite* Mine Complex, the ratio of the common lines of the cable to the air is 3.05. The total capacity current Ic=33.25A was determined mainly by the cable network, with only 0.18A of it being due to the air power lines (Стоилов и др., 2013)

In practice, in the normal mode of operation, not all power lines are included, and the earthing current is lower. For example, for the *Elatzite* Mine Complex, a working regime regarding the capacity earth current is considered that excludes the whole the second feeder from the CRP to KET1, KET3, GTL, and MKTP. Under these conditions, the minimum capacity current Ic is:
min Σ Ic = 22,07 A.

It should be noted that the above mentioned currents are in a "metal" ground connection. In an opencast mine, ground connections are most often due to mechanical failure in the distribution and cable lines. The heaviest case is the breaking of a distribution line and its fall to the ground, whereby the ground connection will be a function of the length of the free-laid conductor on the ground and the transient resistance at the site of the damage.

To explain the phenomenon, an experiment was carried out in which the ground connection was a conductor grounded on a rock mass and on soil. The measurements were carried out at the end of "Open Pit 4" of the *Elatzite* Mine Complex. Experimentally, the ground connection the current at two points of stationary power line "Open Pit 4" was shot:
- point №1 was at a distance of 1800 m from CRP.
- point №2 was at a distance of 1000 m from CRP.

The current of the ground connection was determined in 2 cases: a AC-25 conductor laid on the ground with a length of 50m; and direct connection of one of the phases with the stationary electric current (AC-95) with lighting protection cable (AC-50)

At measurement point 1 (Figure 2), a 6 / 0.23 kV transformer was connected to the power line to power the camcorder. Therefore, the current of the transformer was also recorded in the ground connection circuit. In this measurement, the conductor was laid on a rock mass. Upon completion of the transient process with the transformer currents, the earthed current oscillated within the range of 1.9 ÷ 2.3A due to the occurrence of electric arcs between the free-lying conductor and the ground.
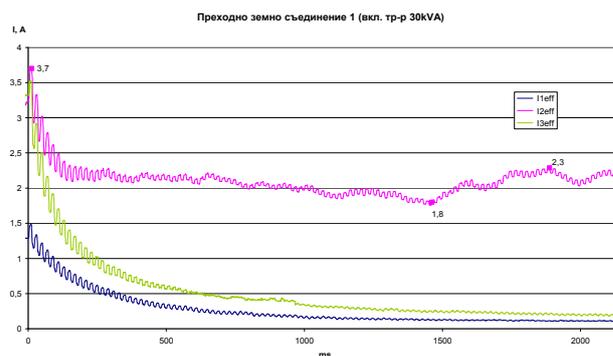

Fig. 2. Electric currents when turning on transformation with transient ground connection at point 1

When measuring at point 2 (fig. 3,) the conductor was laid in a rock mass and soil. The larger part of the conductor lay on soil.

Fig. 3. Current in a transient ground connection at point 2

In figures 4 and 5, the metal ground connection is shown at point 1 and point 2, respectively.

**Fig. 4: Current in metal connection at point 1**
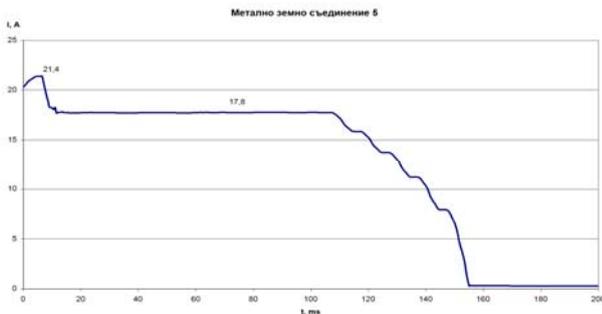
Fig. 5. Current in metal connection at point 2

Table 1.

Point of measurement		i_p, A	I'', A	$I_з$, A
№ 1	Ground connection laid on the ground	10.2		2.3
	Ground connection connected with lightning protection cable	103.4	19.1	15.5
№ 2	Ground connection laid on the ground	18.1		9.3
	Ground connection connected with lightning protection cable	52.4	21.4	17.8

Definition of Table 1 as follows:
i_p - peak value of the current in ground connection;
I'' - superconducting component of ground connection current;
$I_з$, - determined current of the ground connection.

During the experiments, all the conclusions of the CRP were included, which implies the registration of the maximum capacity current for the 6 kV network of the mine. It should be noted that this value is less than the value calculated by cable capacity data due to:
- the resistance of the lightning protection conductor;
- the transient resistance at the connection point of the phase conductor with the lightning protection cable;
- the resistance of the grounded installation in the CRP;
- the possibility that some cables were not under voltage during measurement.

For the calculation of the current I_{3p} of unspecified earth-fault protection, it is necessary to reset the own capacity current of the exit I_c with the impact coefficient K_y taking into account the following:

$$I_{3p} = K_{отс} . K_y . I_c \,, \qquad (2)$$

The impact coefficient depends on the type of network and is theoretically in the range between 1 and 2. From the studies conducted for the particular mine, $K_y = 1{,}2$.

Inevitably, powerful motors and transformers generate zero sequence currents, which can lead to a malfunction of the relay protection. It is necessary to de-energise from these currents by introducing a certain time lag of output $t_{зp}$:

$$t_{3p} = (0{,}1 \div 0{,}5)s \qquad (3)$$

In a study by Stoilov and Dzhustrov (Стоилов и др., 2013), it was found that engines with a continuous start-up process generate zero-sequence currents and voltages only in the start-up phase, and that at 0.1 second from the start, I_0 does not exceed 10A.

The start-up processes in transformers are characterised by longer zero-sequence current generation and are presented in Table 2 (Стоилов и др., 2013):

Table 2.

Power, кVA	Iп/Iпх	$T_в$, s	I_o, A		T_o, s
			t=0	t=0,5s	
1000	22.0	2.0	111	8.3	2.0
630	26.3	1.8	35	1.6	1.4
400	27.2	1.4	38	1.3	1.3
250	32.3	1.5	35	0.5	1.4

When a metal ground connection occurs, a transient process (Figure 6) defined by the capacitive conduction of the power line to the ground is clearly visible. After about 10 ms, a sustained current, also containing higher harmonics, is established.
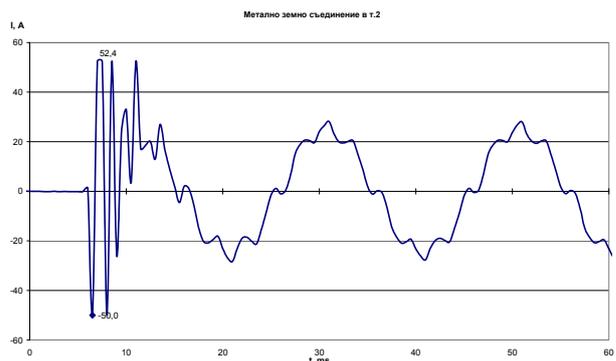

Fig. 6. Momentary values of the current in metal ground compound in point 2

The development of the transition process is similar at point 1 (see Figure 7):

The duration of this process is also about 10 ms, and the maximum amplitude of the shock current depends on the amplitude of the voltage at the moment of the ground connection.
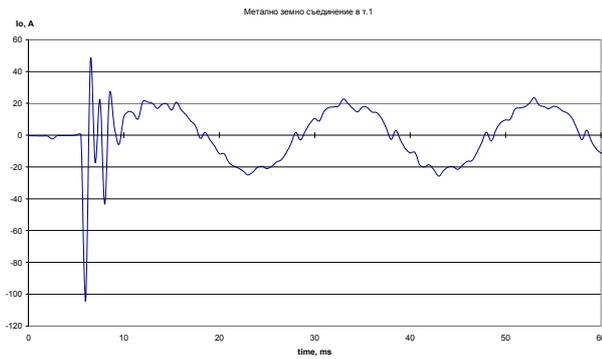
Fig. 7. Momentary values of the current in metal ground compound at point 1

Conclusions

1. In opencast mines, the earth's compounds usually occur through a significant transient resistance

2. The established ground connection is commensurate with the magnitude of the current with zero sequence when switching on transformers after 0.5 s

3. For open pit conditions, it is necessary to introduce at least two steps of protection from earth compounds, if the latter is unspecified.

4. The sensitivity of the protection is determined by (2), with the minimum protection delay time being 0.5÷1.0 s.

5. The setting of the gross level of ground connection protection is made by providing a sensitivity coefficient for a metal earth connection 2, which is

$$I_{зар2} \leq \frac{I_{мзс\,min}}{2},$$

when $I_{мзс\,min}$ is the minimum current of a metal ground connection determined by the minimum working configuration of the power grid. The time delay of this degree is determined by the transition process when a ground connection occurs (Figure 6) and can be considered from 0.02 to 0.04 s.

References

Стоилов, И., К. Джустров. Повишаване ефективността на релейните защити в Рудодобивен комплекс "Елаците мед" АД, Архив "МГУ Инженеринг", С., 2013. (Stoilov, I., K. Dzhustrov. Povishavane efektivnostta na releinite zashtiti v Rudodobiven kompleks "Elatsite Med" AD, Arhiv "MGU Inzhenering", Sofia, 2013.)

Перпелицев, В., И. Стоилов. Анализ на рудничните електрически мрежи средно напрежение с резистивно заземена неутрала, Год. МГУ "Св. Ив. Рилски", т. 56, св. III, С., 2013. - 67-72. (Perpelitsev V., I. Stoilov. Analiz na rudnichnite elektricheski mrezhi sredno naprezhenie s reziztivno zazemena neutrala, God. MGU "Sv. Iv. Rilski", tom 56, svit. III, Sofia, 2013, - 67-72.)

EXPERIMENTAL FILTER TESTS FOR AN INSULATION MONITORING DEVICE FOR IT SYSTEMS

Radi Tenev

Kardzhali Branch of the University of Mining and Geology „St. Ivan Rilski" - Sofia, raditenev@abv.bg

ABSTRACT. IT systems only work effectively with the availability of an insulation monitoring device in real time. The device is connected between the electrical network and the ground. The device's function is to disconnect the network when the insulation resistance drops bellow a preset value. This article discusses the topic of the explorations an insulation monitoring device where an active filter is attempted instead of a choke which attenuate the industrial frequency of 50 Hz. It has been measured and applied a diagram of the filter and the attached features illustrate its operation.

Keywords: insulation resistance, Sallen-Key filter

ЕКСПЕРИМЕНТАЛНИ ИЗСЛЕДВАНИЯ НА ФИЛТЪР ЗА АПАРАТ ЗА КОНТРОЛ НА ИЗОЛАЦИЯТА ЗА МРЕЖИ С ИЗОЛИРАН ЗВЕЗДЕН ЦЕНТЪР

Ради Тенев

Филиал Кърджали на Минно-геоложки университет„Св. Иван Рилски - София, raditenev@abv.bg

РЕЗЮМЕ. Мрежите с изолиран звезден център работят ефективно само при наличието на сигурно устройство за непрекъснат контрол на изолацията в реално време, включено между мрежа и земя. Устройството изключва мрежата при понижаване на изолационното съпротивление под предварително зададена стойност. Настоящата статия разглежда апарат за контрол на изолацията, където е направен опит вместо дросел да се използва активен филтър, който не пропуска промишлената честота от 50 Hz. Дадена е схема на филтъра, а приложените характеристики показват неговата работа.

Ключови думи: изолационно съпротивление, филтър на Сален и Кей

Introduction:

One of the types of insulation control devices that are used in our mining industry is the AZUR apparatus that is highly reliable and meets the requirements of standard 10880-83.

The principle of insulation monitoring is by passing a direct current from a voltage source and the circuit is closed over the ground and the insulation resistance R_F. The magnitude of this constant current is constantly monitored in the process as this is the parameter that informs about the state of R_F insulation resistance. Since the insulation monitoring device is switched on between the network that monitors and the ground, it should have a high resistance to the alternating current and a low resistance to the constant current carrying the information. This high resistance at the AZUR is achieved thanks to a choke-transformer connected to the three-phase network. The choke has high AC resistance and low for the direct current and filters the industrial frequency 50 Hz. If an insulation monitoring. device is implemented without an inductive filter, it will produce a significantly light and compact apparatus,which is significant advantage. The purpose of the study is to select a filter and to examine the parameters of the apparatus at work.
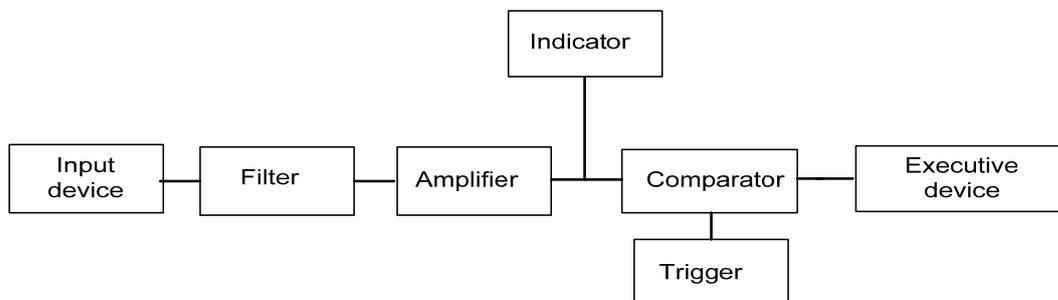

Fig. 1. Block diagram of the insulation control device

Input device:
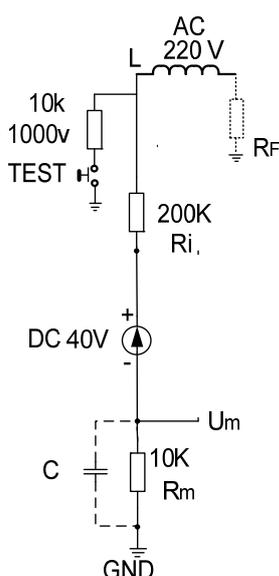
Fig. 2. Input device

The input device is powered by an operating voltage source of 40 V. The voltage source is connected to a 200 KΩ resistor to the mains and even to a ground resistance of 10 KΩ. The parameter which is monitored is taken from the resistor Rm. On the occurrence of an insulation fault the measuring circuit between system and earth closes via the insulation fault R_F, so that a DC measuring current Im proportionate to the insulation resistance results, in accordance with the following equation:

$$I_m = \frac{U_m}{R_i + R_m + R_F} \qquad (1)$$

where:
Im - DC measuring current,
Um - DC measuring voltage,
Ri - Internal resistance of the insulation monitoring device,
Rm - Measuring resistance of the insulation monitoring device,
R_F - Total insulation resistance of the system.

The resistor Rm has two components, constant voltage and alternating voltage. In this case, the variable voltage is a harmful component that needs to be removed. An example: R_F=40000Ω. There are the following voltages on the Rm:

$$U_{m\sim} = \frac{220_\sim . 10.10^3}{(200 + 10 + 40)10^3} = 8,8V \qquad (2)$$

And for Um-is:

$$U_{m-} = \frac{40.10.10^3}{(200 + 10 + 40)10^3} = 1,6V \qquad (3)$$

In this case Um~ should be filtered. This problem may be solved by using a suitable capacitor connected in parallel to Rm. As capacity increases, capacity resistance X_C decreases in accordance with the following equation:

$$X_c = \frac{1}{2\pi f C} \qquad (4)$$

The time constant σ also increases:

$$\sigma = R.C \qquad (5)$$

According to the BDS 10800-83, the trigger time must be 0,1s.[2]. But the increase in capacity reduces the speed of the apparatus, which is a requirement of BDS.

An active filter with operational amplifiers is used to filter the industrial frequency.

When the insulation resistance decreases, the current through Rm increases. If a graph is built, it is in the fourth quadrant. It is more convenient if the graph is in the first quadrant, when the insulation resistance decreases and the current or the voltage will also decrease. To achieve this, a divider of a resistor and a potentiometer is included parallel to the voltage source and the signal is taken from the divider. In this case, when Ri decreases, the measured current decreases. The potentiometer acts as a regulator for adjusting the level of the measured magnitude. Fig. 3 shows the input device finished.
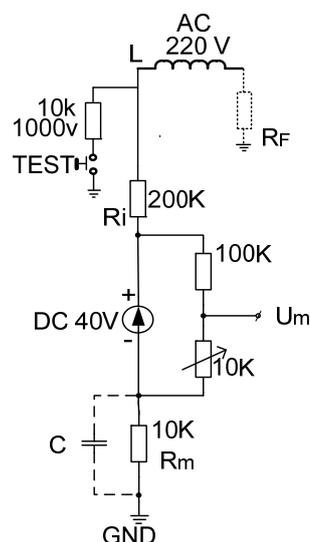

Fig. 3. The input device is complete

It performs the following functions:
1. Provides a high input impedance for the apparatus.
2. Changes the level of the characteristic for a more comfortable R_F measurement.
3. Equipped with a test button according to BDS.

Device filter:
Sallen-Key Law-Pass Filter

To find the circuit solution for this generalized circuit Fig.4, find the mathematical relationships between Ui, Uo, Up and Un, and construct a block diagram. KCL (Kirchhoff's current law) at Uf:

$$U_f\left(\frac{1}{Z1} + \frac{1}{Z2} + \frac{1}{Z4}\right) = U_i\left(\frac{1}{Z1}\right) + U_p\left(\frac{1}{Z2}\right) + U_0\left(\frac{1}{Z4}\right) \qquad (6)$$
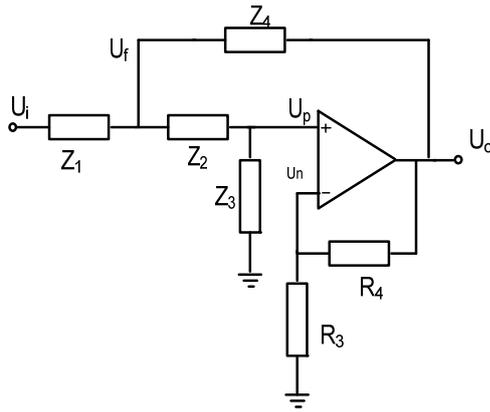
Fig. 4. GeneralizedSallen-Key Circuit

KCL at Up:

$$U_P \left(\frac{1}{Z2} + \frac{1}{Z3} \right) = U_f \left(\frac{1}{Z2} \right) \Rightarrow U_f = U_P \left(1 + \frac{Z2}{Z3} \right) \qquad (7)$$

Substitute Equation (7) into Equation (6) and solve for Up:

$$U_P = U_i \left(\frac{Z2Z3Z4}{Z2Z3Z4 + Z1Z2Z4 + Z1Z2Z3 + Z2Z2Z4 + Z2Z2Z1} \right)$$

$$+ U_0 \left(\frac{Z1Z2Z3}{Z2Z3Z4 + Z1Z2Z4 + Z1Z2Z3 + Z2Z2Z4 + Z2Z2Z1} \right) \qquad (8)$$

KCL at Un:

$$U_n \left(\frac{1}{R3} + \frac{1}{R4} \right) = U_0 \left(\frac{1}{R4} \right) \Rightarrow U_n = U_0 \left(\frac{R3}{R3 + R4} \right) \qquad (9)$$

Gain Block Diagram Fig.4.:

By letting: a(f)= the open-loop gain of the amplifier,

$$b = \left(\frac{R3}{R3 + R4} \right)$$

$$c = \frac{Z2Z3Z4}{Z2Z3Z4 + Z1Z2Z4 + Z1Z2Z3 + Z2Z2Z4 + Z2Z2Z1}$$

$$d = \frac{Z1Z2Z3}{Z2Z3Z4 + Z1Z2Z4 + Z1Z2Z3 + Z2Z2Z4 + Z2Z2Z1}$$

And Ue=Up-Un, the generalized Sallen- Key filter circuit is represented in gain-block form as shown in fig.5.
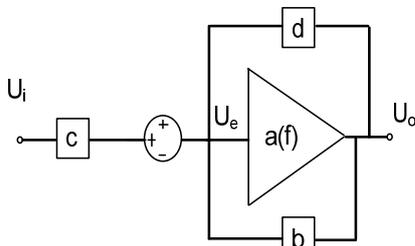

Fig. 5.Gain-Block Diagram of the Generalized Sallen-Key filter

From the gain block diagram the transfer function can be solved easily by observing, $U_0 = a(f)U_e$ and $U_e = cU_i + dU_0 - bU_0$ .Solving for the generalized transfer function on from gain block analysis gives:

$$\frac{U_0}{U_i} = \left(\frac{c}{b} \right) \left[\frac{1}{1 + \frac{1}{a(f)b} - \frac{d}{b}} \right] \qquad (10)$$

Ideal Transfer function

Assuming a(f)b is very large over the frequency of operation, $\frac{1}{a(f)b} \approx 0$, the ideal transfer function from gain block analysis becomes:

$$\frac{U_o}{U_i} = \left(\frac{c}{b} \right) \left[\frac{1}{1 - \frac{d}{b}} \right] \qquad (11)$$

By letting $\frac{1}{b} = K$, $c = \frac{N1}{D}$, and $d = \frac{N2}{D}$,where N1,N2 and D are the numerators and denominators shown above. The ideal equation can be rewritten as:

$\frac{U_0}{U_i} = \left[\frac{K}{\frac{D}{N1} - \frac{K.N2}{N1}} \right]$. Plugging in the generalized impedance terms gives the ideal transfer function with impedance terms.

$$\frac{U_0}{U_i} = \frac{K}{\frac{Z1Z2}{Z3Z4} + \frac{Z1}{Z3} + \frac{Z2}{Z3} + \frac{Z1(1-K)}{Z4} + 1} \qquad (12)$$

Low –Pass Circuit Fig.5

The standard frequency domain equation for a second order low-pass filter is:

$$H_{LP} = \frac{K}{-\left(\frac{f}{fc} \right)^2 + \frac{jf}{Qfc} + 1} \qquad (13)$$

*Wh*ere fc is the corner frequency and Q is the quality factor. When f<< fc Ecuation (10) reduces to K, and the circuits passes signals multiplied by a gain factor K. When f=fc, Ecuation (13) reduces to –jKQ, and signals are enhanced by the factor Q. When f>> fc, ecuation (13) reduces to $-K \left(\frac{fc}{f} \right)^2$ and signals are attenuated by the square of the frequency ratio. With attenuation at higher frequencies increasing by a power of 2, the formula describes a second order low-pass filter. Fig.6 shows the Sallen-Key circuit configuration for low-pass:

$Z1 = R1, \ Z2 = R2, \ Z3 = \frac{1}{sC1} , \ Z4 = \frac{1}{sC2}$
and $K = 1 + \frac{R4}{R3}$
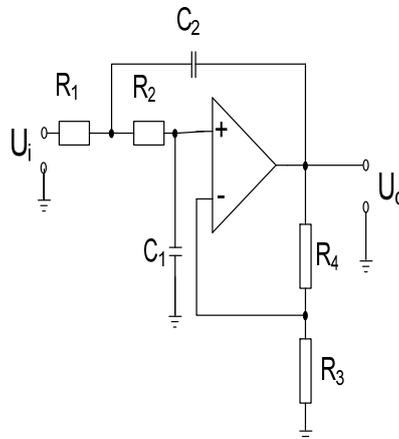
Fig. 6. Low-Pass Sallen-Key Circuit

From Equation (12), the ideal low-pass Sallen-Key transfer function is;

$$\frac{U_0}{U_i}(I_p) = \frac{K}{s^2(R1R2C1C2)+s(R1C1+R2C1+R1C2(1-K))+1} \quad (14)$$

By letting $s = j2\pi f$, $f_c = \frac{1}{2\pi\sqrt{R1R2C1C2}}$,

and $Q = \frac{\sqrt{R1R2C1C2}}{R1C1+R2C1+R1C2(1-K)}$.

Equation (14) follows the same form as Equation (13). With some simplifications, these equations can be dealt with efficiently: the following paragraphs discuss commonly used simplification methods.

Simplification 1:Set Filter Components as Ratios.
Letting $R1 = mR, R2 = R, C1 = C,$ and $C2 = nC,$ results in: $f_c = \frac{1}{2\pi RC\sqrt{mn}}$ and $Q = \frac{\sqrt{mn}}{m+1+mn(1-K)}$. This simplifies things somewhat, but there is interaction between fc and Q. Design should start by setting the gain and Q based on m, n, and K, and then selecting C and calculating R to set fc. Notice that $K = 1 + \frac{m+1}{mn}$ results in Q = ∞. With larger values, Q becomes negative, that is, the poles move into the right half of the s-plane and the circuit oscillates. Most filters require low Q values so this should rarely be a design issue.

Simplification 2:Set Filter Components as Ratios and Gain=1.
Letting R1=mR, R2=R, C1=C, C2=nC, and K=1 results in: $f_c = \frac{1}{2\pi RC\sqrt{mn}}$ and $Q = \frac{\sqrt{mn}}{m+1}$. This keeps gain=1 the pass band, but again there is interaction between fc and Q. Design should start by choosing the ratios m and n to set Q, and then selecting C and calculating R to set fc.

Simplification 3: Set Resistors as Ratios and Capacitors Equal.
Letting $R1 = mR, R2 = R,$ and $C1 = C2 = C,$ results in: $f_c = \frac{1}{2\pi RC\sqrt{m}}$ and $Q = \frac{\sqrt{m}}{1+2m-mk}$. The reason for setting the capacitors equal is the limited selection of values in comparison with resistors. There is interaction between setting fc and Q. Design should start with choosing m and K to set the gain and Q of the circuit and then choosing C calculating R to set fc.

Simplification 4: Set Filter Components Equal. Letting R1=R2=R, and C1=C2=C, results in: $f_c = \frac{1}{2\pi RC}$ and $= \frac{1}{3-K}$. Now fc and Q are independent of one another, the design is greatly simplified although limited. The gain of the circuit now determines Q. RC sets fc- the capacitor chosen and the resistor calculated. One minor drawback is that since the gain controls the Q of the circuit, further gain or attenuation may be necessary to achieve the desired signal gain in the pass band.

Values of K very close to 3 result in high Qs that are sensitive to variations in the values of R3 and R4. For instance, setting K=2,9 results in a nominal Q of 10. Worst case analysis with 1% resistors results in Q=16. Whereas, setting K=2 for a Q of 1, worst case analysis with 1% resistors results in Q=1,02. Resistor values where K=3 leads to Q=∞, and with larger values, Q becomes negative, the poles move into the right half of the s-plane, and the circuit oscillates. The most frequently designed filters require low Q values and this should rarely be a design issue.

Of the frequency characteristics, a Butterworth filter is selected whose characteristic in the bandwidth is too close to the uniform one, called the maximum flat. The slope of the transition section of the filter characteristic of Butterworth is equal to 6Db / oct per pole. There is a non-linear phase-frequency characteristic. The Butterworth filter is used in cases where it is desirable to have the same gain factor for all frequencies in the pass-band. Of the commonly used simplification methods, the forth is selected.

A filter unit is made with the following components.Fig.7.
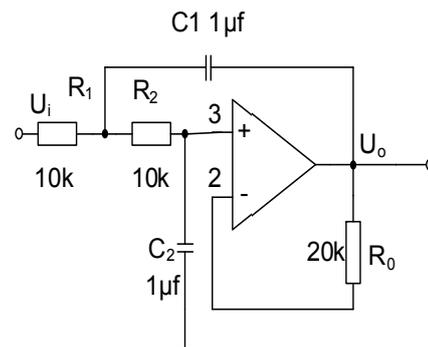
Fig. 7. Low-Pass Filter

With the components so selected, the following characteristics are obtained.

Transfer function $\quad G(s) = \frac{10000,4}{s^2+199,996s+10000}$;
Cut of frequency $\quad$ fc=15,9154943 Hz;
Quality factor $\quad$ Q= 0,5000100002;
Damping ratio $\quad$ ξ=0,99998.
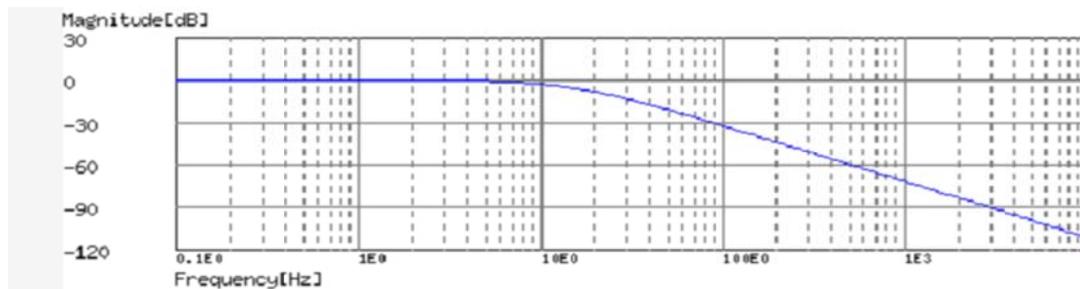
Fig. 8. Frequency response of the Low-Pass Filter

A second-order filter decreases at -12 dB per octave. Fig.8. shows the frequency response of the first filter. Each subsequent filter makes the slope of the frequency response steeper. The filter of the isolation monitoring device is three-stage. The IC LM 324 is used which consists of four operational amplifiers. The first two work as Low-Pass Filter. After the second OA follows a first order Low-Pass Filter. The third OA works as an amplifier and the fourth is a comparator. The potentiometer regulates the amplification of the DC signal.
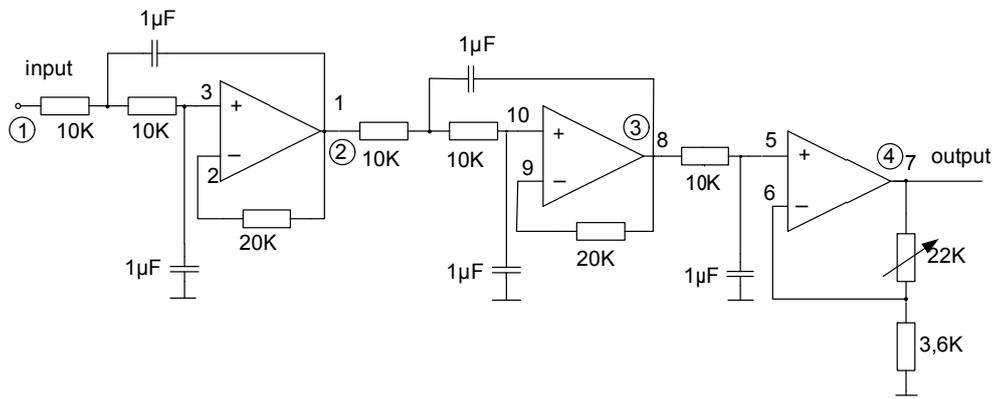
Fig. 9. Filter of the insulation control device. The measuring points are indicated

Experimental studies:

Illustrating the operation of the filter with appropriate oscillograms. A digital oscilloscope SIGLENT is used. The filter is made up of three units, see Fig.9. One unit is not enough to filter the variable component of 50 Hz. Channel 1 of the oscilloscope is connected to the input and channel 2 to the output of the unit. These are points 1and 2. of fig.9.Fig.10.is the oscillograme of the first filter unit. The second oscillogram shows the work of the first two units. Channel 1 is at point 1 and channel 2 at point 3.Fig.11. The next oscillogram, Fig.12 shows the operation of the filter and the amplifier. The ratio between input and output signal is 100 times which means that the AC signal is reduced 100 times. From the above example where U~=8,8V, U~ will be 0,088V at the output. Channel 1 is at point 1 and channel 2 at point 4, which is the output of the amplifier, and hence the signal goes once to the indicator and a second time to the comparator of the device. In addition, another oscillogram for the second unit, point 2 input and 3 output. Fig.13. It is clear that the phase shift between the input and the output signal is approximately 158^0.

Fig. 10. The input and output signals of the first filter unit

Fig. 11. The input and output signals of the first and second filter units

Fig. 12. Input and output signals for the entire filter

Fig. 13. Input and output signal of the second unit. The phase shift is158^0

Conclusion

The experiments were carried out with a real-made insulation monitoring device for voltage of 220 V. The results obtained show that the any inductive filter, such as a throttle, can be replaced by an active filter. Implementing active filters into Insulation Monitoring Devices will significantly reduce their mass and volume.

References

Аппарат защиты от токов утечки рудничный унифици-рованный АЗУР.3 Руководство по эксплуатаций (сов-мещено с паспортом)0.06.466.262 РЭ available at:https://docplayer.ru/51606870-Apparat-zashchity-ot-tocov-utechki-rudnichnyy-unificirovannyy-azur-3-rukovodstvo-po-ekspluatacii-sovmeshcheno-s-pasportom.html(accessed 21 June 2018).

БДС 10800-83. Съоръжения електрически руднични. Апарати за защита от токовете на утечка за мрежи на напрежения до 1200 V с изолиран звезден център. С. (1983) (BDS 10800-83 Suoruzheniya electricheski rudnichni. Aparati za zashtita ot tokove n autechka za mrezhi na naprezeniya do 1200 V s izoliranzvezden tsentur.S.1983).

В.П. Колосюк. Защитное отключение рудничных электроустановок.1980 М. Недра (V.P. Kolosyuk. Zashchitnoeo tklyucheniye rudnichnykh elektroustanovok. 1980 M. Nedra.

Faulkenberry Luces M.1982, An introduction to operational amplifiers with linear IC applications.John Wiley&Sons Inc.

Hofheinz, W.,2000. Protective Mesures with Insulation Monitoring, VDE VERLAG, Berlin.

Karki James, 2002, Analysis of the Sallen-Key Architecture, available at:http://www.ti.com.cn/cn/lit/an/sloa024b/sloa024b.pdf (accessed 28 June 2018).

MEASUREMENT AND CALCULATION OF THE DENSITY OF THE CHARGE OF ELECTRIFIED OIL PRODUCTS USING THE SAMPLING METHOD

Ivan Prodanov[1], Stefan Stefanov[2]

[1] University of Mining and Geology "St. Ivan Rilski", 1700 Sofia, enemko@mail.bg
[2] University of Mining and Geology "St. Ivan Rilski", 1700 Sofia

ABSTRACT. To assess the static electricity hazard in technological operations and fuel stations, it is necessary to know the specific density of the liquid charge. The method discussed in this work is the measuring and calculating of the static charge density of a sample of a petroleum product which is pumped along a turbulent flow pipeline based on the use of the known Faraday cylinder.

Keywords: static electricity, electrification, charge density

ИЗМЕРВАНЕ И ИЗЧИСЛЯВАНЕ НА ПЛЪТНОСТТА НА ЗАРЯДА НА НАЕЛЕКТРИЗИРАНИ НЕФТОПРОДУКТИ ПО МЕТОДА НА ВЗЕМАНЕ НА ПРОБА
Иван Проданов[1], Стефан Стефанов[2]

[1] *Минно-геоложки университет "Св. Иван Рилски", 1700 София, enemko@mail.bg*
[2] *Минно-геоложки университет "Св. Иван Рилски", 1700 София*

РЕЗЮМЕ. За оценка на опасността от статично електричество при технологичните операции и автозареждащите станции е необходимо да се знае специфичната плътност на заряда на течността. В доклада се разглежда метод за измерване и изчисляване на плътността на заряда от статично електричество на проба от нефтопродукт, изпомпван по тръбопровод от турболентен поток, на базата на използването на известния цилиндър на Фарадей.

Ключови думи: статично електричество, електризация, плътност на заряда

Introduction

In the process of filling reservoirs with flammable dielectric liquids, fires and blasts may occur as a result of static electricity discharge. Certain permissible minimum ranges of the electrifying current and of the specific density of the charge of liquid are known within which static electricity does not pose a threat. However, the control of the current and density of the product that is being transported within a reservoir along metal pipes is very difficult. Special measuring equipment in industry is not manufactured and the use of dynamic electrometers mounted directly on the pipelines with gauges placed in the liquid flow is currently still within the field of the laboratory practice only (Стефанов и др., 2013).

Exposition

1. Measuring the charge density of electrified dielectric liquid using the sampling method

A method is considered for measuring and calculating the static electricity charge density of a sample from an oil product that is pumped along a turbulent flow pipeline. The method is based on the use of the famous Faraday cylinder.

In order to implement this method, a special cock is installed on the pipeline, in the immediate vicinity of the tank where the product is injected. This cock makes it possible to take samples in the course of the filling of the tank. The sample is directly inlet into the Faraday cylinder (Fig. 1) which, in this case, is transformed into two coaxially placed vessels isolated from each other.
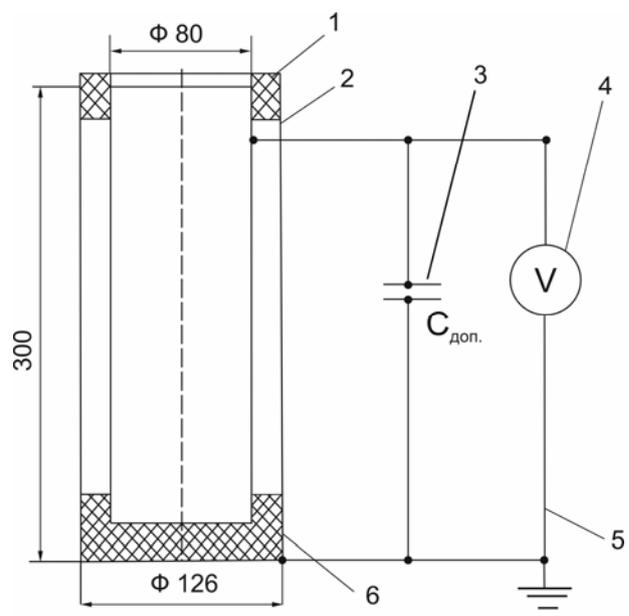

Fig. 1. Diagram of a stand for measuring the charge density of oil products

In Figure1:
1 is the inner cylinder;
2 is the outer cylinder;
3 is an extra volume;
4 is the voltmeter of the electrostatic system;
5 is the connecting wire;
6 is the insulation.

The outer vessel is earthed. The inner vessel is connected to the measuring device by means of a wire with sound insulation. The measuring device could be an ordinary voltmeter from the electrostatic system with a varied measurement range (30, 150, 300V) depending on the required sensitivity and precision of the method. However, any other electrometer with great input resistance could be used as well.

The cylinders are placed one into the other, thus forming the capacitor of the Faraday cylinder with a capacity of C_ϕ. If a sample of electrified liquid is poured into the inner cylinder, then voltage U will be registered after the capacity C_c of the whole system. The system capacity is a sum total of: the capacity of the Faraday cylinder, of the connecting wires, and of the measuring device. If the product charge is great, an additional capacitor $C_{\partial on}$ can be inserted. Thus:

$$C_c = C_\phi + C_n + C_v + C_{\partial on} \qquad (1)$$

Taking into consideration the known capacity and the voltage measured after it, the charge of the selected liquid sample is determined:

$$Q = C_c.U. \qquad (2)$$

Dividing the charge into the volume of the liquid sample, we obtain the specific density of the charge of the product that flows along the pipeline:

$$\rho = \frac{Q}{V}, \quad C/_{m^3} \qquad (3)$$

where V, m^3 is the volume of the selected sample.

The practical application of the suggested method of determining the specific density of the electrified liquid charge is possible under certain conditions: the flow of the oil product moving along the pipeline should be turbulent. In this case, it is assumed that the static electricity charge of the liquid is evenly distributed along the entire section. Consequently, the charge density of the selected liquid sample will correspond to the charge density of the flow in the pipeline. Besides, the time T for filling the Faraday cylinder with the sample has to be much shorter than the time constant of the capacity of the measuring system, i.e. the following condition needs to be met:

$$T << \tau = C.R \qquad (4)$$

where R is the resistance of the insulation of the system comprising the Faraday cylinder, the connecting wires, and the measuring device.

Otherwise, in the course of the filling of the Faraday cylinder with the sample, the success of discharge of the system will be partial and the final result will be higher. If the time constant of the system is $10^2.T$, then for the time necessary to fill the vessel with the sample $T = 20$ s, the time constant of the system needs to be 3000 s. Therefore, at the level of insulation $R = 10^2$ Ω, which is practically feasible, the capacity of the system should be for instance:

$$C_c = \frac{\tau}{\rho} = \frac{3000}{10^{12}} = 3 \quad pF. \qquad (5)$$

The method sensitivity to the charge measured is directly related to the capacity of the system. The less the system capacity, the greater the sensitivity, i.e. the lower charge value can be registered. In turn, the lower capacity results in the decrease of τ. Consequently, in order to maintain the measurement error within constant levels, the system insulation needs to be raised.

2. Example

The isolation material between the cylinders - fluoroplastics;
Insulation of the connecting wires - fluoroplastics;
capacity of the Faraday cylinder - with the connecting wires: 50 pF.

An additional capacity of $C_{\partial on} = 2300$ pF is included parallel to the cylinder. Its purpose is to lower the voltage measured and to raise the time constant of the system discharge.

The insulation of the whole system (including the Faraday cylinder and the connecting wires of the static voltmeter) is no less than 10^2 Ω. Thus, the time constant of the system discharge is $\tau = 2380.10^{-12}.10^{12} = 2380$ s.

The volume of the cylinder is 1 liter, for example. The time taken for its filling is in the range of 20 s. Therefore, the condition for $\tau = 10^2.T$ is fulfilled.

The sensitivity of the system at a deviation of the arrow of the voltmeter C 50 at the scale of 30 V will be as follows:

$$\rho_{min} = 5.2330.10^{-12}.10^8 = 11,7 \quad mC/_{m^3}.$$

Conclusion

It is necessary to take into account that the static electricity in a liquid with a density of $15 \; mC/m^3$ does not pose a risk of ignition of the filling air and vapor mixtures by electrical discharges. Therefore, the obtained sensitivity is sufficient for making a practical assessment of the risk of liquid electrification.

References

Стефанов, С., И. Проданов. Статично електричество – теория и практика. С., Авангард Прима, 2013. (Stefanov, S., I. Prodanov. Statichno elektrichestvo – teoria i praktika. Sofia, Avangard Prima, 2013.)

Попов, Б. Г., В. Н. Веревкин, В. А. Бондарь. В. И. Горшков. Статическое электричество в химической промышленности. Ленинград, Изд. „Химия", 1977. (Popov, B. G., V. N. Verevkin, V. A. Bondar, V. I. Gorshkov. Staticheskoe elektrichestvo v himicheskoi promishlennosti. Leningrad, Izd. "Himiya", 1977.)

Максимов, Б. К., А. А. Обух. Статическое электричество в промышлености и защита от него. М., Энергия, 1978. (Maksimov, B. K., A. A. Obuh. Staticheskoe elektrichestvo v promishlennosti i zashtita ot nego. Moskva, Energiya, 1978.)

MEASUREMENT AND CALCULATION OF THE ELECTRIFYING CURRENT OF ELECTRIFIED OIL PRODUCTS USING THE SAMPLING METHOD

Stefan Stefanov[1], Ivan Prodanov[2]

[1] University of Mining and Geology "St. Ivan Rilski", 1700 Sofia,

[2] University of Mining and Geology "St. Ivan Rilski", 1700 Sofia, enemko@mail.bg

ABSTRACT. To assess the static electricity hazard in the case of the technological operations and at the fuel stations, it is necessary to know the strength of the electrification current. Hereby is presented the problem of measuring and calculating the electrifying current in the process of filling a reservoir with electrifying liquids. A labor stand and the the sampling method are used.

Keywords: static electricity, electrification

ИЗМЕРВАНЕ И ИЗЧИСЛЯВАНЕ НА ТОКА НА ЕЛЕКТРИЗАЦИЯ НА НАЕЛЕКТРИЗИРАНИ НЕФТОПРОДУКТИ ПО МЕТОДА НА ВЗЕМАНЕ НА ПРОБА

Стефан Стефанов[1], Иван Проданов[2]

[1] Минно-геоложки университет "Св. Иван Рилски", 1700 София,

[2] Минно-геоложки университет "Св. Иван Рилски", 1700 София, enemko@mail.bg

РЕЗЮМЕ. За оценка на опасността от статично електричество при технологичните операции и автозареждащите станции е необходимо да се знае силата на тока на електризация. В настоящата работа се разглежда проблемът за измерване и изчисляване на тока на електризация в процеса на запълване на резервоар с наелектризиращи се течности. Използван е лабораторен стенд и методът на вземане на проба.

Ключови думи: статично електричество, електризация

Introduction

In the process of filling reservoirs with flammable dielectric liquids, fires and blasts may occur as a result of static electricity discharge. Certain permissible minimum ranges of the electrifying current and of the specific density of the charge of liquid are known within which static electricity does not pose a threat. However, the control of the current and density of the product that is being transported within a reservoir along metal pipes is very difficult. Special measuring equipment in industry is not manufactured and the use of dynamic electrometers mounted directly on the pipelines with gauges placed in the liquid flow is currently still within the field of the laboratory practice only (Стефанов и др., 2013).

Exposition

1. Method of determining the strength of the electrifying current.

In order to assess static electricity risks during technological operations and at auto-charging stations, it is necessary to know the strength of the electrifying current

The strength of the electrifying current during the motion of the oil product along the pipeline can analytically be calculated according to the Koszman and Gavis equation (Koszman et al., 1962; Попов и др., 1977; Максимов и др., 1978):

$$I = \frac{\pi.\varepsilon_r.\varepsilon_0.R.T.\vartheta}{2.n.F}.N_u\left(1 - \frac{C_s}{C_o}\right)\left(1 - e^{-\frac{l}{\vartheta.\tau}}\right). \quad (1),$$

where:

I is the electrification current in the pipeline;

$\varepsilon_r.\varepsilon_0$ is the permittivity of the oil product;

R is a universal gas constant;

T is the temperature of the oil product in the pipeline;

N_u is the Nusselt parameter;

n is the number of transferred ions;

C_o, C_s is the concentration of ions within the liquid volume and on the walls, respectively;

F is the Faraday constant;

$\tau = \dfrac{\varepsilon_r.\varepsilon_0}{\gamma}$ is the relaxation time.

When calculating the electrification current according to equation (1), it is difficult to determine some parameters that are part of the equation, such as the concentration of ions within the volume of the oil product and on the walls of the

pipeline (C_o, C_s), the number of ions transferred, the diffusion coefficient, etc.

Measuring the electrification current in an operating pipeline is difficult due to the large volume that is pumped, the lack of the necessary equipment, and the complexity of the necessary measurement requirements to be observed. The suggested method makes it possible to calculate the electrification in the actual pipeline based on data from laboratory tests on the electrifiability of the pumped products.

To measure the electrification of oil products in laboratory conditions, a simple stand can be used whose diagram is illustrated in Fig. 1.
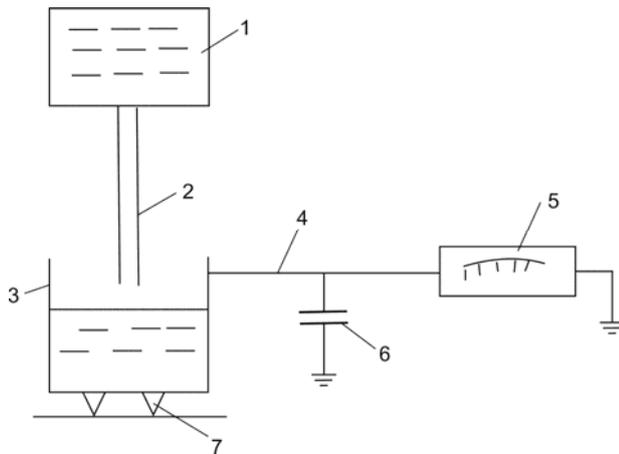

Fig.1. Diagram of a stand for measuring the electrification of oil products

The diagram comprises:
1 – upper tank;
2 – metal earthed pipe;
3 – lower tank isolated from the ground;
4 – shielding;
5 – electrostatic voltmeter;
6 – additional capacitor;
7 – insulators ($R > 10^3 \Omega$).

The tank capacity is 1 to 2 liters and the tanks are isolated one from another. An earthed pipe with a diameter of 5-10 mm and a length of 0.5-1m is attached to the bottom of the upper tank. The lower tank is isolated from the ground and an electrostatic voltmeter is connected via a shielded cable.

Electrification of the oil product is generated by means of pouring the oil product from the upper tank to the lower one. The data of the lower reservoir potential is measured and then the charge initiated by the electrification is calculated. Therefore, the capacity of the system reservoir-voltmeter needs to be known and constant.

The electric capacity of the tank is measured using a microfarad meter.

The amount of the charge accumulated in the lower tank is calculated after the following equation:

$$q = C.U \tag{2}$$

The average electrification current is determined by the ratio:

$$I_1 = \frac{q}{t}, \tag{3}$$

where t is the time of the pouring of the oil product from the upper tank into the lower, s .

The charge formation and accumulation in the pipe of the measuring equipment and of the pipeline that operates on the premises of the oil base are subject to the same law.

The analytical expression obtained from the data generated by the laboratory equipment for the assessment of the electrification current in the pipe is as follows:

$$I_1 = \frac{\pi.\varepsilon_r.\varepsilon_0.R.T_1.\vartheta_1}{2.n.F}.N_u.\left(1 - \frac{C_{s_1}}{C_{o_1}}\right)\left(1 - e^{-\frac{l_1}{\vartheta_1.\tau}}\right). \tag{4}$$

To calculate the strength of the electrification current in the pipeline of the oil bases or the fuel stations, a sample of the pumped product should be taken and tested by means of the stand under consideration. Besides, the concentration and the amount of ions transferred, the molecular diffusion coefficient, and all other parameters need to be the same in the calculation equations for the laboratory stand and for the operating pipeline

Dividing expression (1) by expression (4) and taking into consideration that $C_o = C_{0_1}$ and $C_s = C_{s_1}$, the following expression is obtained of the assessment of the electrification current in the operating pipeline with a length of l :

$$\frac{I}{I_1} = \frac{T.\vartheta.N_u}{T_1.\vartheta_1.N_{u_1}}.\frac{1 - e^{-\frac{l}{\vartheta.\tau}}}{1 - e^{-\frac{l_1}{\vartheta_1.\tau_1}}}. \tag{5}$$

For the long pipes with $e^{-\frac{l_1}{\vartheta_1.\tau}} \rightarrow 0$, expression (5) is as follows:

$$I = I_1.\frac{T.\vartheta.N_u}{T_1.\vartheta_1.N_{u_1}}.\frac{1}{1 - e^{-\frac{l_1}{\vartheta_1.\tau_1}}}. \tag{6}$$

The Nusselt parameter can be expressed through the R_e and S_s parameters in the form of an involution dependency of the type of (Koszman, 1962):

$$N_u = C.R_e^m.S_c^n. \tag{7}$$

where:

$R_e = \dfrac{\vartheta.2.a}{V}$ is the Reynolds parameter;

D is the diffusion coefficient;

a is the pipe radius;

C is the concentration of charge carriers.

For the turbulent liquid mode, we assume that $m = 0.8$ [4]; then the ratio of the Nusselt parameters in expression (5) will be:

$$\frac{N_u}{N_{u_1}} = \left(\frac{\vartheta.a}{\vartheta_1.a_1}\right)^{0,8}, \tag{8}$$

Taking into account equation (8), the ultimate expression for calculating the strength of electrification current in oil base pipelines is written as follows:

$$I = I_1.\frac{1 - e^{-\frac{l}{\vartheta.\tau}}}{1 - e^{-\frac{l_1}{\vartheta_1.\tau_1}}}\left(\frac{\vartheta}{\vartheta_1}\right)^{1,8}.\left(\frac{a}{a_1}\right)^{0,8}. \tag{9}$$

2. Example

When testing petrol ($\gamma = 10^{12}$, $\Omega^{-1}.m^{-1}$; $\varepsilon = 3$) by means of a test laboratory installation, the time for pouring the petrol out of the upper tank into the lower one is $t = 26\ s$, the capacity of the lower tank is $U = 650\ V$, and the capacity of the system lower tank - static voltmeter is $C = 20\ pF$.

The same petroleum product is transported along an operating pipeline with a length of $l = 1000\ m$ at the flow of $Q = 0.08\ \dfrac{m^3}{s}$.

The task is to calculate the strength of electrification current in the pipeline at:

$T = T_1$;

$l_1 = 500\ mm$;

$a = 100\ mm$;

$a_1 = 3\ mm$.

Taking into consideration (2) and (3), the average electrification current is:

$$I_1 = \frac{C.U}{t} = \frac{20.10^{-12}.650}{26} = 5.10^{-10}\ A;$$

the time for charge relaxation is:

$$\tau = \frac{\varepsilon_r.\varepsilon_0}{t} = \frac{3.8,85.10^{-12}.650}{10^{-12}} = 27\ s;$$

the speed in the operating pipeline is:

$$\vartheta = \frac{Q}{\pi.a^2} = \frac{0,08}{3,14.100^2.10^{-4}} = 2,5\ \frac{m}{s};$$

the outflow rate in the laboratory system is:

$$\vartheta_1 = \frac{1,6.10^{-3}}{t.\pi.a_1^2} = 0,2\ \frac{m}{s}.$$

By substituting these data in expression (9), the strength of the electrification current in the operating pipeline is obtained:

$$I = 5.10^{-10}.\frac{1 - e^{-\frac{1000}{2,5.27}}}{1 - e^{-\frac{0,25}{22}}}\left(\frac{2,5}{22}\right)^{1,8}.\left(\frac{0,1}{0,003}\right)^{0,8} =$$

$$= 9.8.10^{-7}\ A.$$

Conclusion

The methodology presented makes it possible to calculate the strength of the electrification current in a pipeline by using data measured in a laboratory stand and also without measuring and determining the diffusion coefficient, the viscosity of the liquid, the ion ratio, and other parameters.

References

Стефанов, С., И. Проданов. Статично електричество – теория и практика. С., Авангард Прима, 2013. (Stefanov, S., I. Prodanov. Statichno elektrichestvo – teoria i praktika. Sofia, Avangard Prima, 2013.)

Попов, Б. Г., В. Н. Веревкин, В. А. Бондарь. В. И. Горшков. Статическое электричество в химической промышленности. Ленинград, Изд. „Химия“, 1977. (Popov, B. G., V. N. Verevkin, V. A. Bondar, V. I. Gorshkov. Staticheskoe elektrichestvo v himicheskoi promishlennosti. Leningrad, Izd. "Himiya", 1977.)

Максимов, Б. К., А. А. Обух. Статическое электричество в промышлености и защита от него. М., Энергия, 1978. (Maksimov, B. K., A. A. Obuh. Staticheskoe elektrichestvo v promishlennosti i zashtita ot nego. Moskva, Energiya, 1978.)

Koszman, I., Y. Gavis, Chem. Eng. Sii, 1962, V 17, № 12.

SIGNATURE ANALYSIS METHODS TO DETECT FAILURES IN ELECTRIC MOTORS

Yasen Gorbunov [1], Tihomir Dzhikov [2]

[1] *University of Mining and Geology "St. Ivan Rilski", y.gorbounov@mgu.bg*
[2] *University of Mining and Geology "St. Ivan Rilski", tihomir.dzhikov@gmail.com*

ABSTRACT. The monitoring and diagnosis of electric motors are a serious challenge for engineers and researchers in the industry where minimising maintenance costs and adherence to production lead times are of utmost importance. Numerous methods exist to solve these tasks, such as monitoring of the mechanical vibrations, thermal inspection, acoustic monitoring, etc. They are based on the fact that for a healthy machine, the shape of the observed signal has some typical profile, also referred to as a signature. The changes in load and the various types of damages lead to the occurrence of additional and atypical harmonics in the spectrum of the signal that have a noticeable impact on the profile of that signal. The choice of a suitable signature analysis method allows for early detection of failures, such as the emergence of a short circuit, a winding disruption, eccentricity or vibrations due to damages of a bearing or to an atypical load. In this way it is possible to perform a planned repair instead of an emergency one, which can be of a considerable economic effect. This paper provides an overview of some basic methods for signature analysis. A particularly promising amongst them is the Motor Current Signature Analysis (MCSA), which is a sensorless and a non-invasive method, and at the same time it allows for remote site-based investigation.

Keywords: motor faults, signature analysis, vibration analysis, health monitoring, Motor Current Signature Analysis (MCSA)

МЕТОДИ ЗА СИГНАТУРЕН АНАЛИЗ ЗА ОТКРИВАНЕ НА ПОВРЕДИ В ЕЛЕКТРИЧЕСКИТЕ МОТОРИ
Ясен Горбунов[1], Тихомир Джиков[2]
[1] *Минно-геоложки университет "Св. Иван Рилски", 1700 София, y.gorbounov@mgu.bg*
[2] *Минно-геоложки университет "Св. Иван Рилски", 1700 София, tihomir.dzhikov@gmail.com*

РЕЗЮМЕ. Контролът и диагностиката на електродвигателите са сериозно предизвикателство за инженерите и изследователите в индустрията, където минимизирането на разходите за поддръжка и спазването на сроковете при производство са от ключово значение. Съществуват множество методи за решаване на тези задачи, такива като следене на механичните вибрации, термично обследване, акустичен мониторинг и др. Те се основават на факта, че за една здрава машина формата на наблюдавания сигнал притежава характерен профил, наричан още сигнатура. Промяната на натоварването и различните видове повреди водят до възникване на допълнителни и нетипични хармоници в спектралния състав, които оказват осезаемо влияние върху профила на този сигнал. Изборът на подходящ метод за сигнатурен анализ позволява ранно откриване на повреди от типа на: възникване на късо съединение, прекъсване на намотка, възникване на ексцентрицитет или вибрации вследствие на повреден лагер или нетипично натоварване. По такъв начин е възможно реализирането на планов вместо авариен ремонт, което може да има съществено икономическо значение. В настоящата статия е направен общ преглед на някои основни методи за сигнатурен анализ. Като особено перспективен сред тях се очертава анализът на формата на тока (Motor current signature analysis-MCSA), който се явява безсензорен и неинвазивен метод, а освен това дава възможност за отдалечено от обекта изследване.

Ключови думи: повреди в електрическите мотори, сигнатурен анализ, вибрационен анализ, анализ на профила на тока

Introduction

In a global aspect, electric drives are amongst the main consumers of electricity as they are involved in all areas of modern life - industry, medicine, and everyday life. According to various sources, electric drives nowadays consume between 50% and 70% of all of the produced electricity. This reserves them a very special place in automation control systems in both manufacturing plants and household appliances. That is why the requirements imposed on their effective use are constantly growing which means deployment of faster and more complex control algorithms. At the same time, the high speed of continuous production requires very high reliability. Unfortunately, even the most sophisticated technologies cannot avoid the possibility of failures. On the one hand, motor faults can emerge due to mechanical problems and on the other hand, they can be electrical in nature. The earlier the

failures are encountered the less are the material and financial losses. Every retardment in obtaining the information of possible faults may affect the whole motor operation, or deteriorate, or even stop the entire manufacturing process. Consequently, large revenue losses and maintenance costs may occur.

Contemporary achievements in physics and material science lead to the invention and production of fast and accurate sensors such as resistive and semiconductor-based strain gauges, piezo transducers, accelerometers, Hall sensors, Rogowski coils, etc. The dramatic development of microelectronics and the increasing computational capability make it possible not only to perform fast data logging but also to implement complex mathematical algorithms into digital hardware that is able to make calculations in real time.

In this paper, some common faults in electrical motors are briefly introduced. Prospective methods adopted for analysis of

motor faults are also discussed such as signature analysis techniques. Some common instrumentation apparatus is also mentioned in the paper.

Faults in electric motors

Faults in electric motors are mainly classified as electric or mechanical. Common failure types include bearing problems (including gearbox), rotor or stator windings, breakage of rotor bar, brushes or slip ring, static or dynamic air-gap irregularities, rotor imbalance, etc. According to a survey held by the Institute of Electrical and Electronics Engineers (IEEE) and the Electric Power Research Institute (EPRI) (IEEE Std. 493-1997; Allbrecht et al., 1986) the percentage of fault occurrence is distributed as shown in Table 1. It can be seen that the bearing faults (mechanical) are prevalent in frequency of emergence followed by stator faults.

Table 1.

Study	Bearing faults [%]	Stator faults [%]	Rotor faults [%]	Others [%]
IEEE	42	28	8	22
EPRI	41	36	9	14

According to (Karmakar et al., 2016), major faults in induction motors can be categorised as:
- mechanical faults – broken rotor bars, load imbalance, air gap eccentricity, bearing damage, rotor and stator windings failure;
- electrical faults – imbalance of the supply voltage/current, single phasing, under/over voltage, reverse phase sequence, earth fault, overload, inter-turn short-circuit fault, crawling;
- faults related to the environment – ambient temperature, external moisture, vibrations due to working in harsh environments.

A non-exhaustive summary of these typical failures is given in Fig. 1 (Siddiqui et al., 2014). A thorough discussion on the causes of AC motor failure analysis that completes the overall picture can be found in (Bonnett, 2000).
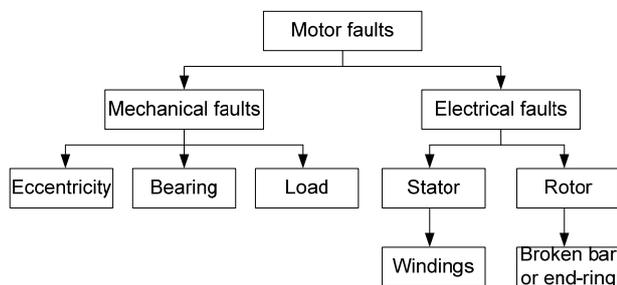

Fig. 1. General classification of motor faults (Siddiqui et al., 2014)

More than 66% of the failures are detected during operation and about 28% are detected during maintenance procedures (IEEE Report, 1985). Rotor faults can be observed either through monitoring the rotor currents, if there are any windings on the rotor at all, or more frequently, by monitoring stator currents. Having said all of the above, the importance of the predictive analysis and the need of preferably non-invasive measurement tools are obvious.

Digital signal processing

Both vibration and current monitoring techniques require conversion of the measured quantity into voltage and subsequent fast data acquisition. This process imposes signal conditioning and filtering in order to limit the spectrum of the signal, subsequent transformation and scaling/normalization, data reduction, and sampling. With properly selected digital filter bandwidths and adequate sampling rates, sigma-delta ADCs allow for supply frequency rejection, which means that no additional signal is introduced during processing. Nowadays, converters available on the market have high dynamic range (up to 24-bit) and high sampling rate in the order of a few hundred MHz. Their capabilities often exceed the performance requirements and provide effective current signature analysis.

The steps involved in digital signal processing are depicted in Fig. 2:
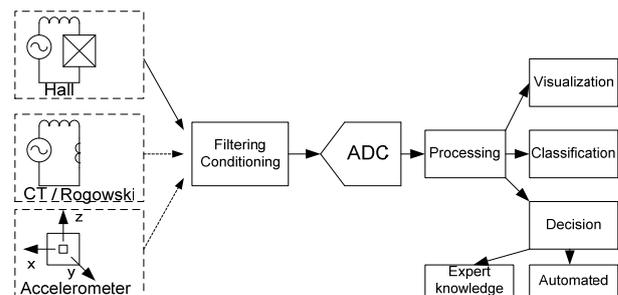
Fig. 2. Digital signal processing and data analysis

As it is shown in the figure the steps of data analysis can also be done digitally concluded with automated visualization, failure classification and decision making. Each of these steps represents a highly sophisticated algorithm although the decision making often requires an expert knowledge.

Primary sensors

The information about the health condition of a machine is obtained by measuring a wide range of signals. These signals include vibration, current or voltage (stator and/or rotor), magnetic flux, torque, acoustic noise, temperature, etc. Some of these quantities can be easily obtained while others are virtually impossible to be read or require constructive modifications, or are simply too expensive. That is why the main sensing components used in motor failure analysis include resistive temperature devices (RTD), accelerometers, Hall sensors, Rogowski coils, and current transformers. The two latter are most widely used for signature analysis (mechanical – vibrations or current related - MCSA).

Analysis methods

Health condition monitoring and analysis methods can be derived in the following general categories (Mehala, 2012, with additions):
1. Thermal model based on:
   - Finite Element Analysis (FEA)
   - Thermal network analysis
2. Root Mean Squared (RMS)
3. Frequency domain
   - Fast Fourier Transform (FFT)
4. Time-Frequency techniques
   - Short Time Fourier Transform (STFT)
   - Gabor Transform (GT)
   - Cohen class distribution
     - Wigner –Ville distribution (WVD)
     - Choi-Williams distribution
     - Cone shaped distribution
   - Wavelet Transform (WT)
5. Time series methods
   - Spectral estimation through ARMA models
   - Welch method
   - MUSIC method
   - Periodogram
6. Cepstrum analysis
7. Park vector approach

The first two categories are discussed in (Siddiqui et al., 2014). The FEA method is based on differential equations and thus it is compute intensive and time consuming, but very precise. The thermal network (Lumped parameter based model) is much simpler, but less accurate than the FEA and can be slow. The RMS method represents a simple statistical calculation but it is much less informative and is mainly used for a rough indication of the motor loading.

The frequency domain analysis uses the Fast Fourier Transform (FFT) and it is the most common signal processing method used for online condition monitoring. This is due to the fact that many mechanical and electrical failures generate signals whose frequencies can be determined by knowledge of motor parameters. These fault signals appear in various sensing signals, including vibration, current, and flux. The FFT analysis is based on the fact that each periodic signal can be decomposed into a sum of sinusoids, thus converting the signal from the time domain into the frequency domain. The vice versa conversion is also possible. In their work, (Marcelo et al., 2012) use FFT to detect real-time asynchronous motor damage – broken rotor rod, bearing failure, eccentricity and short circuit.

The time-frequency techniques include several algorithms amongst which the STFT and WT are the most common. The STFT method provides strong capabilities to diagnose faults in the transient conditions. It has good time resolution but has poor frequency resolution. In contrast with the FFT, the wavelet transform decomposes the signal into a set of non-sinusoidal waves. It is usually applied to impulse waveforms that are not convenient to be represented as a sum of sinusoidal components. This transform is being initially used for seismic analysis. It provides capabilities to extract local parameters of the signal with very good precision. (Siddiqui et al., 2012) use the WT method for broken rotor bar fault detection in induction motors.

The cepstrum analysis is a result of taking the inverse Fourier transform (IFT) of the logarithm of the estimated spectrum of a signal. The word "cepstrum" is derived by exchanging the two halves of the word "spectrum". (Bogert et al., 1963) describe it as "the power spectrum of the logarithm of the power spectrum". As with the WT, the original application of this method is the detection of echoes in seismic signals. Operations on cepstra are labelled quefrency analysis, liftering, or cepstral analysis.

The Park vector method is a relatively new technique, which is applied in the diagnosis of rotor faults, inter turn stator faults, and unbalanced supply voltage (Ourici et al., 2012). An undamaged machine theoretically shows a perfect circle when plotting the two axes, namely the active stator current and the reactive stator current (d, q), obtained from the Park transform. An unbalance due to turn faults may result in a more elliptic representation of the plot giving a clear indication of a motor fault.

After the analysis stage of the digital signal processing, a decision making algorithms take place. The most common ones include the category of statistical classification algorithms which solve the problem of identifying to which of a set of categories some new set belongs, and the category of intelligent methods like artificial neural networks (ANN) (Ourici et al., 2012) and fuzzy logic (Benbouzid et al., 2001; Siddique et al., 2003). These methods will not be discussed in this paper as the topic is too broad.

Instrumentation apparatus

Numerous tools exist regarding the signature analysis both in terms of the vibration and of the MCSA measurements. Some commercial tools exist for vibration measurement, such as the portable Fluke 810 Vibration Tester (worth 9000 EUR), Fluke 805 Vibration Meter (2000 EUR), MIDE Shock & Vibration Accelerometer Loggers (about 850 – 1700 EUR), and for current signature, power quality and motor analysis, such as IRIS Power MDSP3 that detects rotor cage winding faults including broken rotor bars, cracked shorting rings and unequal air gaps (5000 EUR), Fluke 438-II (8500 EUR) or SEMAPI Test-I-Go (12000 EUR). All mentioned tools are very high-quality, powerful, portable, and versatile solutions but for some users and cases they are quite pricey. On the other hand, very low-cost and even open-source solutions exist, such as the Arduino microcontroller platform equipped with the corresponding accelerometer, Hall effect or current probes whose price can be as low as 50 EUR, or the TI MSP432 ARM MCU that is powerful enough to do calculations in real time. The high-end of low-cost solutions includes single board computers (SBC), such as the Raspberry Pi and TI Beagle Bone. Beside the proprietary software solutions, the common software used for offline analysis or plotting the results and taking a decision is based on mathematical packages, such as Matlab, Scilab or Octave, and some popular programming languages as Python and its libraries Numpy, Scipy and Matplotlib.

Since the data processing path can be too long and thus significantly slow, nowadays, programmable logic devices become more and more common, such as the Field Programmable Gate Arrays (FPGAs). Because these integrated circuits don't have hard logic architecture (ALU, registers, etc.) but only logic gates and memory, they are capable of implementing parallel running algorithms. It makes it possible to embed the signal conditioning, analog to digital conversion, signal decomposition (FFT or WT), and an artificial neural network onto a single device. This way, a true real time data processing and decision making can be done.

Conclusions

A number of diagnostic methods exist for identifying different failure modes of electric motors, such as mechanical vibration control, thermal imaging, acoustic monitoring, etc., but most of these methods require expensive sensors or interference in the design of electric motors. It is well known that the various types of damage affect the shape of the current. This allows it to be analysed in a sensorless and non-invasive way which is mainly done by performing Motor current signature analysis (MCSA) or Wavelet Transform (WT) technique. The analysis of the current profile is done by observing its harmonic spectrum and searching for typical frequencies (artifacts), as is the case with the mechanical vibration analysis. If there is a fault, harmonics emerge that are not typical for the healthy machine. This method allows early detection of failures such as increased risk of short circuit, winding disconnection, eccentricity or vibrations due to damaged bearing or load abnormalities. The discussed techniques make it possible to transform the maintenance process from reactive to preventive to predictive one. In this way, it is possible to implement a planned instead of an emergency repair, which is of utmost importance in the production. This makes the topics discussed in the research paper relevant, practical, and with a good potential economic impact.

References

Agoston, K. Vibration Detection of the Electrical Motors using Strain Gauges. 9th International Conference Interdisciplinarity in Engineering, INTER-ENG 2015, 8-9 October 2015, Tirgu-Mures, Romania, Procedia Technology 22, 2016. - 767–772, doi:10.1016/j.protcy.2016.01.037

Allbrecht, P., Appiarius J., McCoy, R., Assessment of the Reliability of Motors in Utility Applications-Updated. IEEE transactions on Energy Conversion, Vol. 1, No. 1,1986.

Arashloo, R. Salehi, A. Jalilian, Design, Implementation and Comparison of Two Wavelet Based Methods for the Detection of Broken Rotor Bars in Three Phase Induction Motors. 1st Power Electronic & Drive Systems & Technologies Conference, PEDSTC, 2010. - 345–350.

Benbouzid, M., Nejjari, H., A Simple Fuzzy Logic Approach for Induction Motors Stator Condition Monitoring. IEEE, 2001.

Bogert, B., Healy, M., Tukey, J., The Quefrency Alanysis of Time series for Echoes: Cepstrum, Pseudo-Autocovariance, Cross-Cepstrum, and Saphe Cracking. In: Proc. of the Symp. on Time Series Analysis, (Ed. M. Rosenblatt), Wiley, NY, 1963.

Bonnett, A. Root Cause AC Motor Failure Analysis with a Focus on Shaft Failures, IEEE Transactions on Industry Applications, Vol. 36, No. 5, 09/10, 2000.

Ece, D., Gerek, O., Induction Motor Fault Diagnosis Via Current Analysis on Time Domain, Proc, 17th IEEE Int. Conf., Signal Processing and Communications Applications, 2009. - 488-491.

IEEE Report, Report of Large Motor Reliability Survey of Industrial and Commercial Installations, Part I. IEEE Transactions on Industry Applications, Vol. IA-21, No. 4, 07/08, 1985.

IEEE Std. 493-1997, IEEE Recommended Practice for The Design of Reliable Industrial and Commercial Power Systems, Appendix H. 1997.

Karmakar, S., Chattopadhyay, S., Mitra, M., Sengupta, S., Induction Motor Fault Diagnosis Approach through Current Signature Analysis. ISBN 978-981-10-0623-4, Springer, 2016.

Marcelo, C., Fossatti, J. P., Terra, J. I., Fault diagnosis of induction motors based on FFT. IntechOpen, In book: Fourier Transform - Signal Processing, DOI: 10.5772/37419, April 2012, Available from: https://www.intechopen.com/books/fourier-transform-signal-processing/fault-diagnosis-of-induction-motors-based-on-fft.

Mehala, N. Current Signature Analysis for Condition Monitoring of Motors. International Journal of Electronics and Computer Science Engineering, ISSN 2277-1956/V1N3, 2012. - 1629-1633.

Menacer, A. et al., Stator current analysis of incipient fault into asynchronous motor rotor bars using Fourier fast transform. J. Electr. Eng. 55 (5–6), 2004. - 122–130.

Mohanty, A. Machinery Condition Monitoring Principles and Practices. Indian Institute of Technology, CRC Press, ISBN-13: 978-1-4665-9305-3, 2015.

Neelam, Mehala. Condition Monitoring and Fault Diagnosis of Induction Motor using Motor Current Signature Analysis. Ph.D. Thesis, Electrical Engineering Department, NIT Kurukshetra, Oct. 2010.

Ourici, A., Ouari, A., Park's Vector Approach to detect an inter turn stator fault in a doubly fed induction machine by a neural network. Computer Science & Information Technology, DOI 10.5121/csit.2012.2503, 2012.

Pons-Llinares, J., Antonino-Daviu, J., Roger-Folch, J., Morinigo-Sotelo, D., Duque-Perez, O., Eccentricity Diagnosis in Inverter Fed Induction Motors via the Analytic Wavelet Transform of Transient Currents. XIX International Conference on Electrical Machines (ICEM), 2010. - 1-6.

Randall, R. A History of Cepstrum Analysis and its Application to Mechanical Problems, Mechanical Systems and Signal Processing. ISSN 0888-3270, Volume 97, December 2017.

Siddique, A., Yadava, G., Singh, B., Applications of Artificial Intelligence Techniques for Induction Machine Stator Fault Diagnostics: Review. IEEE, 2003.

Siddiqui, K., Giri, V., Broken Rotor Bar Fault Detection in Induction Motors using Wavelet Transform. Int. Conf Proc, IEEE, Computing, Electronics and Electrical Technologies [ICCEET], Chennai, India, March 2012. - 1-6.

Siddiqui, K., Sahay, K., Giri, V. Health Monitoring and Fault Diagnosis in Induction Motor - A Review. International Journal of Advanced Research in Electrical, Electronics and Instrumentation Engineering, Vol. 3, Issue 1, January 2014, ISSN 2320-3765. - 6549-6565.

Treetrong, J. Fault Detection of Electric Motors Based on Frequency and Time-Frequency Analysis using Extended DFT. International Journal of Control and Automation, Vol. 4 No. 1, March 2011.

INFORMATION MODEL FOR CITY MONITORING BY SMART LIGHTING

Mila Ilieva-Obretenova

University of Mining and Geology "St. Ivan Rilski", 1700 Sofia, milailieva@abv.bg

ABSTRACT. City monitoring includes a variety of services like informing for parking places, pedestrian planning, situational awareness (access to photos, audio, video), environmental planning, traffic planning. This could be achieved by improving the Smart Lighting technology. Smart Lighting was designed for energy efficiency. The new aim is safety for the citizens. It is reached by embedding different sensors and cameras in street lighting.
This paper offers an information model for city monitoring through Smart Lighting. The model is designed for user interface developers, city authorities, and citizens. The hypothesis is as follows: the description of the objects containing the data should be represented as a software model. It is sufficient that the software of each component be detailed with elements up to the level of service logic. The model should possess the following features: The components containing the data are represented as physical entities. For each component, software is represented as a set of functions. Functions are grouped according to the areas of open system interconnection (OSI): configuration, security, maintenance, accounting, and performance. The focus is on the configuration area because it contains the data on the execution of the service logic. Software components in the configuration area are detailed up to attributes and operations that direct the logic to the next element of its execution. Design methodology for the information model includes defining of classes of managed objects for service components. The result is an information model design for city monitoring by Smart Lighting. This is a model of management services and their components. The object-oriented method is used. The classes of managed Objects are defined according to managed units. The Guidelines for the Definition of Managed Objects (GDMO) from the Network Management Standards are followed. The UML (Unified Modeling Language) is used for the model description. On this stage, objects are represented with names, "Part of"- relationships, associations, attributes, and operations. On the next stage, new attributes and operations will be added to the objects managed. With this level of defining, the model is a good base for the development of user interface. The model is also applicable for monitoring the processes in an underground mine. Lighting with sensors and cameras could be applied there and the same services could be provided: employee planning, collecting information for a specific location, environmental planning, retrieving event information.

Keywords: Information model, city monitoring, Smart Lighting, safety for the citizens

ИНФОРМАЦИОНЕН МОДЕЛ ЗА НАБЛЮДЕНИЕ НА ГРАД ЧРЕЗ УМНО УЛИЧНО ОСВЕТЛЕНИЕ (SMART LIGHTING)
Мила Илиева-Обретенова
Минно-геоложки университет "Св. Иван Рилски", 1700 София, milailieva@abv.bg

РЕЗЮМЕ. Наблюдението на един град включва разнообразие от услуги като информиране за свободни паркоместа, насочване на пешеходци, информация за дадено място (достъп до снимки, видео), наблюдение на параметрите на околната среда, информиране за трафика. Това може да се постигне чрез усъвършенстване на технологията Smart Lighting. Първоначалната цел на Smart Lighting е постигане на енергийна ефективност. Новата цел е сигурност за гражданите. Тя се постига чрез вграждане на различни сензори и камери в уличните лампи.
Статията предлага информационен модел за наблюдение на град чрез Smart Lighting. Моделът е предвиден за разработчици на потребителски интерфейс, органите на реда и гражданите. Хипотезата е следната: описанието на обектите с данните трябва да представя модел на софтуер. Софтуерът на всеки компонент е достатъчно да се детайлизира с елементи до ниво логика на услуга. Моделът трябва да притежава следните качества: Компонентите с данните се представят като физически единици. За всеки компонент се представя софтуер като множество от функции. Функциите се групират в съответствие с областите за взаимодействие на отворени системи (OSI): конфигурация, защита, поддържане, таксуване и технически характеристики. Фокусираме върху област конфигурация, защото тя съдържа данните за изпълнението на логиката на услугите. Софтуерните компоненти в област конфигурация се детайлизират до атрибути и операции, които насочват логиката към следващия елемент при нейното изпълнение. Методологията за проектиране на информационния модел включва дефиниране на класове управлявани обекти за компонентите на услугите. Резултатът е проект на информационен модел за наблюдение на град чрез Smart Lighting. Това е модел на услугите за управление и техните компоненти. Използван е обектно-ориентиран метод. Класовете управлявани обекти са дефинирани в съответствие с управляваните единици. Следвани са Препоръки за дефиниране на управлявани обекти (GDMO) от стандартите за управление на мрежи. За описание на модела е използван UML (Унифициран език за моделиране). На този етап компонентите на услугите са представени чрез имена, отношения „Част от", асоциации, атрибути и операции. На следващия етап ще се добавят нови атрибути и операции към управляваните обекти. С това ниво на дефиниране моделът представлява добра основа за разработване на потребителски интерфейс. Моделът е приложим и за наблюдение на процесите в подземна мина, където могат да се приложат лампи със сензори и камери, и могат да се предложат аналогични услуги като насочване на служителите, събиране на информация за дадено място, наблюдение на параметрите на средата, информиране за събития.

Ключови думи: информационен модел, наблюдение на град, Smart Lighting, сигурност за гражданите

Introduction

City monitoring includes a variety of services, like informing for parking places, pedestrian planning, situational awareness (access to photos, audio, video, and other media), environmental planning, traffic planning, etc. This could be achieved by improving Smart Lighting technology. Initially, Smart Lighting was designed for energy efficiency. The new aim is safety for the citizens. It is achieved by embedding different sensors and cameras in street lighting (Velinov, 2018). Nowadays, a few cameras are located in big cities in Bulgaria: Sofia "Orlov most", Sofia "Serdika" Underground station, Plovdiv "International Fair", Varna "Hristo Botev Boulevard", Bourgas "Stefan Stambolov Boulevard", Berkovitsa

"City center Berkovitsa", Pamporovo "Ski track Snezhanka", Pamporovo "Ski track Studenets", and Chepelare "Mechi chal" (https://nova.bg/camera , 2018). Smart Lighting services offer a lot of details for the users (https://developer.currentbyge.com/cityiq , 2018).

The Parking Planning service provides parking metadata that is collected from intelligent nodes installed on all street lights along public roadways or in parking lots. Each time a vehicle enters or leaves a parking space, a timestamped event is created and stored in the cloud. This data can be obtained from a single sensor or a group of sensors and can provide valuable insights about parking activity in a given region. The data can also be used to improve traffic and parking convenience.

The Pedestrian Planning service provides pedestrian metadata that is collected from intelligent nodes installed on all street lights along public roadways or in parking lots. As pedestrians pass by these sensors, the service creates and stores a timestamped event, counting each event. This data can be obtained from a single sensor or a group of sensors, to provide insights to city officials and local businesses about pedestrian movement in a given region. The data can also be used to enhance safety and convenience.

The Situational Awareness service provides access to images, video, and other media collected from intelligent nodes installed on all street lights along public roadways. You can retrieve media on demand (streaming data) or historical media data. Examples of use cases for these images and videos include enhancing situational awareness, improving traffic flow, and verifying where vehicles are parked. The media can be requested using a date range beginning with near real-time and ending based upon data availability. This data can be obtained on-demand directly from a single sensor or node, as needed, to provide insights to city officials that enhance awareness. This service can be used in concern with other "Intelligent Cities" services to address a variety of use cases.

The Environmental Planning service provides environmental sensor data collected from intelligent nodes installed on all street lights along public roadways. This data can be obtained from a single sensor or a group of sensors, as needed, to provide timely environmental information to city officials that directly affect urban dwellers and their activities.

The Traffic Planning service provides vehicle metadata collected from intelligent nodes installed on all street lights along public roadways. As vehicles pass by these sensors, information such as speed, direction lane use, and volume (counts) are collected and stored with a time-stamp in the cloud. The data can be viewed from any number of nodes in a given region and can present both historical and near real-time information. The density, range, and flexibility of this sensor data can provide insights into traffic patterns at different intervals. Along with facilitating the planning for future safety and convenience enhancements, the data can reveal opportunities to optimise traffic flows.

Scope

The paper aims to offer an information model for city monitoring by Smart Lighting. The model is designed for user interface developers, city authorities, and citizens.

Thesis

The model should include descriptions of management services in Smart Lighting and their components.

Hypothesis

The description of the management services in Smart Lighting and their components should include software definitions. Each component's software is sufficiently defined with elements of the level of managed object. The model should possess the following features: management service components are represented as physical entities; software as a set of functions is represented for each component; functions are grouped according to OSI (ISO/IEC/IS, 1989) areas: configuration, security, maintenance, accounting, and performance; focusing on a configuration area because it contains the data for service logic execution; software components in a configuration area are detailed up to attributes and operations that direct the logic to the next element of its execution.

Methodology

The methodology for the design of an information model for city monitoring by Smart Lighting includes definitions of managed objects classes for services provided to subscribers and providers. Definitions are represented verbally and by UML (Unified Modelling Language) diagrams (Fowler, 2004; Gentleware, 2018). UML diagrams are classified into two types: behavior diagrams and structure diagrams. Class diagrams, a type of structure diagrams, are appropriate for the description of city monitoring management. A class diagram describes types of objects in the system and the different kind of static relationships between them. Diagrams also show "Part of"-relationships, features, and operations of classes and the limits of the way in which the objects are connected. The "Part of"-relationship is shown with a rhombus and a line. Features are one term, but they are represented with two quite different notations: attributes and associations. The notation for an attribute describes a distinct feature like a text (second row) in a rectangle, envisaged for a class. The association is a directed line between two classes and its direction is from class-source to class aim. A feature's name is set on the aimed end of the association with its majority. The end-aim of the association is connected to the class which is the feature's type. The majority of a feature is a note for how many objects could complete the feature. Operations are actions which a class could realise. Obviously, they correspond to the methods of a class. There is a distinction between Operation and Method, however. The operation is the name used for a method – a declaration of a procedure. The method is a code which the procedure consists of. Operation and Method are different by polymorphism. The model has the impact of a similar model for telecommunications management (Magedanz, 1994).

Results

In this section, the designed model for management in Smart Lighting is represented: a model of management services and their components. The object-oriented method is used. The classes of managed objects are defined according to managed units. The Guidelines for the Definition of Managed Objects (GDMO) (ISO/IEC/IS, 1989) from the Network Management Standards are followed. The UML is used for model description. At this stage, objects are represented with names, "Part of"-relationships, associations, attributes, and operations.

Managed Objects classes for service configuration in Smart Lighting

Managed Object (MO) **SConfiguration** represents a service configuration needed for the provider or tailored on special order for a subscriber. MO **SComponent** contains all parts of a service which must be distributed on the network infrastructure. MO **Template** represents the description of the entry format for each service in a Smart Lighting network. MO **Resource** represents the description of a specialised resource (camera, sensor) used by a specific service. MO **Program** represents the description of a program with service logic. MO **TriggerInfo** represents the description of a trigger needed for service execution direction. MO **SDFData (Service Data Function Data)** represents an entry for a specific service subscriber. MO **SubsConfiguration** represents the subscriber's requirements for the configuration of the provided services. MO **ParkPlanning** contains the description of the Parking Planning service. MO **PedPlanning** contains the description of the Pedestrian Planning service. MO **GetMedia** contains the description of the Situational Awareness service. MO **EnvPlanning** contains the description of the Environmental Planning service. MO **TrafficPlanning** contains the description of the Traffic Planning service. Fig. 1 shows the UML diagram of Managed Objects classes for service configuration in Smart Lighting.
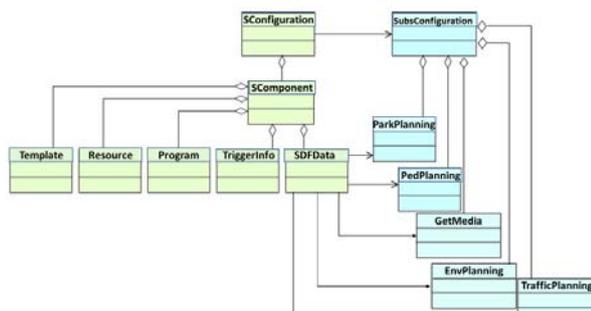

Fig. 1: UML diagram of Managed Objects classes for service configuration in Smart Lighting

Attributes and operations of Managed Objects classes for service configuration in Smart Lighting

MO **Resource** has the following attributes:
Attribute **Camera** describes the unique Identifier for each camera. Attribute **Sensor** describes the unique Identifier for each sensor.

MO **Program** has the following attributes:
Attribute **AssetUID** describes the Identifier for a unique asset. This is a key attribute by which information query for a specific asset is performed. Attribute **LocationUID** describes the

Identifier for the unique location in an observed area. This is a key attribute by which an event query in a specific area is performed. Attribute **EventType** describes the Identifier of type events. This is a key attribute by which a pedestrian query by number, direction, and speed is performed. Attribute **TimeStamp** describes the actual data and time when the event occurs. Attribute **GeoCoordinates** describes the GPS coordinates of the four angles of the parked vehicle. Attribute **ObjectID** describes the unique Identifier (plate number) of a specific vehicle. Attribute **VehicleType** describes the type of specific vehicle i.e. vehicle, truck, bus, building machine, agricultural machine. Attribute **DirectionUnit** describes the measurement unit for pedestrian direction, i.e. degree. Attribute **SpeedUnit** describes the measurement unit for pedestrian speed, i.e. m/s. Attribute **Unit** describes the unit, by which specific magnitude is measured, i.e. K, HPa, south-southwest, %. Attribute **PowerOf10** describes the factor of 10, i.e. -1 (10^{-1}). The measure in K multiplies with 10^{-1}, i. e. 2700 x 10^{-1} K=270 K, 270 K-273 15=- 3,15° C. Attribute **ImagePollUrl** describes the link which shows photos captured from a specific device. Attribute **VideoPollUrl** describes the link which shows video captured from a specific device. Attribute **Status** describes the status in response to a request for video or photos. The status could be INPROGRESS when the request is in process or SUCCESS when the request is completed. Attribute **MedialD** describes the Identifier used for a specific type media or the Identifier for a specific node.

Attribute **MediaType** describes a specific media type: IMAGE provides a list of images in JPG, PNG, and GIF formats. Depending on the position of the camera, it will return the best resolution image available: either 320x240 for black and white or 1920x1080 for color; VIDEO provides a list of videos in H.264 format. Attribute **MediaLogID** describes the Identifier for each entry in the list. Attribute **MediaFileName** describes the file name of the captured media. Attribute **MediaTimeStamp** describes the time when the media was captured from the node. Attribute **ExternalRefID** describes the Identifier of an external pointer. Attribute **EntryTimeStamp** describes the time when the captured media was entered in the database. Attribute **Size** describes the maximum number of records to return per page; if none specified, the default value of 2 is used automatically. Attribute **Number** indicates the page number, the default is 0.

MO **Program** has the following operations:
Operation **Counter_direction** calls the procedure for computing of a pedestrian's direction in interval west, northwest, north, northeast or east direction (270° - 0° - 90). Operation **Counter_dir_pedCount** calls the procedure for counting the serial number of a pedestrian who moved in a specific direction (the same as in Counter_direction). Operation **Counter_dir_speed** calls the procedure for computing the average speed of a pedestrian in a specific direction (the same as in Counter_direction). Operation **Direction** calls the procedure for computing a pedestrian's direction in interval west, southwest, south, southeast, and east direction (270° - 180° -90°). The procedure calculates the direction opposite the one in Counter_direction. Operation **PedCount** calls the procedure for counting the serial number of a pedestrian who moved in the direction opposite the one in Counter_direction. Operation **Speed** calls the procedure for computing the

average speed of a pedestrian opposite the one in Counter_direction. Operation **Counter_dir_vehicleCount** calls the procedure for counting the serial number of vehicles in a specific direction. (As with the pedestrians, the movement is calculated in two directions, the serial number of the vehicles in a specific direction is counted, and the average speed in this direction is calculated.) Operation **VehicleCount** calls the procedure for counting the serial number of vehicles in the direction opposite the one in Counter_dir_VehicleCount.

Operation **Max** calls the procedure for determining the maximum value of a specific magnitude for a defined period, i.e. humidity, wind direction, pressure, and temperature. Operation **Mean** calls the procedure for computing the mean value for a defined number of digits. Operation **Median** calls the procedure for determining the median in a defined interval of values. (The median is the value separating the higher half of a data sample from the lower half.) Operation **Min** calls the procedure for determining the minimum value of a specific magnitude for a defined period. Operation **Sort** calls the procedure for sorting values of attributes: Asset UID, Media File Name, Media Time Stamp, Media Type. Operation **Duration** calls the procedure for counting the duration of an event. Operation **SortDir** calls the procedure for sorting in an ascending or a descending order. Operation **Ignore Case** calls the procedure for determining whether the request is interrupted or not (for service Get Media). Operation **getAssetUIDrtd** calls the procedure for capturing different events registered by a unique device in real time. Operation **getLocationUIDrtd** calls the procedure for capturing different events for a unique location in real time. Operation **getAssetUIDhd** calls the procedure for capturing different events registered by a unique device as historical data. Operation **getLocationUIDhd** calls the procedure for capturing different events for a unique location as historical data.

MO **TriggerInfo** has the following attributes:
Attribute **Pkin** indicates the event of parking enter. Attribute **Pkout** indicates the event of parking escape. Attribute **Pedevt** indicates a pedestrian appearance. Attribute **Tfevt** indicates the event of traffic appearance (vehicle). Attribute **Humidity** indicates the event of humidity counting in an exact moment. Attribute **Orientation** indicates the event wind orientation counting in an exact moment. Attribute **Pressure** indicates the event of pressure counting in exact moment. Attribute **Temperature** indicates the event of temperature counting in an exact moment. Attribute **Click** indicates the event of click on a link.

MO **SConfiguration**, MO **SComponent**, MO **Template**, MO **SDFData**, MO **SubsConfiguration**, MO **ParkPlanning**, MO **PedPlanning**, MO **TrafficPlanning**, MO **EnvPlanning,** and MO **GetMedia** are described only by name and number.
Table 1 shows theattributes of MO **Resource.** Table 2 shows the attributes and operations of MO **Program.** Table 3 shows the attributes of MO **TriggerInfo.**

Table 1.
Attributes of MO Resource

Resource
Camera[1] : String
Sensor[1] : String

Table 2.
Attributes and operations of MO Program

Program
AssetUID[1] : String
LocationUID[1] : String
EventType[8] : String
TimeStamp[1] : String
GeoCoordinates[4] : List
ObjectID[1] : String
VehicleType[5] : String
DirectionUnit[1] : String
SpeedUnit[1] : String
Unit[4] : String
PowerOf10[1] : String
ImagePollUrl[1] : String
VideoPollUrl[1] : String
Status[2] : String
MediaID[1] : String
MediaType[2] : String
MediaLogID[1] : String
MediaFileName[1] : String
MediaTimeStamp[1] : String
Size[0..1] : int
Number[1] : int
Counter_direction(…): void
Counter_dir_pedCount(…): void
Counter_dir_speed(…): void
Direction(…): void
PedCount(…): void
Speed(…): void
Counter_dir_vehicleCount(…): void
VehicleCount(…): void
Max(…): void
Mean (…): void
Median(…): void
Min(…): void
Sort(…): void
Duration(…): void
SortDir(…): void
IgnoreCase(…): void
getAssetUIDrtd(AssetUID, EventType): EventType1, EventType2
getLocationUIDrtd(LocationUID, EventType): EventType1, EventType2
getAssetUIDhd(AssetUID, EventType, StartTime, EndTime): void
getLocationUIDhd(LocationUID, EventType, StartTime, EndTime, size, page): void

Table 3.
Attributes of MO TriggerInfo

TriggerInfo
Pkin[1] : String
Pkout[1] : String
Pedevt[1] : String
Tfevt[1] : String
Humidity[1] : String
Orientation[1] : String
Pressure[1] : String
Temperature[1] : String
Click[1] : String

The chosen granularity for the description of the managed objects gives an idea of the work volume which should be completed in the development phase. The proposed model represents an abstract description of service management in Smart Lighting. Only the functional area Configuration is considered here. In comparison with other models, i.e. for telecommunications management, attributes and operations for the managed objects are also listed here. The disadvantage could be found in the limited number of details.

Conclusion

The paper represents the design of an information model for city monitoring by Smart Lighting. The model corresponds to the responsibilities of the Service Subscriber and Service Provider actors. The classes of Managed Objects are defined which represent the managed resources for the network elements following the object-oriented method. The classes of Managed Objects are organised in a hierarchy which shows the correlation between them and relates to easier implementation. At this stage, the software for management services is detailed with elements up to the level service components. The chosen classes of Managed Objects are defined by name, "Part of"-relationships, associations, attributes, and operations. At the next stage, new elements could be added to the functional area Configuration and details could be developed for other functional areas. Nevertheless, the model is a good basis for prototype development of user interface.

The model is also applicable for monitoring the processes in an underground mine where lighting with sensors and cameras could be installed and where similar services could be provided, like employee planning, information capturing for specific location, environmental planning, events information, etc.

References

Fowler, M. UML Distilled: A Brief Guide to the Standard Object Modeling Language. 3rd ed. Addison-Wesley Professional, 2004.

Gentleware AG, Poseidon for UML CE 8.0, www.gentleware.com (accessed 2018).

https://nova.bg/camera (accessed 2018).

ISO/IEC/IS 7498-4 CCITT Recommendation X 700: Information Processing – Open Systems Interconnection – Basic Reference Model – Part 4: Management Framework, 1989. - 19-30.

Magedanz, T. An integrated management model for intelligent networks, München, Wien: Oldenburg, 1994.

Redefining the future, https://developer.currentbyge.com/cityiq (accessed 2018);

Velinov, K. et al., Web-based Database for Luminaries and Application in Street Lighting, Proceedings, VII Balkan Conference on Lighting BalkanLight 2018, Sofia, 2018. - 201-204.

DETERMINING THE NATURAL FREQUENCY ON A STEPPED SHAFT WITH A TRANSITIONAL CURVED SECTION

Gergana Tonkova[1] , Violeta Trifonova–Genova[2]

[1]*University of Mining and Geology "St. Ivan Rilski", 1700 Sofia, g_pis @abv.bg*
[2]*University of Mining and Geology "St. Ivan Rilski", 1700 Sofia, violeta.trifonova@yahoo.com*

ABSTRACT. The article discusses the topic of determining the natural frequency in a specific shaft. The shaft consists of three segments. The second one is fulfilled with a rounded radius. In the process of operation, the shaft acts by its natural vibrations. An approximate method is applied for their determination. According to the method, each segment of the shaft is divided into portions along its length. The computational scheme is a free beam, propped up with two camps at its ends. It is loaded with concentrated forces whose values are equal to the weights of the individual portions. Their application points are in the middle of the width of the portions selected by the package engineer. The displacements in the points of this simple beam are calculated by the differential equation of the elastic line. The solution to this equation is realised through its numerical integration. For the curved segment, an algorithm is applied to determine the radii, weights and stiffness. For the entire shaft, the reaction forces and bending moments in the application points of the forces are obtained. The inclines of the elastic line and the displacements in these points are calculated by numerical integration. The presented solution to determining the natural frequency of shaft with a transitional section confirms the validity of the analytical expressions of the above values.

Keywords: stepped shaft with a curved segment, natural frequency, approximated method, differential equation of the elastic line.

ОПРЕДЕЛЯНЕ НА ЧЕСТОТАТА НА СОБСТВЕНИ ТРЕПТЕНИЯ НА СТЪПАЛЕН ВАЛ С ПРЕХОДЕН УЧАСТЪК
Гергана Тонкова[1], Виолета Трифонова – Генова[2]
[1] *Минно-геоложки университет "Св. Иван Рилски", 1700 София, g_pis @abv.bg*
[2] *Минно-геоложки университет "Св. Иван Рилски ", 1700 София, violeta.trifonova@yahoo.com*

РЕЗЮМЕ. В статията се разглежда въпросът за определяне на собствените трептения в конкретен вал. Той се състои от три участъка, като вторият е изпълнен със закръгление с определен радиус. В процеса на работа върху вала действат собствени трептения. За тяхното определяне е приложен приблизителен метод. Според него всеки участък от вала се разделя на сегменти по дължината му. Изчислителната схема е греда, подпряна с два лагера в краищата й. Тя е натоварена със съсредоточени сили, чиито стойности са равни на теглата на сегментите. Приложните им точки са в средите на избраните от конструктора ширини на сегментите. Преместванията в точки от простата греда се определят чрез диференциалното уравнение на еластичната линия. Решението на това уравнение се реализира посредством численото му интегриране. За преходния участък е приложен алгоритъм за определяне на радиусите, теглата и коравините на сегментите. За целия вал са получени опорните реакции и огъващите моменти в приложните точки на силите. Чрез числено интегриране са получени наклоните на еластичната линия и преместванията в същите точки. Представеното решение за определяне на честотата на собствените трептения във вал с преходен участък потвърждава верността на аналитичните изрази за описаните по-горе величини.

Ключови думи: стъпален вал, собствени трептения, приблизителен метод, диференциално уравнение на еластична линия.

Introduction

The natural frequency of a stepped shaft is the object of investigation by specialists calculating the shafts. The approximate method is well known. It applies numerical integration to resolve the differential equation of the elastic line (Feodosev, 1965). Refining this method, an algorithm for the transition section of the shaft is added (Trifonova-Genova et al., 2017). This algorithm consists of eleven steps. They include formulae by which the current diameter and the stiffness of each section are obtained. The main objective of this article is to apply this algorithm to a concrete stepped shaft with a curvilinear transition.

Methods

1. Formulation of the problem

A stepped cylindrical shaft is presented at Figure 1 (Anchev et al., 2011). The lengths of three sections are: $l_1 = 12\ cm$, $l_2 = 0.5\ cm$ and $l_3 = 5.5\ cm$. The radius of the transition zone is: $r = 0.5\ cm$, the diameters of the first section and the beginning of the second and the third section of the relevant shaft are, respectively, $D_1 = 5.6\ cm$, $D_{2,o} = 5.0\ cm$, and $D_3 = 4.0\ cm$.

2. Method for determining the of internal forces

To determine the natural frequency, the approximate method is applied (Feodosev, 1965). According to it, the shaft is divided into portions with sized widths in the first and the third sections: $\Delta x_1 = \Delta x_3 = 1\,cm$, and in the second section - $\Delta x_2 = 0.1\,cm$.
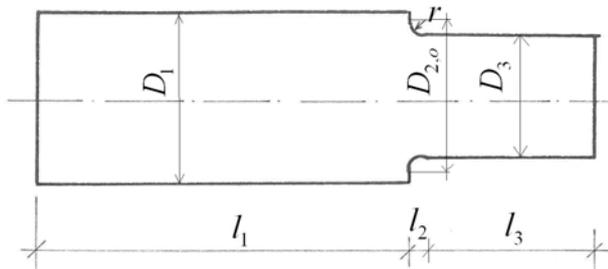

Fig.1. Stepped shaft with a curved segment

Current diameter $D_{2,i}$ in the second segment (section)

For determining this diameter for each segment of this section, the algorithm of (Trifonova-Genova et al., 2017) is applied. For given values of arrows, the chords and the diameters are calculated. The results are given in Table 1.

Table 1.
Diameters of a segment with a transitional curved section

Point of segment	f_i mm	a_i mm	$D_{2,o}$ mm
13	0.5	4.4	46
14	1.5	7.5	43
15	2.5	8.7	41
16	3.5	9.5	40
17	4.5	10.0	40

Stiffness of the segment of the shaft

The Young's modulus of shafts is taken by (Kisiov, 1978) ($E = 1.98.10^4\,\kappa g/cm^2$). With a known diameter of each segment of the shaft, the moment of inertia is calculated. The stiffness of the segments in the three sections are given in Table 2.

Table 2.
Stiffness of the segments of the shaft

Section	points	$EJ_y\,10^6\,[kgcm^2]$
1	1-12	95.536
2	13	43.516
2	14	33.227
2	15	27.464
2	16	24.881
2	17	24.881
3	18	24.869
3	19-23	24.869

Weight of the segments

The volumetric weight of the material of the shaft is $\gamma = 7.8.10^{-3}\,kg/cm^3$, but the weight of the segments is given in Table 3.

Table 3.
Forces

Section	points	$P_i^I\,[kg]$
1	1-12	0.1921
2	13	0.0128
2	14	0.0111
2	15	0.0105
2	16	0.0100
2	17	0.0098
3	18	0.0480
3	19-23	0.0981

The segment with the principal point number 18 has a width of $0.5\,cm$. This is the reason why the weight is half of the weight of the segments to follow.

The reactions of a support

The computational scheme is a free beam loaded by weights. The values of the first iteration are given in Table 3. The reactions of support are calculated with the methods of statics (Vulkov, 2004; Vulkov et al, 2013). Their values are: $A^I = 1.635\,kg$, $B^I = 1.262\,kg$.

Bending moment diagram

The moments in the individual points are determined with the methods of the resistance of the materials (Vulkov, 2011). The values of first iteration are given in Table 4.

Table 4.
Bending moments

point	M_i^I $[kgcm]$	point	M_i^I $[kgcm]$
A	0	13	5.758
1	0.818	14	5.689
2	2.261	15	5.620
3	3.512	16	5.550
4	4.571	17	5.478
5	5.437	18	5.275
6	6.112	19	4.696
7	6.595	20	3.827
8	6.885	21	2.860
9	6.984	22	1.794
10	6.890	23	0.631
11	6.604	B	0
12	6.126		

3. Natural frequency

Natural frequency is obtained through the following relations. In the beginning, the following proportion of the bending moments for each point is calculated from Table 4 to the stiffness from Table 2. This proportion is multiplied by the width of each segment. With the method of numerical integration, the slope of an elastic line is obtained (Feodosev, 1965).

The displacements w_i are represented by an equation which has two coefficients. They are obtained by the boundary conditions: $w_1(0) = 0$, $w_n(l) = 0$. For the concrete shaft, these coefficients are: $C_1^I = -0.5827.10^{-6}$ and $C_2^I = 0$. The displacement for the concrete position x_i of point i in the computational scheme is determined.

Finally, two multiplications are composed. The first includes the displacement and the force at each point. The second involves the displacements elevated to the second degree and the force. The values are given in Table 5.

Table 5.
Results of the first iteration

	x_i	w_i^I	$P_i^I w_i^I$	$P_i^I\left(w_i^I\right)^2$
		10^{-6}	10^{-6}	10^{-12}
		$[cm]$	$[cm]$	$[kgcm]$	$[kgcm^2]$
A	0	0	0	0
1	0.5	0.283	0.054	0.015
2	1.5	0.833	0.160	0.133
3	2.5	1.347	0.259	0.348
4	3.5	1.813	0.348	0.631
5	4.5	2.222	0.427	0.948
6	5.5	2.567	0.493	1.265
7	6.5	2.843	0.546	1.552
8	7.5	3.046	0.585	1.783
9	8.5	3.177	0.610	1.939
10	9.5	3.236	0.622	2.011
11	10.5	3.225	0.620	1.998
12	11.5	3.151	0.605	1.907
13	12.05	3.070	0.039	0.120
14	12.15	3.053	0.034	0.103
15	12.25	3.035	0.032	0.096
16	12.35	3.014	0.030	0.091
17	12.45	2.991	0.029	0.088
18	12.75	2.903	0.139	0.405
19	13.50	2.577	0.253	0.652
20	14.50	1.989	0.195	0.388
21	15.50	1.285	0.126	0.162
22	16.50	0.510	0.050	0.025
23	17.50	0.291	0.029	0.008
B	18.00	0	0	0
Σ			6.228	16.671

After summing the last two columns, the square of the natural frequency is calculated: $\left(\omega^I\right)^2 = 366,494.10^6 \ s^{-2}$. The natural frequency is $\omega^I = 19.144.10^3 s^{-1}$ by the first iteration of the approximate method (Kisyov, 1978).

The second iteration takes into account that, in process of vibration, the shaft is loaded not only with the force of weight but with the force of inertia as well. From the first approximation, the values of displacements and the square of the frequency are also used. For the second iteration, the force P_i^{II} is calculated according to the formula given in (Trifonova-Genova et al., 2017). After that, the reactions of support, the bending moments, the slope of the elastic line, and the displacements of the points are determined in the computational scheme, as well as both multiplications analogically to the second iterations. The values are given in Table 6.

Table 6.
Results of the second iteration

	x_i	w_i^{II}	P_i^{II}	$P_i^{II} w_i^{II}$	$P_i^{II}\left(w_i^{II}\right)^2$
		10^{-6}		10^{-6}	10^{-12}
		$[cm]$	$[cm]$		$[kgcm]$	$[kgcm^2]$
A	0	0	-	0	0
1	0.5	0.274	0.020	0.006	0.002
2	1.5	0.808	0.060	0.048	0.039
3	2.5	1.311	0.097	0.127	0.166
4	3.5	1.771	0.130	0.230	0.408
5	4.5	2.178	0.159	0.347	0.756
6	5.5	2.523	0.184	0.465	1.172
7	6.5	2.801	0.204	0.571	1.600
8	7.5	3.006	0.219	0.657	1.976
9	8.5	3.139	0.228	0.716	2.246
10	9.5	3.197	0.232	0.743	2.374
11	10.5	3.186	0.231	0.737	2.349
12	11.5	3.109	0.226	0.703	2.186
13	12.05	3.027	0.015	0.044	0.134
14	12.15	3.010	0.013	0.038	0.114
15	12.25	2.991	0.012	0.036	0.106
16	12.35	2.970	0.011	0.034	0.100
17	12.45	2.947	0.011	0.032	0.095
18	12.75	2.858	0.052	0.149	0.426
19	13.50	2.532	0.094	0.239	0.605
20	14.50	1.947	0.073	0.142	0.276
21	15.50	1.255	0.047	0.059	0.074
22	16.50	0.498	0.019	0.009	0.005
23	17.50	0.280	0.011	0.003	0.001
B	18.00	0	0	0	0
Σ				6.135	17.210

The calculation from the first iteration are repeated and the natural frequency is obtained: $\omega^{II} = 18,701.10^3 \ s^{-1}$. The value is compared to the value of the first iteration and a difference of 2.29% is obtained. This is sufficient for the practice accuracy. Therefore, the iterations are terminated and the value is finally chosen.

4. Key Findings

In this article, the approximate method is applied for calculating the value of natural frequency in a concrete shaft with a transitional curvilinear section. The algorithm is applied for this section and the values of diameters and weights are obtained. The successive parameters, like the reactions of the supports, the bending moments, the slopes, and the displacements of points in the free beam are given here. Finally, the natural frequency for two iterations is calculated.

Conclusion

The numerical results of this work confirm the formulae and the algorithm for stiffness in the curvilinear section. They give a more precise solution to the problem of determining the natural frequency in a shaft with a curvilinear section. This is the advantage of the proposed method. It can be extended to shafts with more sections.

No matter how weak the curvature in a curvilinear section is, it is desirable to take it into account in each real shaft.

References

Анчев, А, Ичкова, М. Определяне на коефициента на концентрация на напреженията при опън-натиск по МКЕ. - Известия на ТУ Габрово, т. 42, 2011. - 22-24. (Anchev, A., Ichkova, M. Opredelyane na koefitsienta na kontsentratsia na naprezheniata pri opun–natisk po MKE. – Izvestia na TU Gabrovo, t. 42, 2011. - 22-24.)

Вълков, М. Съпротивление на материалите, част 1 - еластостатика. Изд. къща „Св. Ив. Рилски“, 2011. - 300 с. (Vulkov, M. Suprotivlenie na materialite, chast 1 - elastostatika. Izd. kushta "Sv. Iv. Rilski", 2011. - 300 p.)

Вълков, М. Теоретична механика, част 1 - Статика. Изд. къща „Св. Ив. Рилски“, 2004. - 204 с. (Vulkov, M. Teoretichna mehanika, chast 1- Statika. Izd. kushta "Sv. Iv. Rilski", 2004. - 204 p.)

Вълков, М., Ст. Пулев. Ръководство за решаване на задачи по теоретична механика. Част I. Статика. С., Изд. къща „Св. Ив. Рилски“, 2013. - 133 с. (Vulkov, M., S. Pulev. Rukovodstvo za reshavane na zadachi po teoretichna mehanika. Chast I. Statika. Sofia, Izd. kushta "Sv. Iv. Rilski", 2013. - 133 p.)

Кисьов, И. Съпротивление на материалите. С., ДИ "Техника", 1978. - 594 с. (Kisyov, I. Suprotivlenie na materialite. Sofia, DI "Tehnika", 1978. - 594 p.)

Феодосев, В. И. Съпротивление на материалите. С., Техника, 1965. - 547 с. (Feodosev, V. I. Suprotivlenie na materialite. Sofia, Tehnika, 1965. - 547 p.)

Trifonova-Genova, V., G. Tonkova. One approach for determining natural frequency of a stepped shaft. Journal of mining and geological sciences, vol. 60, Part III., 2017. - 39-43.

THE MOVEMENT OF A POINT SET IN CARTESIAN COORDINATES AND STUDIED IN THE MATHCAD ENVIRONMENT

Asen Stoyanov

University of Mining and Geology "St. Ivan Rilski", 1700 Sofia

ABSTRACT. The movement of a point M within the time interval $t_0 \div t_1 \, (s)$ is specified by the law $x = x(t) \quad y = y(t)$. The trajectory and the position of point M on it are determined for the moment of time $t = t_1 (s)$. The radial and transverse components of the velocity and acceleration of the point are represented in a matrix form and all the kinematics characteristics of the movement are graphically depicted.

Keywords: transverse velocity, radial velocity, transverse acceleration, radial acceleration, MathCAD

ДВИЖЕНИЕ НА ТОЧКА ЗАДАДЕНО В ДЕКАРТОВИ КООРДИНАТИ И ИЗСЛЕДВАНО В СРЕДА НА MATHCAD
Асен Стоянов
Минно-геоложки университет "Св. Иван Рилски", 1700 София

РЕЗЮМЕ. Движението на точка M е зададено в интервала от време $t_0 \div t_1 \, (s)$ със закона $x = x(t)$ и $y = y(t)$. Траекторията и положението върху нея на т. M са определени за момента от врема $t = t_1 (s)$. Радиалните и трансверзалните компоненти на скоростта и ускорението на точката са представени в матрична форма, като всички кинематични характеристики на движението са графично изобразени.

Ключови думи: трансверзална скорост, радиална скорост, трансверзално ускорение, радиално ускорение, MathCAD

Introduction

The article examines a classical problem related to the kinematics of a point. The movement of the point is set in a coordinate way. The trajectory formed by its movement within the examined interval of time is part of a hyperbola.

When the motion of the point is set at polar coordinates, its velocity and acceleration are defined as the geometric sum of the radial and transversal components – see Fig.2. B) and C) The article shows how these operations are performed using the MathCAD math package.

Solution to a problem with the MathCAD package

The material point M moves within the time interval $t_0 \div t_2$ according to the law $x = \dfrac{-3}{t+2}; \ y = 3.t + 6$ (Yablonsky, 1978) – see Figure 1.

For the moment $t = t_1$, it is necessary to determine:

- The position of point M on the trajectory – see Fig.1.A);
- The velocity, the full, tangential, and normal acceleration of point $M - \vec{v}, \vec{a}, \vec{a_\tau} \ u \ \vec{a_n} -$ see Fig.2.A);
- The transverse $\vec{v_{tr}}$ and the radial $\vec{v_{rad}}$ components of the velocity $\vec{v_M}$ – see Fig.2.B);
- The transverse $\vec{a_{trx}}$ and the radial $\vec{a_{rady}}$ components of the acceleration $\vec{a_M}$ – see Fig.2.C);
- The radius of curvature $\rho(t)$ of the trajectory at moment t_1 – see Fig.2.D).

The calculations and graphical visualisation have to be performed using the MathCAD package.

$$x(t) := \frac{-3}{t+2} \qquad y(t) := 3 \cdot t + 6 \qquad t0 := 0 \qquad t1 := 1.6 \qquad t2 := 2$$
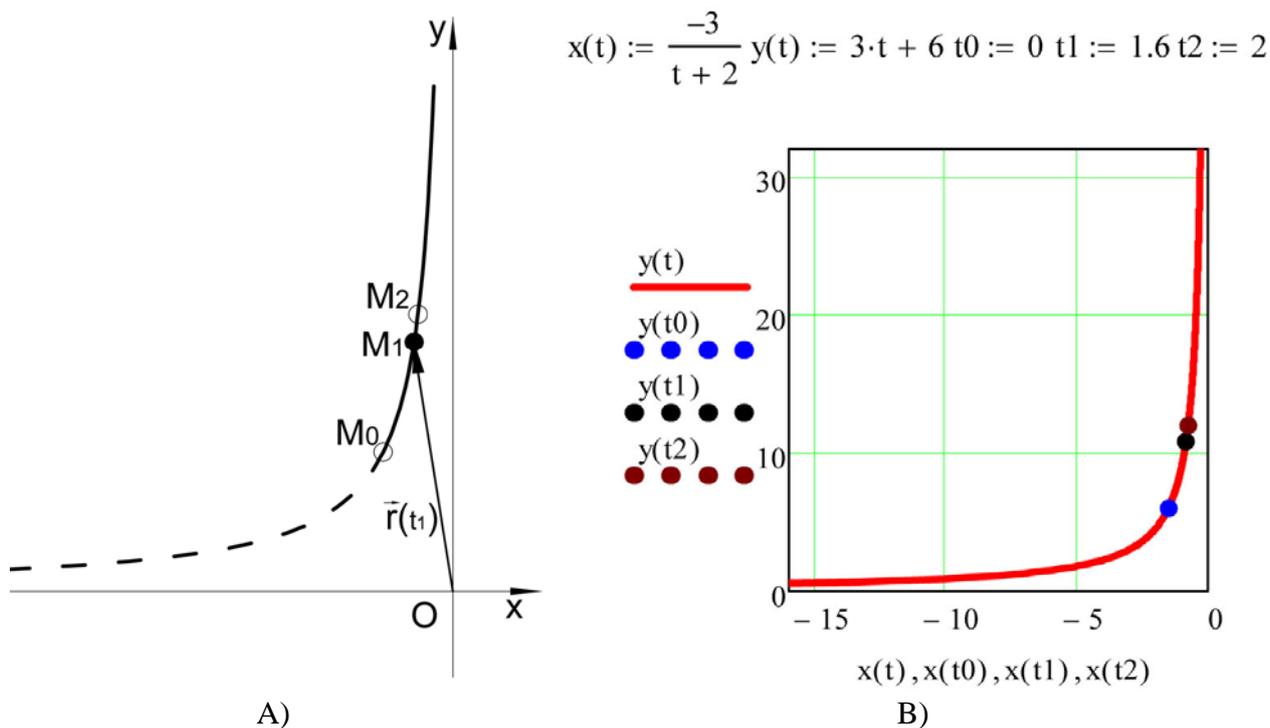
Fig.1. The trajectory of point M and its positions for moments t_0, t_1, and t_2, interpreted with: A) Excel и AutoCAD; B) MathCAD;

The problem is solved within MathCAD environments using the following algorithm:
- The output data is entered – see Fig.1.B);
- In the studied section, the trajectory of point M is visualised graphically for the time interval $t_0 \div t_2$ – see Fig.1.B);
- The law of the change of the velocity of point M is determined analytically and graphically;
- The law of the change of the acceleration of point M is determined analytically and graphically;
- The laws of the change of the tangential and normal acceleration of point M are determined analytically and graphically;

- The law of the change of the radius-vector $\vec{r}(t)$ of point M is determined analytically;
- The law of the change of the transverse and radial component of the velocity of point M is determined analytically and graphically;
- The law of the change of the transversal and radial component of the acceleration of point M is determined analytically and graphically;
- The law of the change of the radius of curvature of the trajectory $\rho(t)$ is determined.
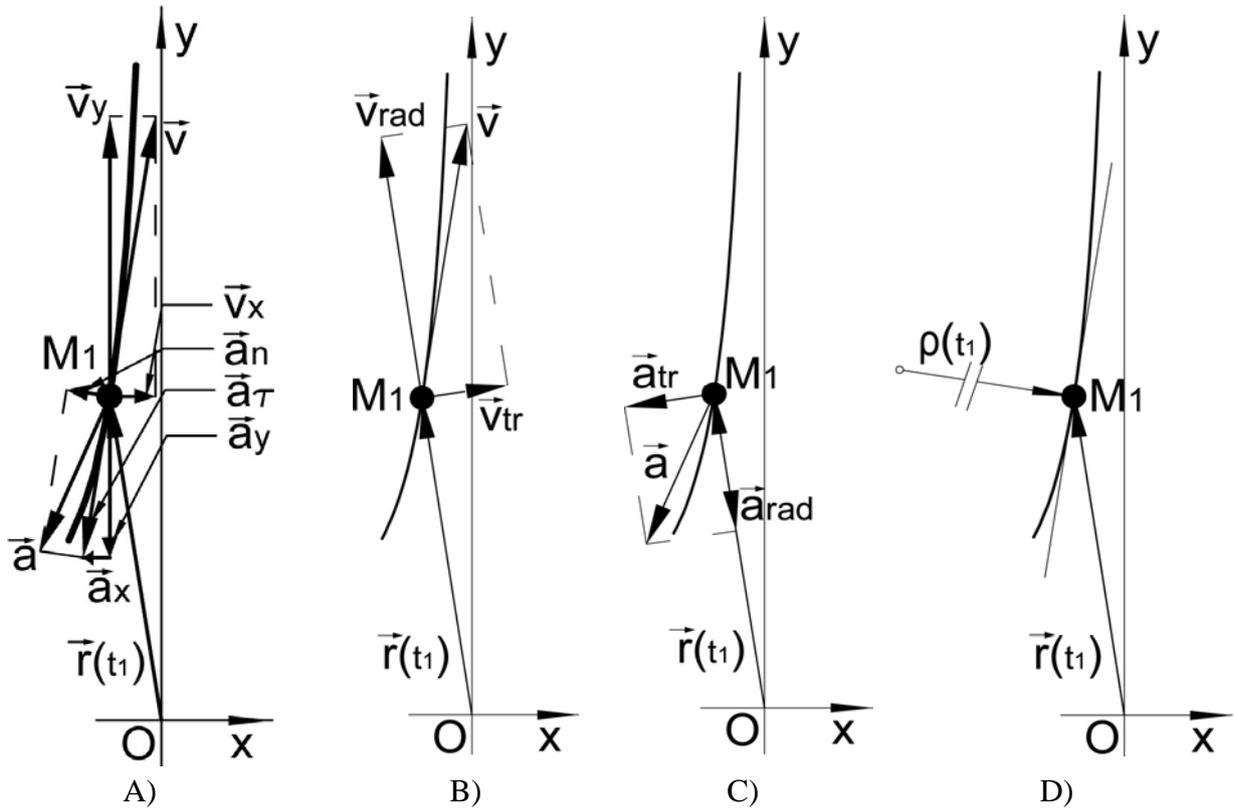
Fig. 2. Kinematics characteristics of point M for the moment t_1

$$vx(t) := \frac{d}{dt}x(t) \quad vy(t) := \frac{d}{dt}y(t) \quad v(t) := \sqrt{vx(t)^2 + vy(t)^2} \quad ax(t) := \frac{d}{dt}vx(t) \quad ay(t) := \frac{d}{dt}vy(t)$$

$$a(t) := \sqrt{ax(t)^2 + ay(t)^2} \quad a\tau(t) := \frac{vx(t) \cdot ax(t) + vy(t) \cdot ay(t)}{v(t)} \quad an(t) := \sqrt{a(t)^2 - a\tau(t)^2} \quad \rho(t) := \frac{v(t)^2}{an(t)}$$

$$r(t) := \sqrt{x(t)^2 + y(t)^2} \quad vradx(t) := x(t) \cdot \frac{vx(t) \cdot x(t) + vy(t) \cdot y(t)}{r(t)^2} \quad vrady(t) := y(t) \cdot \frac{vx(t) \cdot x(t) + vy(t) \cdot y(t)}{r(t)^2}$$

$$vrad(t) := \sqrt{vradx(t)^2 + vrady(t)^2} \quad vtrx(t) := \frac{-x(t) \cdot y(t) \cdot vy(t) + y(t)^2 \cdot vx(t)}{r(t)^2}$$

$$vtry(t) := \frac{x(t)^2 \cdot vy(t) - x(t) \cdot y(t)\, vx(t)}{r(t)^2} \quad vtr(t) := \sqrt{vtrx(t)^2 + vtry(t)^2} \quad v(t) := \sqrt{\left(|vtr(t)|\right)^2 + vrad(t)^2}$$

$$vx(t1) = 0.231 \quad vy(t1) = 3 \quad v(t1) = 3.009 \quad \rho(t1) = 70.61 \quad an(t1) = 0.128 \quad a\tau(t1) = -9.893 \times 10^{-3}$$

$$a(t1) = 0.129 \quad vtrx(t1) = 0.46 \quad vtry(t1) = 0.036 \quad vradx(t1) = -0.229 \quad vrady(t1) = 2.964$$

$$vrad(t1) = 2.973 \quad vtr(t1) = 0.462 \quad aradx(t) := x(t) \cdot \frac{ax(t) \cdot x(t) + ay(t) \cdot y(t)}{r(t)^2}$$

Fig.3. Analytical expressions for determining the kinematics characteristics of point M and their values at moment $t = t_1\,(s)$ (Бертяев, 2005; Brent Maxfield, 2009; Доев и др., 2016).

$$\text{arady}(t) := y(t) \cdot \frac{\text{ax}(t) \cdot x(t) + \text{ay}(t) \cdot y(t)}{r(t)^2} \qquad \text{arad}(t) := \sqrt{\text{aradx}(t)^2 + \text{arady}(t)^2}$$

$$\text{atrx}(t) := \frac{-x(t) \cdot y(t) \cdot \text{ay}(t) + y(t)^2 \cdot \text{ax}(t)}{r(t)^2} \qquad \text{atry}(t) := \frac{x(t)^2 \cdot \text{ay}(t) - x(t) \cdot y(t)\, \text{ax}(t)}{r(t)^2}$$

$$\text{atr}(t) := \sqrt{\text{atrx}(t)^2 + \text{atry}(t)^2} \qquad a(t) := \sqrt{\left(|\text{atr}(t)|\right)^2 + \text{arad}(t)^2} \qquad a(t1) = 0.129$$

Fig.3. Analytical expressions for determining the kinematics characteristics of point M and their values at moment $t = t_1\,(s)$ (Бертяев, 2005; Brent Maxfield, 2009; Доев и др., 2016).
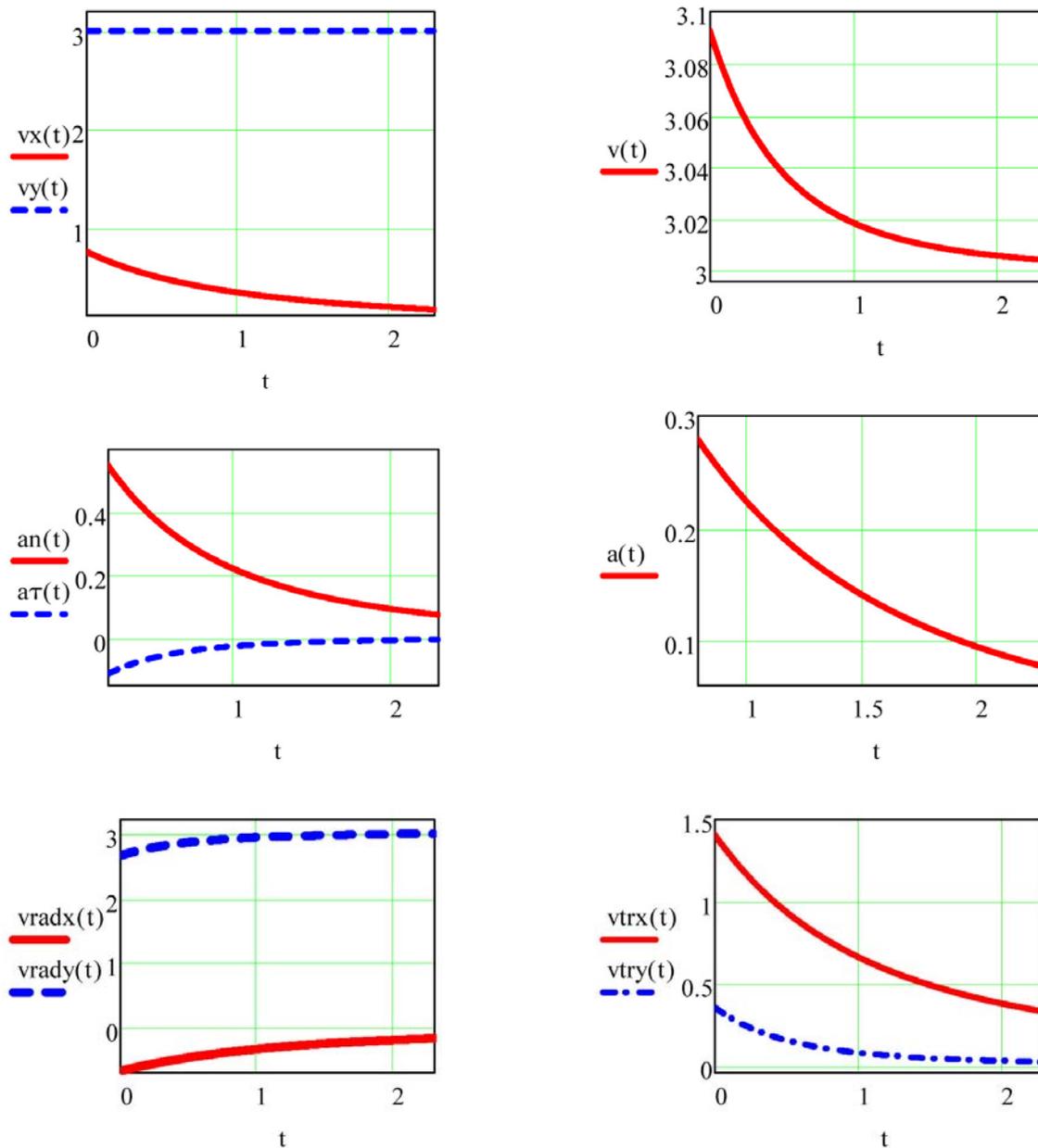
Fig. 4. Graphs expressing the dependence of the kinematic characteristics of point M on time $t\,(s)$ (Brent Maxfield, 2009; Доев и др., 2016)
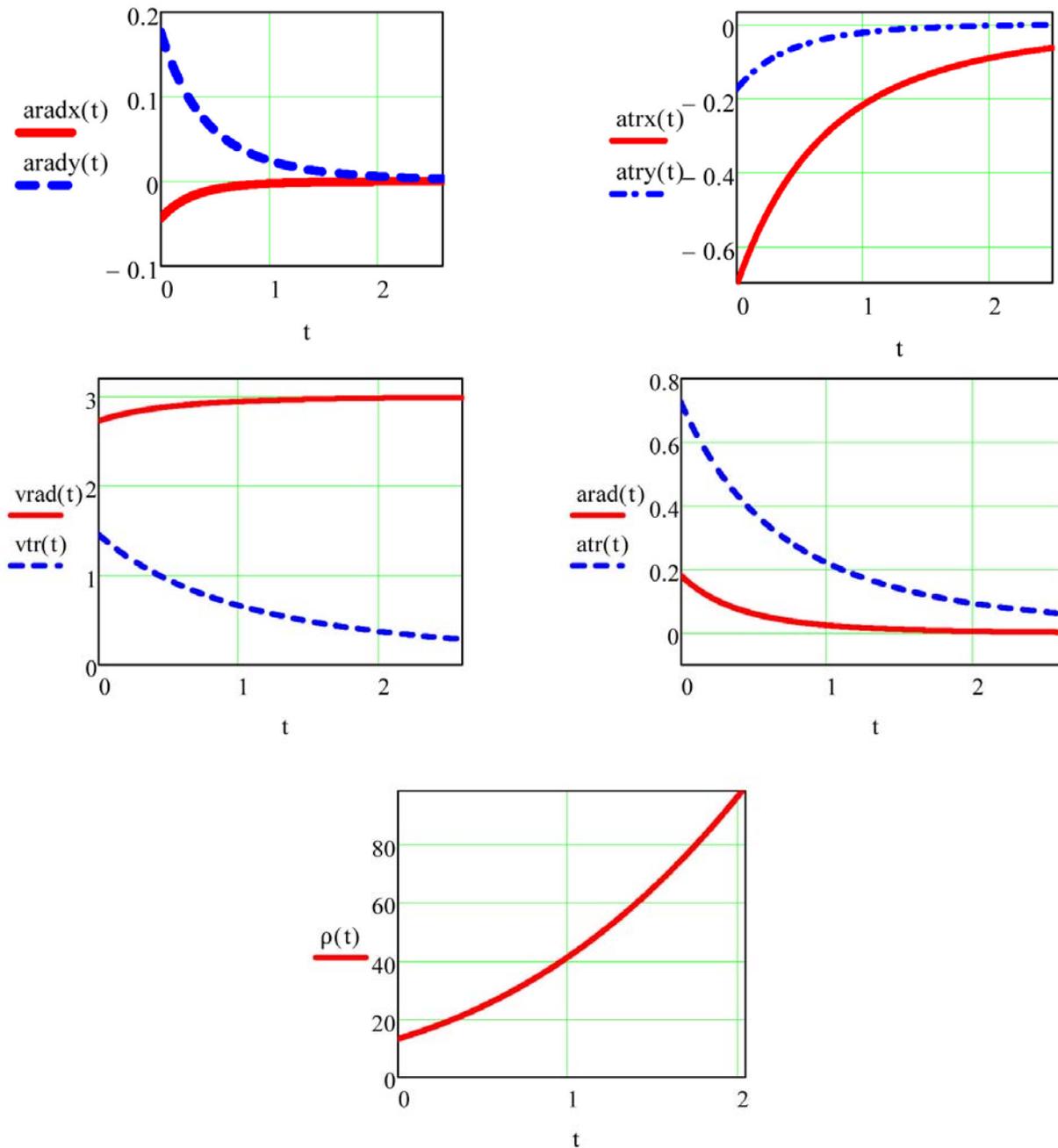
Fig. 4. Graphs expressing the dependence of the kinematic characteristics of point M **on time** $t\,(s)$ **(Brent Maxfield, 2009; Доев и др., 2016)**

Conclusion

An idea for a short solution is given by using the MathCAD package. The example complements the kinematics teaching aids in Bulgaria.

A similar problem has been solved by Doev and Doronin (Доев и др., 2016).

This article makes the solution more complete and detailed. The kinematics characteristics of the point are clearly detailed in Fig. 2. In addition to the graphical changes of the velocity and acceleration, Fig. 4. shows the changes in their components as well.

Finally, the task can be solved by hand as well. The partially automated solution overcomes the occurrence of mathematical difficulties and makes it possible to track the changes in kinematics magnitudes. It is compact and adaptable to the changes in the input data of the problem.

References

Бертяев, В. Теоретическая механика на базе MathCAD практикум. Санкт–Петербург, „БХВ–Петербург", 2005. – 739 с. (Bertyaev, V. Teoreticheskaya mehanika na baze MathCAD praktikum. Sankt-Peterburg, "BHV-Peterburg",

2005. - 739 p.)

Brent Maxfield Essential MathCAD for Engineering, Science, and Math. 30 Corporate Drive, Suite 400, Burlington, MA 01803, USA, 525 B Street, Suite 1900, San Diego, California 92101-4495,USA, 84 Theobald's Road, London WCIX 8RR, UK, Copyright 2009. - 501 p.

Доев, В. С., Ф. А. Доронин. Сборник заданий по теоретической механике на базе MathCAD. Санкт Петербург, Москва, Краснодар, Лань, 2016. - 585 с.

(Doev, V. S., F. A. Doronin. Sbornik zadaniy po teoreticheskoy mehanike na baze MathCAD. Sankt-Peterburg, M., Krasnodar, Lan, 2016. - 585 p.)

Яблонский, А. А. Сборник заданий для курсовых работ по теоретической механике, М., Высшая школа, 1978. (Yablonskiy, A. A. Sbornik zadaniy dlya kursovaih rabot po teoreticheskoy mehanike, M., Visshaya shkola, 1978.)

MODELS IN DESIGNING DOCUMENT MANAGEMENT SYSTEMS

Kremena Arsova – Borisova[1], Veselin Christov[2]

[1] *University of mining and geology "St. Ivan Rilski", 1700 Sofia, kremena.arsova@mgu.bg*
[2] *University of mining and geology "St. Ivan Rilski", 1700 Sofia, veso@mgu.bg*

ABSTRACT. In all organizations, they use and accumulate large quantities of various documents - contracts, annexes, minutes, invoices, bank statements, mission statements and reports, advance reports, offers, customs declarations, bills of lading, references, proposals, orders, requests, applications, drawings, sketches, plans, decisions, notary deeds and others. Documents can be both paper and electronic. Typically, document management systems are used to handle a large quantity of documents. The article examines the different models in the design of these systems: information, functional, structural, the database system, etc. An experimental document management system is presented to test the models under consideration.

Keywords: document management system, DMS, design model

МОДЕЛИ ПРИ КОНСТРУИРАНЕ НА СИСТЕМИ ЗА УПРАВЛЕНИЕ НА ДОКУМЕНТИ
Кремена Арсова – Борисова[1], Веселин Христов[2]
[1] *Минно геоложки университет „Св. Иван Рилски", 1700 София, kremena.arsova@mgu.bg*
[2] *Минно геоложки университет „Св. Иван Рилски", 1700 София, veso@mgu.bg*

РЕЗЮМЕ. Във всички организации си използват и натрупват големи количества от разнообразни документи – договори, анекси, протоколи, фактури, банкови извлечения, командировъчни заповеди и отчети, авансови отчети, оферти, митнически декларации, товарителници, справки, предложения, заповеди, молби, заявления, чертежи, скици, планове, решения, нотариални актове и други. Документите може да са както на хартиен, така и на електронен носител. Обикновено при работа с големи количества документи се използват системи за управление на документи. В статията се разглеждат различните модели при конструирането на тези системи: информационен, функционален, структурен, на системата от бази от данни и др. Представена е експериментална система за управление на документи, при която се изпробват разгледаните модели.

Ключови думи: система за управление на документи, СУД, конструктивен модел

Introduction

Each organization has a real need for a document management system (DMS). DMS exist to organize, store and retrieve information accurately and effectively. They are designed to organize files and recordings in electronic form. They are a mean of providing more compact storage, universal access for retrieval, a higher level of data security and privacy. Its base features include [Björk, Bo-Christer, 2001]: acquisition, storage, classification, indexing, version editing, maintenance, use, document security. When documents are in a structured system, more complex processing procedures, such as tracking the life cycle of each document, are possible. They are designed to provide the data warehouse where documents are created, managed and stored for easier access by different users and departments within an organization [Löwnertz, K., 1998].

When designing such a system, it is necessary to plan carefully the various models that define its design and operation so that it is as efficient, easy and safe as possible. [Ralph H. Sprague, Jr, 1995].

An experimental document management system has been designed and developed, in which such design models have been implemented.

Design Models in DMS

In the process of planning and building a DMS it is necessary to consider and clarify a number of issues related to its functioning. The solutions found determine the design models embedded in the future EMS. Properly selected models should provide system evolution and scalability. Such models are:

System architecture. It determines whether the system will function as a separate local application for a single user or will serve a team of users.

The operating system file system is generally used as a local DMS, but in this case, the structuring of document storage and searching does not particularly support users. There is no further description of the documents, they cannot be grouped by additional signs, the life cycle and the movement of the documents cannot be traced. In some word-processing systems, for example, Microsoft Word has built-in local DMS components, but it is limited to documents created with this

word-processing system. In general, local DMSs are rarely created and used.

Collective DMSs can be organized in two major ways: distributed processing and client-server technology.

In distributed processing, a single user's work is stored on his computer and a system for searching, accessing, and moving documents between users is organized. This way of working is closer to the thinking of traditional users. On the other hand, it is very complex for implementation and maintenance, and creates a number of problems with the security of storage and authorized access to documents. The number of users is limited.

Client-server technology is a network architecture type. The administration is centralized. The server is a computer running dedicated server software and a network operating system that makes its resources available to other computers on the network. On the other hand, the client is a computer that accesses the server resources. The term client may also mean software programs accessing server programs. Access to resources is controlled through authentication and access rights. User accounts are created and stored on the server. The client is the active partner in the communication, and the server is a passive partner, waiting for requests, processing and returning a response. Each server can receive queries from a large number of clients simultaneously. The connection between the client and the server is accomplished through a specific protocol (a set of rules of the dialogue between the two partners).

Most DMSs are based on this architecture. Various variations are possible: the databases (DBs) for the documents are on the server and the documents themselves are on the client computers or the documents and the DBs are on the server. It is possible that most of the DMS is in the form of a client module of the user computers. This is a good solution for a document system limited within an organization. The disadvantage is that access to the DMS can only be done by computers where this module is installed. If access is needed from anywhere, then the solution is a Web based DMS, where it is all deployed on a server and accessed via a web browser.

Functional model. It describes the functions that the DMS implements. Depending on what documents the system is intended for, it may be specialized or general purpose. For example, a specialized DMS is the one that organizes the design documentation of a building organization. Such systems have some specific functions related to special operations with documentation such as selection of tender documents. The main functions of the general purpose DMSs include acquisition, storage, classification, indexing, version editing, searching, using, printing, sending to specific destinations, electronic signature stamping, security, document lifecycle; creation and maintenance of user accounts and user groups, user profiles, specific user access rights, personalized user interface, etc. A separate aspect of the functional model is the administration of the system.

Structural model. It defines the modules and subroutines of the software and DMS hardware requirements. This model is in direct connection with the chosen architecture and functional model. It also depends on the database system, the security model, the user and the information models of the system. In

server DMSs, the technical characteristics and positioning of the server or servers, their connection to the computer network, the operating systems, the organization of the data warehouse, etc. are of particular importance. The choice of the programming language and database management system (DBMS) depend on the architecture, the structural and the functional model.

Structure of databases. Mostly, relational databases are used in the DMS. It is important to properly build the individual bases and their system organization: there must be no data excesses, the system has to be properly normalized and it is possibly to add new bases. It is necessary to maintain the appropriate data for the documents and the users and for who and when they used the documents.

To these design models can be added:
- An **information model** describing the movement of documents and user data inside the system;
- A **security model** covering all issues related to secure document storage, recovery from user errors and system crash and malfunctions, user accounts and profiles, organizing users in groups, access rights, user tracking, etc.;
- An **user model** of the system that defines the user interface, user personalizing, organizing collaborative work on the same document, etc.

Experimental DMS description

The Experimental DMS is implemented as a desktop application through a client - server architecture. Resources from Microsoft are selected to the realization. The Visual Basic programming language for Visual Studio 2010 and the .NET Framework 4.0 platform are used to implement the client part. For the implementation of the server side of the application, MS SQL Server 2014 Express and Transact-SQL are used. The Inno Setup compiler (installation software written on Delphi) is used to create the application's installation system.

For system implementation about the server 6 tables, 11 procedures, 4 functions and 326 rows of program code are made. With respect to the client part - 7 forms and 1490 rows of program code are produced. The main activities of the system are:

- Add a document to the system and allocate it to a specific directory - To add a document to the system, the user first describes the document by adding additional information about it - chooses its type; the directory in which it will be recorded; comments and labels, then indicates the required document and adds it;

- Use of function keyboard keys - The user is given the opportunity unless provided by the interface controls to use relevant function keys: INSERT function key - pressing its trigger event "click" on the Add button; Function key F2 - Pressing the button activates the event "click" on the Edit button; with the DELL function key - when it clicks, the event triggers the click of the Delete button; Function key ENTER - when pressed (in a text box) this triggers the radio button click event (if there is one above the text box);

- Searching and retrieving electronic documents (records) - In the submenu "Entering and correcting" of the menu "Data entry", in the tab "Main data", the user has the possibility to search and retrieve records according to the following criteria: Code - search is performed in whole or in part in the text field code; Document type - searching by document type selected from combo box; Folder - searching by folder name selected by the combo box; Document name - searches are made in whole or in part; Comment - search is made on a wholly or partially entered comment; Labels - searching based on user-tagged labels;

- Sorting - The system allows sorting of data;

- Generate sequential document type numbers - The system automatically generates a sequential number and adds it to the code corresponding to each document type. For example, the user adds a document type Archive (the code is ARH), and if no documents of this type are added to the system, then its ID will be ARH1. If there are already 10 documents of this type in the system, the newly added will be code ARH11;

- Link between documents - The system allows the user to add additional documents to one master document. For example, we have a document that contains a contract and several other documents that are annexes to this contract;

- Revisions (versions) - Allows you to store and manage various document revisions. This feature is useful for documents that require frequent updates. When adding a document, the system checks by its name if it exists in the system and if not, then by default add rev0 to its name. If a document with the same name exists when it is added to the system, its Rev + revision number for this document is added to its name;

- Opening a document - In "Correction and Input" submenu the system allows the user to open a marked from him document by clicking on "Path";

- Show the size of the document and its file extension - The system provides information about the size and file extension of each document;

- System Administration and Security - Different levels of access may be required for different users (when correcting and deleting documents). The system allows a user to be restricted in their access to correct and delete data. In addition, a user with a lower access level cannot correct or delete a document added by a higher-level user. Access levels are set in menu "Users";

- Remembering the last user who used the program - The system keeps information about the last user who used it and when it was rebooted, In this case it is not necessary to fill in the User field, but only its password.

Figure 1 shows a schematic diagram of the structural model of the experimental system client part, and Figure 2 illustrates the scheme of the database system.


**Fig. 1. Structural model of the experimental system client part**

Users

	Column Name	Data Type	Allow Nulls
🔑	Id	char(10)	☐
	Name	char(15)	☐
	idAccess	int	☐
	pass	char(10)	☐
			☐

Tag

	Column Name	Data Type	Allow Nulls
🔑	id	int	☐
	name	char(50)	☐
	CDB	char(10)	☐
	CDATE	datetime	☐
	CTIME	datetime	☐
	MDB	char(10)	☐
	MDATE	datetime	☐
	MTIME	datetime	☐
			☐

Folders

	Column Name	Data Type	Allow Nulls
🔑	id	int	☐
	name	char(50)	☐
	CDB	char(10)	☐
	CDATE	datetime	☐
	CTIME	datetime	☐
	MDB	char(10)	☐
	MDATE	datetime	☐
	MTIME	datetime	☐
			☐

Docs

	Column Name	Data Type	Allow Nulls
🔑	Id	int	☐
	Kod	char(13)	☐
	TipDoc	char(3)	☐
	idTag	char(500)	☐
	Pat	char(500)	☐
	Note	char(500)	☐
	Rev	int	☐
	Name	char(50)	☐
	Ext	char(5)	☐
	idFolder	int	☐
	Size	char(20)	☐
	CDB	char(10)	☐
	CDATE	datetime	☐
	CTIME	datetime	☐
	MDB	char(10)	☐
	MDATE	datetime	☐
	MTIME	datetime	☐
			☐

DopDocs

	Column Name	Data Type	Allow Nulls
🔑	id	int	☐
	idDocs	int	☐
	name	char(50)	☐
	ext	char(5)	☐
	pat	char(50)	☐
	note	char(500)	☐
	size	char(20)	☐
	folder	char(50)	☐
	rev	char(10)	☐
	CDB	char(10)	☐
	CDATE	datetime	☐
	CTIME	datetime	☐
	MDB	char(10)	☐
	MDATE	datetime	☐
	MTIME	datetime	☐
			☐

TipDoc

	Column Name	Data Type	Allow Nulls
🔑	id	char(3)	☐
	name	char(50)	☐
	CDB	char(10)	☐
	CDATE	datetime	☐
	CTIME	datetime	☐
	MDB	char(10)	☐
	MDATE	datetime	☐
	MTIME	datetime	☐
			☐

Fig. 2. Database System of the experimental system

Conclusion

Document management systems are an important part of the software of any organization that works with documents. Their quality largely determines the effective work of these organizations. Planning and developing such a system requires careful consideration and selection of the various design models that will be built into it. Such models are system architecture, functional model, structural model, database system, information model, system security model, user model, etc.

To illustrate this model approach, an initial version of an experimental document management system is being developed. It could be evaluated by:

- adding a metadata classification function;
- adding a feature that will prevent specific users from accessing certain menus and features;
- adding a search function using metadata;
- adding a keyword search feature;
- adding a semantic analysis function to determine a search connection;
- adding web functionality so that it can be accessed via mobile phones, tablets, etc.;
- giving an ability to upload multiple documents simultaneously.

References

Björk, Bo-Christer, 2001. Document management - a key technology for the construction industry, Information and Communications Technology (ICT) in the Practice of Building and Civil Engineering, proceedings of the 2nd worldwide ECCE Symposium, Espoo, Finland 6-8.6.2001, Association of Finnish Civil Engineers, Helsinki, Finland, pp. 35-43;

Löwnertz, K., 1998. Change and Exchange – Electronic Document Management in Building Design, Licentiate Thesis, Dept. of Construction Management and Organization, Royal Institute of Technology, Stockholm, Sweden;

Ralph H., Sprague, Jr., 1995. Electronic Document Management: Challenges and Opportunities for Information Systems Managers, MIS Quarterly, Vol. 19, No.1 (Mar.,1995), Management Information Systems Research Center, University of Minnesota.